Spring 5-15-2020

Transcriptional and Epigenetic Regulation of Cerebellar Development and Function

Naveen C. Reddy
Washington University in St. Louis

WASHINGTON UNIVERSITY IN ST. LOUIS

Division of Biology and Biomedical Sciences
Neurosciences

Dissertation Examination Committee:
Azad Bonni, Chair
Harrison Gabel
Kristen Kroll
Robi Mitra
David Ornitz

Transcriptional and Epigenetic Regulation of Cerebellar Development and Function

by
Naveen Cherukupalli Reddy

A dissertation presented to
The Graduate School
of Washington University in
partial fulfillment of the
requirements for the degree
of Doctor of Philosophy

May 2020
St. Louis, Missouri

Table of Contents

List of Figures

Acknowledgments

I am grateful to have had the opportunity to attend Washington University. The rigorous scientific community and investment in training future scientists has prepared me for a bright future.

I am thankful to have had the opportunity to be mentored by Dr. Azad Bonni. While I am certainly proud of the research projects that we have completed, my time in the Bonni lab has meant more than that. Azad and the Bonni lab have created an amazing environment for scientific, personal and future growth. I am extremely lucky to have worked with such wonderful people.

I would also like to thank Dr. David Ornitz, Dr. Kristen Kroll, Dr. Rob Mitra and Dr. Harrison Gabel for their support and advice as thesis committee members throughout my training. I want to additionally thank Harrison for his co-mentorship in the final stages of my training.

I would also like to thank each of the funding institutions and groups that have allowed me to achieve my dissertation research aims, including the National Institutes of Health grants (1RF1MH11707001, 5R01NS08439305) and the Washington University Center for Cellular Imaging.

Naveen C Reddy

Washington University in St. Louis

May 2020

Dedicated to my loving family.

ABSTRACT OF THE DISSERTATION

Transcriptional and Epigenetic Regulation of Cerebellar Development and Function

by

Naveen Cherukupalli Reddy

Doctor of Philosophy in Biology and Biomedical Sciences

Neurosciences

Washington University in St. Louis, 2020

Professor Azad Bonni, Chair

Precise control of gene expression is essential for neural development and function. This control is regulated by the interplay of chromatin remodelers and transcription factors (TFs). To better understand these mechanisms involved in gene regulation, we pursue two questions: 1) what are the roles of the chromatin remodeler CHD7 in cerebellar development and 2) what are the roles of the MEF2 TF family in cerebellar function.

CHD7 mutations are causative for CHARGE syndrome, a heterogeneous disorder affecting many organ systems, occurring in 1:10,000 newborns. Recent MRI studies have identified cerebellar hypoplasia and foliation defects in a large portion of CHARGE syndrome patients. To identify the how a decrease in CHD7 activity leads to cerebellar defects seen in patients, we conditionally knockout CHD7 in granule cell precursors of mouse cerebellum. Surprisingly, we see a stereotyped folding pattern along the typically smooth mediolateral axis. We then characterize cellular processes and identify a switch in the preferred axis of granule cell precursor division prior to onset of irregular folding. Upon assessing transcriptomic and epigenomic functions of CHD7, we find CHD7 to regulate gene programs implicated in human

disorders of brain folding. Additionally, we show that CHD7 reduces accessibility of enhancers with corresponding reduction in enhancer activity and proximal gene expression.

The recruitment of chromatin remodelers to specific regions is accomplished by multiple factors including transcription factors. Thus, TFs also play a vital role in proper gene regulation. Furthermore, transcription factors can bind accessible regions and recruit other factors important for transcription to occur. The latter part of this dissertation will address the roles of paralogous transcription factors, MEF2A and MEF2D, and their roles in cerebellar function.

MEF2A and MEF2D are highly expressed in cerebellar granule cells, the most abundant neuron in the brain. Using single and double conditional knockout of MEF2 family TFs, we find that MEF2A and MEF2D play functionally redundant roles in cerebellar-dependent motor learning. Although both TFs are highly expressed in granule neurons, transcriptomic analyses show MEF2D is the predominant genomic regulator of gene expression in vivo. Strikingly, genome-wide occupancy analyses reveal upon depletion of MEF2D, MEF2A occupancy robustly increases at a subset of sites normally bound to MEF2D. Importantly, sites experiencing compensatory MEF2A occupancy are concentrated within open chromatin and undergo functional compensation for genomic activation and gene expression. Finally, motor activity induces a switch from non-compensatory to compensatory MEF2-dependent gene regulation. These studies uncover genome-wide functional interdependency between paralogous TFs in the brain.

Collectively, our studies on CHD7 and MEF2 provide further understanding of the roles of two critical classes of gene regulators in cerebellar development and function. These studies have set the basis for understanding how TFs and chromatin remodelers control gene expression. Future studies will address how knockout of chromatin remodelers affect TF occupancy, and conversely, how TF depletion prevents chromatin remodeler recruitment.

Chapter 1:

Epigenetic and transcriptional regulation of gene expression

1.1 Introduction to gene regulation

1.1.1 Gene expression

It is widely known that genetic material is conserved and not lost during proper development (Gurdon et al., 1975; Wilmut et al., 1997). Consequently, the trillions of cells found in complex multicellular organisms such as humans are comprised of the same genome (Reik, 2007). Simply stated, skin cells have the same genome as brain cells and liver cells. How, then, have these cells developed to have such vastly different morphologies and functions?

Cell-type specification and function rely on the ability of cells to interpret molecular and environmental signals and to precisely and temporally control gene transcription. Transcription typically begins when RNA polymerase binds a gene promoter, a DNA sequence usually located just upstream of a gene. However, distal regulatory elements, known as enhancers, are primarily responsible for spatiotemporal control of gene expression (Kim and Shiekhattar, 2015). These regulatory elements can function over long distances to modify promoter activity. Throughout evolution, cells have developed complex mechanisms to aid in regulating gene expression.

Cellular mechanisms that control gene expression can be largely divided into proteins that modify the chromatin state, chromatin remodelers, and those that recruit cofactors in order to dynamically regulate transcription, such as transcription factors. Additionally, the intricate combinatorial expression of and interplay between transcription factors and chromatin remodelers adds yet another layer of complexity to gene regulation that is vital for essentially all developmental and functional processes.

1.1.2 Chromatin remodelers

One copy of the human genome stretches over two meters when fully extended. However, it must be packaged into a cell nucleus that averages less than 10um in diameter. In order to achieve this feat, cells have developed chromatin, a complex made up of DNA and histone proteins. 147 base pairs wrapped around an octomer of histone proteins H2A, H2B, H3, and H4 create the fundamental unit of chromatin, the nucleosome (Zhou et al., 2019).

As described previously, gene expression is vastly dynamic and dependent on many factors. Similarly, the chromatin state is also highly plastic and sets the stage for transcriptional control of gene expression by facilitating or preventing access to nucleosomal DNA by remodeling the structure, composition and positioning of nucleosomes. This process is known as chromatin remodeling (Lai and Pugh, 2017).

Chromatin remodeling occurs primarily through two mechanisms 1) covalent histone-modifying complexes such as histone acetyltransferases, deacetylases and 2) methyltransferases, and adenosine triphosphate (ATP)-dependent chromatin remodeling complexes (Clapier et al., 2017). ATP-dependent chromatin remodelers share a common ATPase domain belonging to the SNF2 family of DNA helicases (Hota and Bruneau, 2016). ATP-dependent chromatin remodelers hydrolyze ATP, producing energy that is utilized to evict histones from DNA, slide nucleosomes along DNA and exchange histone variants. These functions lead to a change in the accessibility of the DNA, either promoting or inhibiting the ability of other nuclear factors, such as transcription factors, to bind and further regulate transcription (Manning and Yusufzai, 2017, Reiter et al., 2017).

1.1.3 Transcription factors

The action of chromatin remodelers to define chromatin state and accessibility sets the stage for proceeding steps in gene expression regulation, which are largely controlled by the coordinated action of DNA binding proteins called transcription factors (TFs) (Takahashi and Yamanaka, 2006, Farley et al., 2015, Siersbaek et al., 2014). TFs bind 6-12 bp DNA sequences, known as a consensus motif, which tend to be evolutionarily conserved (Jolma et al., 2013). Often, the simultaneous binding of a diverse combination of TFs at an enhancer and/or promoter is required for accurate regulation of gene expression (Long et al., 2016). Once bound, TFs recruit cofactors, such as the Mediator complex or the acetyltransferase CBP/p300, which mediate assembly of the basal transcriptional complex at core promoters (Spitz and Furlong, 2012). This coordinated action of TFs on distinct regulatory elements drives gene expression outcomes.

Additionally, TFs can aid in altering and maintaining the chromatin state, further affecting gene regulation. Certain TFs known as pioneer factors bind exposed nucleosomal DNA and recruit chromatin remodelers to create a more accessible chromatin environment (Zaret and Carroll, 2011). Additional TFs can then bind accessible regions and maintain chromatin state by outcompeting nucleosomes (Lambert et al., 2018, Grossman et al., 2018). Although the number of chromatin remodelers and TFs are limited, the combinatorial expression of these regulators is exceedingly vast, allowing for a multitude of different gene expression programs and developmental outcomes.

1.2 Cerebellar development and organization

1.2.1 Cerebellar development

The gross structural complexity of the cerebellum hides a relatively simple, stereotyped cellular organization comprised of a limited number of morphological cell types. Cerebellar cells can be divided into two broad categories: 1) GABAergic cells that include Purkinje, Basket, Stellate, Golgi and Lugaro cells and 2) glutamatergic cell that include unipolar brush cells and granule neurons. Bergmann glia and GABAergic cells originate from the ventricular zone, distinguished by Ptf1a expression. Whereas glutamatergic neurons originate from the rhombic lip. The deep cerebellar nuclei contain both GABAergic interneurons and glutamatergic projection neurons, and thus, originate from the ventricular zone and rhombic lip (Martinez et al., 2013).

Granule neurons, account for over 70% of all cell in the mature cerebellum. These cells are born between E12.5 and E17 in mice. Granule cell precursors (GCps) migrate from the rhombic lip and deposit in an anterior to posterior manner in the cerebellar anlage. This new germinal layer is known as the external granule layer (EGL) and is identified by Atho1 expression. GCps continue to proliferate postnatally in the outer portion of the EGL, accounting for more than 90% of all granule neurons. This rapid postnatal proliferative phase of GCps, initiated by molecular signals such as Shh, begins around P3 and lasts until P16, leading to rapid expansion and foliation of the cerebellum (Chang et al., 2019). As GCps become post-mitotic, they move into the inner EGL where they begin to migrate tangentially along the medial-lateral axis. Granule neurons then extend two fibers parallel to the pia mater as they begin migrating radially to their final resting point, the internal granule layer (IGL). These parallel fibers reside in the molecular layer and become granule neuron axons that form synapses with Purkinje cells, the

major output of the cerebellum. Once granule neurons pass the Purkinje cell layer and reach the IGL, they extend dendrites that form synaptic connections following a period of pruning and maturation (de la Torre-Ubieta and Bonni, 2011).

1.2.2 Cerebellar organization

As mentioned before, a relatively simple, stereotyped cellular organization underlies the complex structure of the cerebellum. Sensory information from pre-cerebellar nuclei is transmitted form mossy fibers to granule neurons and Golgi cells. Inhibitory action of Golgi cells can directly regulate granule neuron excitatory function. Granule neurons then relay information to Purkinje cells through parallel fibers. This can occur through direct excitatory inputs onto Purkinje cell dendritic spines or indirect inhibitory inputs through molecular layer interneurons, Basket and Stellate cells (White et al., 2014). Purkinje cells also receive input from the inferior olivary nucleus through climbing fibers. Climbing fiber inputs are critical for cerebellar forms of associative learning.

1.3 Introduction to CHD7

1.3.1 CHD7

The human chromodomain helicase DNA binding protein 7 (CHD7) gene spans 189kb on chromosome 8 and consists of 38 exons. This gene produces a 336 kDa chromatin remodeling protein. CHD7 contains two N-terminal chromodomains that may facilitate binding to methylated histones, a SANT domain allowing for histone tail binding, two BRK domains that

are characteristic of group III CHDs, an ATP-helicase domain and less well-defined C-terminal domains (de Dieuleveult et al., 2016, Bajpai et al., 2010).

These domains are vital for proper chromatin remodeling necessary for development. Complete loss of CHD7 in mice is embryonically lethal. Similarly, complete loss of CHD7 specifically in neuronal progenitors is lethal shortly after birth (Yu et al., 2013). Thus, CHD7 is crucial for early development of many systems. Neuronal expression of CHD7 begins as early as E8.5 in cerebral cortex where it regulates proliferation and migration of cells within germinal zones (Jiang et al., 2012). At E12.5 CHD7 expression can be found in other cortical areas as well as the EGL of the cerebellum (Bosman et al., 2005, Feng et al., 2017a).

Although CHD7 homozygous mutations are lethal, heterozygous mutations leading to haploinsufficiency are not. In humans, heterozygous mutations of CHD7 are causative for CHARGE syndrome (Jongmans et al., 2006). Heterozygous mutations in mice lead to phenotypes that mimic multiple aspects of CHARGE syndrome (Yu et al., 2013).

As mentioned previously, chromatin remodelers regulate development by acting on chromatin to modify many regulatory elements. Accordingly, CHD7 seems to primarily function at distal regulatory elements that are enriched for the poised and active markers, H3K4me1 and H3K17ac, respectively. This suggests that CHD7 works at active and poised enhancers. Further supporting this notion is the de-enrichment of repressive marks, H3K27me3 and H3K9me3, at CHD7 bound regions. Recent studies have shown that CHD7 acts at cell-type specific enhancers and super-enhancers, both thought to regulate tissues and cell-type specific developmental processes. Interestingly, Chd7 depletion in neuroepithelial cells resulted in redistribution of H3K27ac from cell-type specific enhancers to other enhancers, causing a fate switch from neuroepithelial to neural crest-like cells (Chai et al., 2018). Additionally, CHD7 has been shown

affect gene expression by regulating the accessibility of chromatin in granule neurons of genes essential for granule neuron differentiation (Feng et al., 2017a). These finding demonstrate the importance of CHD7 in enhancer activation leading to proper gene regulation and neuronal differentiation.

1.3.2 CHARGE Syndrome

CHARGE syndrome is a rare disorder that arises in early fetal development and occurs in roughly 1:10,000 newborns (van Ravenswaaij-Arts and Martin, 2017). Thus, children with CHARGE syndrome have multiple organ defects and developmental issues at birth, requiring immediate surgical intervention.

CHARGE was first identified as a cluster of anomalies occurring together in 17 patients by Dr. Bryan Hall. Soon after, Hittner and colleagues publish 10 case reports on patients with similar abnormalities. Two years later, in 1981, Pagon and colleagues published a series of work and coined the term CHARGE association. CHARGE is an acronym for common features present in patients: coloboma of the eye, heart defects, atresia of the choanae, retardation of growth or development, genital or urinary defects, and ear anomalies or deafness (Martin, 2010).

Although CHARGE was first identified in 1971, it wasn't until 2004 that CHD7 was shown to be responsible for CHARGE, officially classifying CHARGE as a syndrome (Vissers et al., 2004). Nearly 500 pathogenic mutations have been identified, of which, 38% are nonsense, 32% are frameshift, 13% are missense and 17% are splice site mutations. These mutations span 37 of 38 coding exons and most intronic sequences. De novo mutations account for 97% of CHD7 mutations causative for CHARGE syndrome (Janssen et al., 2012).

Although hundreds of mutations have been identified, no connection have been made linking disease severity to a subset or type of mutations. This is partially due to the extreme heterogeneity and severity of features present in CHARGE syndrome patients. Due to heterogeneity of features seen in CHARGE patients, Blake proposed diagnostic criteria in 1998. However, these criteria are constantly changing as we better understand CHARGE syndrome. Blake's criteria have been updated by Verloes and more recently by other groups (Legendre et al., 2017). All diagnostic criteria created have grouped features into two categories, major and minor. Some criteria changes have included adding new features or even replacing "major" features with more prevalent "minor" features.

Interestingly, brain structural defects are now one of the minor criteria used for diagnosis of CHARGE syndrome (Legendre et al., 2017). Specifically, recent MRI studies have revealed cerebellar abnormalities in approximately 50% of CHARGE syndrome patients. These abnormalities include hypoplasia of the cerebellar vermis, found in 35% of patients scanned, and foliation defects, found in 25% of patients (Yu et al., 2013). The prevalence of these abnormalities is similar to other clinical features of CHARGE syndrome, supporting the addition of cerebellar abnormalities to the features seen in CHARGE syndrome. Although the role of CHD7 in cerebellar hypoplasia has been characterized, little is known about how CHD7 regulates cerebellar folding.

1.3.3 Cerebellar foliation

A defining feature of the cerebellum is its unique folding pattern, made up of a distinct number of folia separated by fissures. In most species, fissures run perpendicular to the anterior-posterior (AP) axis, creating a symmetrical pattern of foliation across the cerebellar midline. This

commonality among most species suggests genetic determination of folia (Altman and Bayer, 1997 – Dev Cb System). These folia, subdivided into lobules, are thought to not only be a means of accommodating more cells by increasing surface area but also a means of facilitating and organizing more complex functional circuits (Welker, 1990 – foliation; Sudarov and Joyner, 2007 – cerebellar morphogenesis). Interestingly, specific folia have been shown to regulate distinct sensory-motor tasks (Sillitoe and Joyner, 2007). Similarly, spinocerebellar mossy fibers project to subset of lobules in the cerebellar vermis (Sotelo, 2004 – cellular genetic).

Folding of the mouse cerebellum begins in late embryogenesis begins with formation of four primary fissures, and consequently, five cardinal lobes. These cardinal lobes are shared between all mammals. As the cerebellum continues to develop postnatally, secondary fissures form leading to creation of the ten canonical lobules seen across the anterior-posterior axis. These ten lobules are conserved in humans; however, they show increased levels of foliation (Legue et al., 2016, Sudarov and Joyner, 2007).

In stark contrast to the highly lobulated AP-axis is the relatively smooth medial-lateral (ML) axis of the cerebellar vermis. This striking preference of the cerebellum to fold in the AP-axis is thought to occur due to a preferred axis of cerebellar expansion. Studies aimed at understanding this preference have focused primarily on granule cell precursors, as GCp proliferation accounts for the majority of cerebellar expansion. Remarkably, these studies have identified a preference for GCps to preferentially divide along the AP-axis (Legue et al., 2015). The ability of GCps to regulate folding through divisional preference is further supported by computational modeling (Lejeune et al., 2019).

Although the preference of GCps to divide along the AP-axis provides a cellular mechanism for the preference of cerebellar lobulation along the AP-axis, it does not explain the

stereotypy of fissures. The stereotypy of fissures is thought to occur due to the creation of anchoring centers, through concerted action of granule neurons, Purkinje cells, and Bergmann glia (Sudarov and Joyner, 2007). While multiple lines of evidence suggest that cerebellar folding is under strict genetic control of cellular processes, the molecular and cellular processes that occur during folding have not yet been elucidated.

Chapter 2:

Conditional knockout of CHARGE Syndrome protein CHD7 leads to cerebellar polymicrogyria

2.1 Summary

A wide spectrum of brain folding anomalies are associated with cognitive and neurological deficits. Recently, defects in cerebellar foliation were identified in patients with CHARGE syndrome, a multi-system disorder predominantly caused by mutations in chromatin remodeler CHD7. To investigate the cellular and molecular basis of cerebellar folding abnormalities in the context of CHARGE syndrome, we conditionally knockout CHD7 in granule cell precursors of mouse cerebellum. This results in a strikingly consistent pattern of folding along the normally smooth mediolateral axis of the cerebellum. We characterize the spatiotemporal onset of folding and identify a switch in the preferred axis of granule cell precursor division as a potential cellular basis for ectopic cerebellar folding. We also identify connections between CHD7-dependent gene programs and molecular pathways implicated in human disorders of brain folding. We then assess the epigenetic role of CHD7 and identify CHD7 to bind to and specifically reduce the accessibility of enhancers. This reduction in accessibility correlates with a reduction in enhancer activity and corresponding proximal gene expression.

2.2 Introduction

Epigenetic factors are critical regulators of gene expression in neurons (Gallegos et al., 2018). Among these factors, the chromodomain helicase DNA-binding (CHD) family of ATP-dependent chromatin remodelers have been implicated in neural development and neurological disease (Son and Crabtree, 2014, Sokpor et al., 2017). CHD7 haploinsufficiency is the major cause of CHARGE, presenting in 1:10,000 newborns as a heterogeneous constellation of signs, including coloboma of the eye, heart defects, atresia of the choanae, retardation of growth or development, genital or urinary defects, and ear anomalies or deafness (Zentner et al., 2010). Neurodevelopmental defects and neurological signs suggest dysregulation of nervous system development occurs in CHARGE syndrome (Whittaker et al., 2017). Recent studies have identified cerebellar hypoplasia and/or foliation defects as relatively prominent neuroanatomical abnormalities in CHARGE patients (Whittaker et al., 2017, Feng et al., 2017). Thus, disrupted CHD7 activity in CHARGE patients may affect developmental processes critical for the expansion and proper folding of the cerebellum.

The association of brain folding anomalies with a diverse array of neurodevelopmental disorders demands a thorough assessment of the mechanisms underlying the folding process and factors contributing to its dysregulation (Kroenke and Bayly, 2018). In addition to extreme examples of folding defects associated with neurological deficits, such as lissencephaly, polymicrogyria and pachygyria, subtler folding abnormalities have been detected in individuals with autism spectrum disorder, and schizophrenia (Piao et al., 2005, Miterko et al., 2018). Despite a potential connection between folding abnormalities and neurological deficits, the molecular and cellular mechanisms governing the folding process have remained elusive for scientists.

Recent work to elucidate mechanisms of brain folding has primarily focused on the human cerebral cortex (Lawton et al., 2019). Due to the lissencephalic cortex of mice, the gyrencephalic ferret has served as an alternative model to study mechanisms of cerebral folding. However, technological limitations are significant in gyrencephalic animal models due to lack of genetic tools, among other issues. In response, scientists have recently identified several mouse models that closely recapitulate cortical folding (Borrell, 2018). Although these models achieve folding, they show low penetrance and inconsistent patterns of folding between animals. Whereas the location of primary sulci and gyri within a given gyrencephalic species, including humans, is robustly conserved, the cortical folding thus far achieved in mouse models is of a highly variable pattern, in addition to its low penetrance (Kroenke and Bayly, 2018). Evidence that the gyral and sulcal pattern observed in human brains is heritable supports the existence of genetic mechanisms that define the patterns of cortical folding (de Juan Romero and Borrell, 2017). Studies suggest that the lack of consistent folding patterns in mouse models of cortical folding may be due to the lack of genetic domains normally present in ferrets and other gyrencephalic species (Del Toro et al., 2017).

In contrast to the mouse cerebral cortex, mouse cerebellum is densely folded and partitioned into zones, each with its own distinct gene expression patterns that likely delineate physiologically meaningful subdivisions. As in humans, the mouse cerebellum is densely folded with a simple alignment of 8-10 stereotypical folds along the anterior-posterior axis (Lawton et al., 2019). Thus, combined with the genetic tools available in mouse, this allows for precise developmental interrogation to identify and analyze the in vivo molecular, cellular and tissue level behaviors driving growth and folding (Sudarov and Joyner, 2007). Although multiple lines

of evidence suggest that cerebellar folding is under strict genetic control, the molecular and cellular processes that occur during folding have not yet been elucidated.

Here, we report our discovery of strikingly penetrant and stereotyped sulcal formation along the normally smooth mediolateral axis of mouse cerebellum, following genetic ablation of CHARGE syndrome protein CHD7 (CHD7 cKO) in granule cell precursors. The full penetrance and consistency of this ectopic folding phenomenon allowed us to identify cellular and molecular processes that spatiotemporally coincide with the onset of folding, which occurs between p3 and p4. We demonstrate that CHD7 cKO granule cell precursors undergo a shift in axis of division from normally dividing along the anterior-posterior axis to dividing along the mediolateral axis. The consequent mediolateral expansion of the proliferating outer zone of the cerebellum compared to the hypoplastic inner core supports the prevailing theory that increased rate of expansion of the outer relative to the inner zone mechanically induces cortical folding. In addition, integrative genome-wide analysis at the onset of folding in mouse cerebellum reveals that CHD7-regulated genes are convergent with molecular pathways affected in polymicrogyria, a disorder of excessive folding. In accordance with these findings, we identify excessive cerebellar folding in the context of clinically-diagnosed CHARGE syndrome. Furthermore, epigenetic profiling reveals that CHD7 regulates gene expression through enhancer activity. These findings offer novel molecular and cellular mechanisms that contribute to folding in the mammalian brain that will not only be relevant to our understanding of folding during neurodevelopment, but also during disease.

2.3 Results

Conditional knockout of CHARGE syndrome protein CHD7 results in stereotyped cerebellar microgyria

Cerebellar foliation defects are one of the more prevalent neuroanatomic abnormalities thus far detected in CHARGE patients (Yu et al., 2013). Mutations leading to haploinsufficiency of CHD7 contribute to approximately 90% of CHARGE syndrome cases (Legendre et al., 2017). In the developing mouse cerebellum, CHD7 is strongly enriched in granule cell precursors (GCps), whose expansion primarily along the anterior-posterior axis is thought to give rise to cerebellar foliation (Legue et al., 2016, Sudarov and Joyner, 2007, Feng et al., 2017).

Therefore, to elucidate the interrelationship of CHD7 and cerebellar foliation, we employed an Atoh1-promoter-driven Cre-recombinase transgene to conditionally knockout CHD7 (CHD7 cKO) selectively in the granule cell lineage during its specification in the rhombic lip (Whittaker et al., 2017). Recombination of the CHD7 conditional allele occurred during the early stages of EGL formation at E14.5 (Whittaker et al., 2017). Postnatally, efficient CHD7 deletion was evident in GCps of the anterior and central cerebellar vermis, whereas the most posterior (IX and X) lobules were spared of CHD7 deletion, in agreement with previous reports on the activity of the Atoh1-Cre transgene. CHD7 deletion was also evident in the cerebellar hemispheres.

Remarkably, knockout of CHD7 resulted in a striking pattern of cerebellar folds along the normally smooth mediolateral axis of the cerebellum (Fig. 2.1A). Histological analyses and nano X-ray computed tomography of adult cerebellum both revealed that the spatial organization of the additional folds was highly consistent between mice, with 8 folds detected in CHD7 cKO mice compared to one smooth surface in control mice (Fig. 2.1A, B, C). Intact molecular and

granule cell layers were detected, indicating the maintenance of distinct cerebellar cortex layers (Fig. 2.1A). In accordance with these findings, pathologic analysis of human cerebellum from a clinically-diagnosed CHARGE syndrome patient revealed multifocal cerebellar polymicrogyria. In addition, CHD7 cKO resulted in a significant increase in the length of the adult cerebellum compared to control mice (Fig. 2.1D). To our knowledge, this is the first genomic knockout leading to highly stereotyped and fully penetrant folding of the brain. Fortuitously, this offers an advantageous model to study the genetic and cellular processes underlying brain folding.

To determine whether CHD7 is required for the proper function of granule neurons, we first subjected CHD7 cKO mice to the cerebellar-dependent eyeblink conditioning learning paradigm (supplemental figure) (Heiney et al., 2014, Valnegri et al., 2017). During this associative task, mice learn to blink in response to an initially neutral conditioned stimulus (blue light) after repeated pairing with an eyeblink-eliciting unconditioned stimulus (periocular air puff). As expected, the learned eyelid blink conditioned response (CR) gradually increased each session day in control littermate mice. Strikingly, the rate of CRs was significantly reduced in CHD7cKO mice, indicating a deficit in cerebellar-dependent motor learning (supplemental figure). In other analyses, general motor coordination assessed by the DigiGait assay and ambulatory activity assessed by the open field test were not affected following knockout of CHD7 (supplemental figure). Thus, it appears that CHD7 is required for the performance of fine associative motor tasks, rather than gross motor coordination.

Next, we investigated the spatiotemporal onset of folding in CHD7 cKO mice. Temporal analysis of cerebellar folding by nano X-ray computed tomography allowed us to identify the developmental time point at which the first sulcus became visually apparent, postnatal day 3 (P3) in the anterior basal lobules (Fig. 2.1E). By P3.5, folding advanced from the initial midline

sulcus to two symmetrical folds. By P4, we could detect four pronounced folds symmetrically surrounding the midline of the cerebellum (Fig 2.1F).

CHD7 regulates preferred axis of granule cell precursor division

The highly consistent spatiotemporal onset of abnormal cerebellar folding in CHD7 cKO mice led us to evaluate cellular processes occurring during the emergence of ectopic folds. Around P3, the cerebellum undergoes extensive granule cell precursor proliferation in the EGL, thought to be important for foliation of the cerebellum. To assess the effect of CHD7 depletion on GCp proliferation, we subjected control and CHD7 cKO mice to immunohistochemistry analysis with antibodies recognizing phosphorylated histone H3 (pH3), a marker of dividing cells. This revealed no significant change in mitotic index of GCps between CHD7 cKO and control mice (Fig. 2.2A). At P3, some GCps are also becoming post-mitotic and radially migrate towards the internal granule layer. In vivo electroporation of granule cell precursors in CHD7 cKO and control mice revealed no significant difference in granule cell radial migration 48 hours later (Fig. 2.2B).

During normal cerebellar development, granule cell precursors have their preferred axis of division along the anterior-posterior axis of the cerebellum. This leads to increased anterior-posterior expansion of the cerebellum, which is thought to give rise to the uniaxial foliation that occurs in this direction. Axis of division is assessed by measuring the angle of axis around which a cell is dividing relative to the pia mater (Fig. 2.2D, E). In a given 2D section of the cerebellum, a vertical division represents cells dividing parallel to the pia mater and thus expanding along the length of the given section. By contrast, a horizontal division represents a cell undergoing division perpendicular to the pia mater, which is not preferentially expanding the brain along the

length of that plane, as a horizontal division can be detected in all planes. We did not see a difference in the number of horizontal divisions between CHD7 cKO and control mice (Fig. 2.2F), as expected given the lack of proliferation defect. Immunohistochemical analysis of the axis of division in the anterior-posterior and medio-lateral sections of the cerebellum revealed that in control mice there was a higher ratio of vertical to horizontal divisions in the anterior-posterior plane, whereas the number of vertical compared to horizontal divisions in the medio-lateral plane was similar (Fig. 2.2F, G). This indicated that preferential expansion occurs along the anterior-posterior axis in control mice, which corroborates previous findings on axis of division in normal cerebellar development.

By contrast, CHD7 cKO granule cell precursors showed a significant decrease in the ratio of vertical to horizontal divisions in the anterior-posterior direction and a significant increase in the medio-lateral direction (Fig. 2.2G). This indicated that granule cell precursors in CHD7 cKO mice undergo a shift in axis of division from normally dividing along the anterior-posterior axis to dividing along the mediolateral axis. The consequent mediolateral expansion of the proliferating outer zone of the cerebellum compared to the hypoplastic inner core supports the prevailing theory that increased rate of expansion of the outer relative to the inner zone mechanically induces folding of the brain.

CHD7 regulates gene pathways implicated in polymicrogyria

As CHD7 is a chromatin remodeler, we next characterized the effect of conditional CHD7 knockout on granule cell precursor gene expression at p4, during the folding process. To isolate granule cell precursors from the EGL of the anterior basal cerebellum – the region displaying pronounced folding – we performed laser microdissection of the EGL from lobules I –

V, followed by RNA-sequencing of five biological replicates from control and CHD7 cKO mice, each (Fig 2.3A). We identified 2,145 CHD7-repressed genes which were upregulated following CHD7 conditional knockout, and 2,095 CHD7-activated genes which were downregulated following CHD7 conditional knockout (Fig 2.3B). ChIP-sequencing for CHD7 in the anterior basal cerebellum of p4 mice revealed 22,515 CHD7 genomic binding sites. These sites were reduced in CHD7 cKO mice, indicating specificity of called peaks (Fig. 2.3C). CHD7 was found to occupy transcription start sites, active and poised enhancers, as well as a small number of other regions (Fig. 2.4D). Direct target genes were identified based on association of significantly CHD7-dysregulated genes with a CHD7 peak within 100kb on the genome. This analysis yielded 1,106 CHD7-bound repressed genes and 1,236 CHD7-bound activated genes. We next evaluated whether CHD7-direct target genes were enriched in molecular pathways implicated in dysregulated folding. Gene ontology analysis of genes associated with polymicrogyria in humans revealed three major pathways: Integrin signaling, cytoskeletal regulation by RhoGTPase, and gonadotropin releasing hormone receptor pathway. Interestingly, the first two of these pathways were also discovered as enriched molecular pathways for CHD7 direct target genes (Fig. 2.3E). In accordance with these findings, we identify excessive cerebellar folding in the context of clinically-diagnosed CHARGE syndrome (Fig. 2.3F).

CHD7 activates gene expression via regulation of enhancer activity

Next, we were interested in understanding how CHD7 regulates such vast gene programs affecting many biological processes. As CHD7 has been shown to govern nucleosome sliding in vitro and suggested to play a role in chromatin accessibility in vivo, we began by performing ATAC-seq of P4 control and cKO granule cells. We first began by assessing the effect of CHD7

cKO on the chromatin accessibility. Aggregate analysis of ATAC-seq data of all sites occupied by CHD7 revealed a decrease in chromatin accessibility (Fig 2.4A). Additionally, 96% of CHD7 binding sites overlap significantly called accessible regions and 82% of accessible regions with CHD7 occupancy show a reduction in accessibility upon CHD7 depletion (Fig. 2.4B).

As previously stated, CHD7 primarily binds to promoters, active enhancers and poised enhancers. Promoters were defined by adding 500bp flanking regions to all UCSC genome browser identified TSS. Active enhancers were defined as H3K27ac positive non promoters; while, poised enhancers are those that lack H3K27ac but are positive for H3K4me1. When comparing CHD7 occupied versus non-occupied regions, these distinct types of regulatory elements all showed a reduction in accessibility upon CHD7 depletion (Fig. 2.4C). Interestingly, we identified a similar robust reduction in accessibility at both active and poised enhancers, and a more modest effect at promoter regions (Fig. 2.4C).

Next, we were interested in assessing whether the observed changes in genomic accessibility by CHD7 influence enhancer activity, using H3K27ac and RNA Pol II levels as surrogates for enhancer activity. We first binned CHD7 bound enhancers that showed significant reduction in accessibility (CHD7 activated enhancers) into three similarly sized groups based on fold change (1= low, 2 = medium, and 3 = high). The same was done for CHD7 bound enhancers that show an increase in accessibility upon CHD7 depletion (CHD7 repressed enhancers). Quantitative assessment revealed that changes in enhancers activity correlated with accessibility changes of CHD7 activated enhancers but not CHD7 repressed enhancers (Fig. 2.4D).

As cooperative binding of transcription factors, co-factors, chromatin remodeling enzymes, and ultimately RNA Pol II complex at enhancers mediate the activation of target gene expression, we subsequently measured the change in proximal gene expression (Franco et al.,

2019). Interestingly, changes in proximal gene expression correlated with changes seen at CHD7 activated but not repressed enhancers. These data suggest that CHD7 activates gene expression programs by modulating enhancer activity.

2.4 Discussion

Cerebellar foliation defects identified in CHARGE patients led us to perform conditional knockout of CHARGE syndrome protein CHD7 in granule cell precursors of the developing mouse cerebellum. Fortuitously, we identify the first genetic mouse model in which a consistent folding pattern is achieved in the brain, an integral feature of physiological folding in human and other gyrencephalic species. We isolate the temporal onset of folding as p3 to p4 and characterize events that spatiotemporally coincide with this developmental window. We demonstrate increased mediolateral expansion of granule cell precursors due to a switch in their axis of division from the anterior-posterior to the mediolateral axis of the cerebellum. At the molecular level, we identify a role for CHD7 in regulating cytoskeletal and integrin-signaling pathways, which converge with gene programs dysregulated in polymicrogyria. Accordingly, we identify excessive cerebellar folding in the context of clinically-diagnosed CHARGE syndrome.

Unlike the folds of the cerebrum, the folds of the cerebellum are aligned such that the external surface appears to be covered in parallel grooves. As studies of folding have primarily focused on the cerebral cortex, the cerebellum offers an alternative system from which we may gain novel insights into the genetic and cellular mechanisms involved in brain folding. The developing cerebellum is distinct from the cerebral cortex, as it has a temporary external granule cell layer of proliferating granule cell precursors that cover the surface and generate growth by dividing primarily in the anterior-posterior direction. The process of foliation is initiated by the formation of specific multicellular anchor points at the position of prospective fissures, identified by indentations on the surface of the developing cerebellum. Recent work has suggested that anchoring center initiation is driven by tissue-scale mechanical forces that arise due to differential growth. Recent cellular and tissue scale mechanical modeling support that the

anterior-posterior oriented granule cell division leads to the formation of anchoring centers and the characteristic oriented parallel grooves of the cerebellum. Here, we provide experimental evidence in support of the role of axis of division in folding of the cerebellum. Genetic manipulation of CHD7 leads to a shift in granule cell precursor axis of division to the mediolateral axis and the emergence of folding perpendicular to normal cerebellar folia. The potential causality of mediolateral folding due to a switch in axis of division is supported by computational modeling showing that a uniaxial mode with wrinkles perpendicular to the dominant direction of granule cell expansion will arise. As cerebellum is also densely folded into parallel grooves in humans, this could represent a conserved cellular mechanism of folding regulated by CHD7 in higher order species.

Increased mediolateral expansion due to a switch in oriented cell division supports the prevailing “buckling due to differential expansion” theory, in which compressive forces arise in the outer layer of the brain because of its tangential expansion relative to the inner zone. Prior to our study, differential expansion of the outer zone of the brain primarily focused on the fact that gyrencephalic species have a greater abundance of proliferating basal radial glial cells of the outer subventricular zone of the cerebral cortex. These basal radial glial cells extend basal fibers which creates a dramatic divergence of the radial fiber scaffold, leading to tangential dispersion of radially migrating neurons and hence to the tangential expansion and folding of the cortical surface. Here, we have newly implicated axis of division as a proliferative mechanism of tangential expansion that leads to folding. Thus, although brain regions are composed of distinct networks and morphologies, folding in both the cerebral cortex and cerebellum appear to result from variations of the same principle, in which an outer grey matter zone tangentially expands at a higher rate than the underlying core. Furthermore, the temporal period in which folding occurs

in CHD7 cKO mice is prior to extensive parallel fiber extension and perpendicular to the direction of predicted tension from parallel fibers, which provides further evidence that counters the once popular axon-tension hypothesis, which posited that tension along parallel fibers, the axons of granule cells, could explain why the cerebellar cortex is highly elongated but also folded like an accordion into lobules.

While we focus on the perinatal role of CHD7 in regulating axis of division of granule cells on the surface of the cerebellar anlage, CHD7 also plays a temporally distinct role during embryonic cerebellar development. Although perinatal proliferation levels of the external granule layer are unaffected in CHD7 cKO, during embryonic development CHD7 regulates the expansion of granule cell precursors by maintaining high levels of Fgf8 in the mid-hindbrain organizer. Diminished FGF signaling contributes specifically to hypoplasia of the cerebellar vermis. Thus, CHD7 cKO affects cerebellar development in two distinct phases: 1) embryonically, reduces granule cell precursor proliferation leading to a hypoplastic cerebellum; 2) perinatally, reorients granule cell precursor axis of division in the external granule layer. Perhaps the perinatal role of CHD7 cKO in enhanced mediolateral expansion of the external granule layer compounds with its embryonic role in proliferation. These consecutive insults may synergize to increase differential expansion of the outer and inner zone of the cerebellum, leading to folding in the mediolateral axis. This hypothesis aligns with increasing evidence that relevant cellular and molecular mechanisms occur days to weeks before actual tissue folding, and the effect of mechanical factors depends on specific initial conditions that must be set in advance by early developmental processes.

The highly stereotyped gyral and sulcal patterns in gyrencephalic species suggests the influence of a deeply imprinted deterministic program, possibly genetic. Strikingly, the similarity

of folding patterns between monozygotic twins is statistically above the general population, including higher-order fissures. Prior to our study, no mouse models of brain folding had recapitulated the consistent patterns of folding that occur between individuals in a gyrencephalic species. In response, scientists suggested that this may be due to a noticeable lack of genetic domains in the lissencephalic mouse cortex, when compared to gyrencephalic species such as ferret.

In our study, we provide the first genetic manipulation that leads to fully penetrant and consistent patterns of ectopic folding in mouse cerebellum. Our ability to recapitulate consistent folding patterns seen in gyrencephalic species may result from the fact that the mouse cerebellum, unlike the cerebrum, is divided into well-defined genetic compartments. Although the cerebellar cortex is often described as having a uniform cellular composition, it is in fact heterogeneous in its molecular properties. The cerebellar cortex is divided into an array of lobules and parasagittal patterns that segment all of its cell classes, creating an almost grid-like pattern of genetic organization across the cerebellum. Interestingly, gene expression patterns delineate functionally and anatomically distinct entities in the cerebellum. One of the best-studied examples of brain organization is the parasagittal Purkinje cell zonal map. The topographic inputs and outputs of the Purkinje cell zones form functional modules. Gene expression reveals patterns of Purkinje cell stripes that demarcate the parasagittal modules. Modules are derived from lineage patterning mechanisms that instruct specific classes of sensory afferents to target particular regions of the cerebellum, and to some extent particular folds. Thus, the mouse cerebellum offers the opportunity to determine the role of genetic compartmentation on the folding process.

Although not yet shown experimentally, the new folds of the CHD7cKO cerebellum appear as though they may respect the boundaries of functionally distinct parasagittal module. With further evaluation, this may shed light on a long-standing debate as to how folding is accomplished, and how it might relate to brain function. Perhaps in folding of the cerebellum and other brain regions, form follows function. In the case of CHD7 cKO folding may have arisen to accommodate the increased number of neurons within each parasagittal module due to mediolateral expansion, which aligns with the theory that folds occur in higher order species due to the need to accommodate increased neuronal number.

The spatiotemporal predictability of folding in CHD7 cKO mouse cerebellum allows us to pinpoint developmental events that intersect this developmental window. Interestingly, the folding patterns in CHD7 cKO mice seem to spatiotemporally coincide with the highly transient appearance of a category of parasagittal Purkinje cell stripes. Whether Purkinje cell stripes create regional environmental variability for developing granule cells that leads to folding should be possible to test in future studies using genetic manipulation of Purkinje cell distribution. One possibility is that Purkinje cell stripes represent compartments of the cerebellum that differentially responds to mechanical force from the mediolateral expansion of CHD7 cKO granule cell precursors. Previous studies have shown that Purkinje cell stripes also border cell dense ribbons of migratory granule cells, called granule cell raphe that transiently connect the external granule layer and internal granule layer. The highly transient presence of granule cell raphe between p0 and p6, seems to spatiotemporally coincide with the onset of folding in CHD7 cKO mice. Perhaps, in the context of increased mediolateral expansion in the CHD7 cKO, the granule cell raphe represents sites of decreased resistance for radial migration of granule cells into the internal granule layer. An additional possibility is that another feature that correlates

with the parasagittal modules of the cerebellum, such as variability of Bergmann glia , could play a role in the location and onset of sulcal formation.

The highly defined perinatal period during which we see mediolateral folding in CHD7 cKO may represent a highly transient and critical developmental window in which the cerebellum has the potential to undergo folding in this axis. In addition to the convergence of multiple developmental events that spatiotemporally coincide with folding onset in CHD7 cKO, other experimental evidence exists indicating this may be a window of susceptibility to deregulated folding. X-ray irradiation of rats during the prenatal period, GD-21, resulted in remarkably abnormal cerebellar foliation, in which the number of lobules was larger and the direction of the fissures was almost vertical, whereas the direction of most fissures was horizontal in the control. In contrast, no apparent foliar abnormalities were found in the cerebellum exposed to radiation on p4. Thus, the last day of gestation until p4 represents a critical window in which perturbation of granule neuron precursors results in excessive folding in the mediolateral axis.

Numerous genetic tools are available in mice that are not available in gyrencephalic mammalian models. In addition to the spatiotemporal predictability and high penetrance of folding in CHD7 cKO, the ability to genetically manipulate CHD7 at different timepoints during granule precursor development will allow for further interrogation into the critical period during which CHD7 activity can affect folding. As chromatin regulators like CHD7 regulate numerous developmental processes, finer spatiotemporal genetic manipulation of CHD7 in mouse cerebellum will allow us to more accurately hone in on the mechanisms sufficient for induction of folding in the cerebellum. Additionally, genetic manipulation of molecular and cellular processes in granule cell precursors can inform us further on their roles in folding. Moreover,

genetic manipulation of the compartmentation of the cerebellum may allow us to understand whether and how folds are formed in relation to the underlying genetic and functional architecture of the brain.

Beyond elucidating general principles for folding that can be applicable to the cerebral cortex, studying folding of the cerebellum, in and of itself, is critical due to the association of cerebellar structural abnormalities with human neurodevelopmental disorders of cognition. The cerebellum has been traditionally considered to be primarily involved in sustaining or supporting motor control. A preponderance of empirical evidence, however, which we detail below, suggests a crucial role for the cerebellum in many domains of human cognition and perception (including implicit learning and predictive processing). Further, alterations in cerebellar structure and function may contribute to atypical development. In addition to foliation defects present in CHARGE patients, the relationship between cerebellar anomalies and autism is well established and in contrast to other brain regions, gross and microscopic changes in the cerebellum are most frequently associated with autism (Becker & Stoodley, 2013). In particular, neonatal cerebellar damage confers a large non-heritable risk (up to 40%) for developing Autism Spectrum Disorders (ASD) later in life, revealing the cerebellum's vulnerability during sensitive periods in neurodevelopment (as the cerebellum undergoes continued post-natal development relative to other brain structures. This background provides an important motivation to more fully characterize the architecture of cerebellum in typical and atypical development. As in human, mouse cerebellum is densely folded, making this a relevant model to understand mechanisms that could shape the cerebellum in humans. Additionally, we provide evidence that the genomic distribution and direct targets of CHD7 in mice are relevant to humans at a similar developmental age. Furthermore, our finding of excessive folding in human cerebellum of a

patient with CHARGE syndrome lend further support that dysregulation of CHD7-dependent mechanisms in the cerebellum may lead to pathological folding in human disease. Additionally, our finding that CHD7 regulates gene targets mutated in polymicrogyria raises awareness of the potential role of chromatin regulators in folding disorders of the brain, adding this category of transcriptional regulators to what has primarily included downstream effectors of cytoskeleton and cell-adhesion. Collectively, our study presents an advantageous genetic model to interrogate the molecular, cellular, and mechanical aspects of the folding process.

2.6 Future Directions

Here we demonstrate that cKO of CHD7 using the Math1-Cre line leads to fully penetrant, stereotyped abnormal folding of the mammalian brain. However, it is difficult to precisely determine which cellular process led to the observed folding defect as both Math1 and CHD7 express early in granule neuron development. In order to get a better understanding of how the multiple stages of granule neuron development lead to the observed folding phenotype, we need to further deconstruct the temporal role of CHD7 in these cells. Thus, tamoxifen-inducible Math1-CreERT2 mice can be used to knockout CHD7 in GCps at various stages of embryonic and postnatal development. This allows us to determine whether folding defects arise due to a single or a combination of CHD7 dependent developmental processes.

Additionally, due to the highly spatiotemporal consistency in folding, we can use our current model to explore genetic programs important for stages of folding such as fissure formations and anchoring center composition. Initial study will be focused on comparing genomic similarities of normal AP-axis to abnormal ML-axis folds and fissures. Such analyses may yield insight into the evolving transcriptome and epigenome during various stages of the folding process.

Furthermore, the cerebellum is characterized by many genetic and functional domains. For instance, genetically distinct populations of Purkinje cells separate the cerebellum in genetic compartments known as parasagittal stripes. Knockout of the transcription factor En1 leads to a change in spatial profiling of these parasagittal stripes (Sillitoe et al., 2008, White et al., 2014). Interestingly, the abnormal folding of the cerebellum due to depletion of CHD7 seems to coincide spatially and temporally with parasagittal Purkinje cell stripes. It will be interesting to

see whether cerebellar compartmentation is altered in CHD7 cKO mice. For example, we may see a switch in certain parasagittal stripes from ML-axis to AP-axis or vice.

Similarly, redistribution of granule neurons due to reorientation of cell division may lead to functional reorganization of the cerebellum. Not only are granule neurons important for fine tuning cerebellar function, but granule cell proliferation and migration are also vital for proper Purkinje cell distribution. Furthermore, relatively small, sub lobular cerebellar regions have been shown to be important for specific cerebellar tasks.

These studies will aid in better understanding how cerebellar defects could underly CHARGE syndrome symptoms such as motor and learning delays. Furthermore, these studies could help us identify downstream players that could be modulated in order to rescue cerebellar folding in CHD7 cKO mice. As many gene programs are shared among cerebellar and cortical development, future studies could also aid in understanding cortical folding.

2.7 Figures

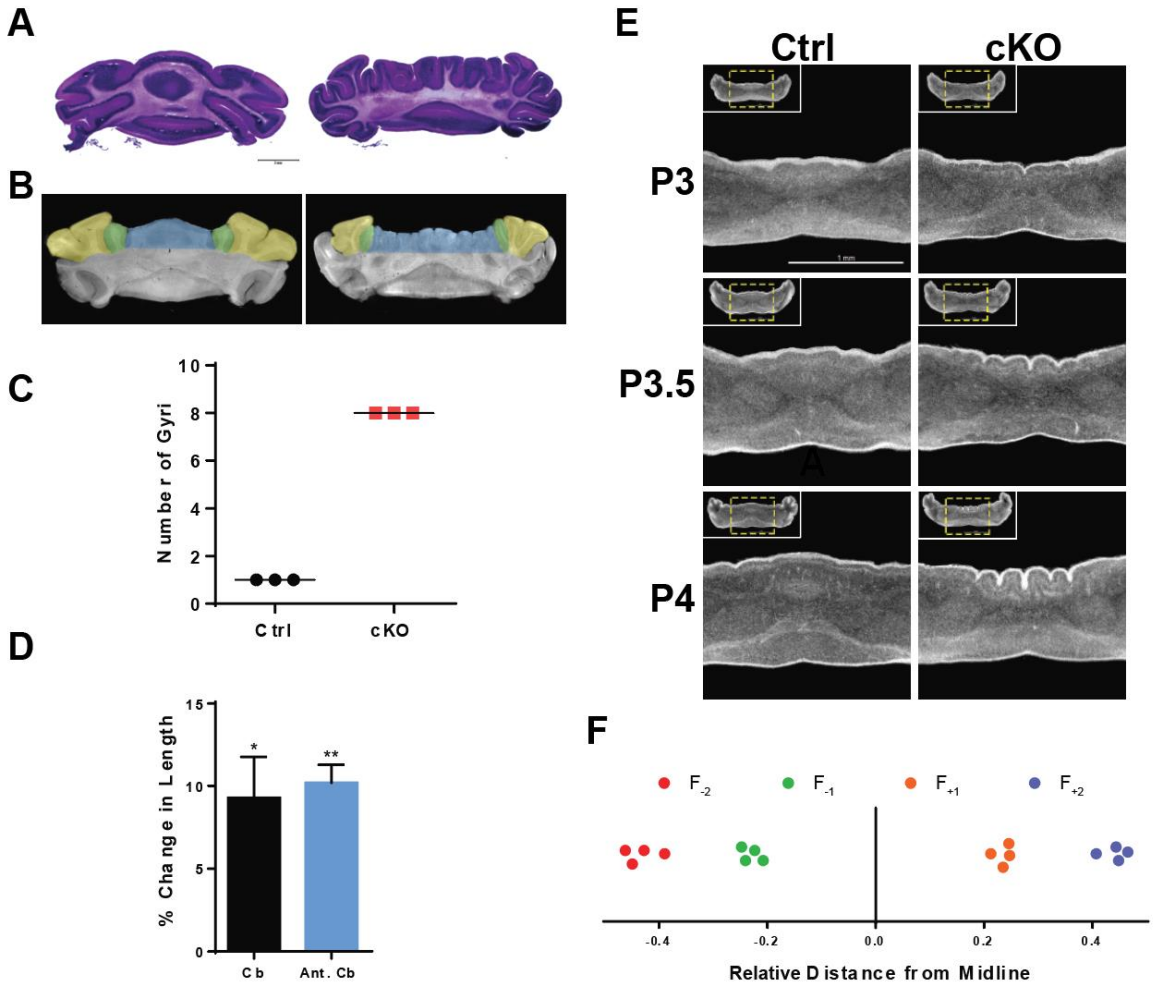

Fig. 2.1 Conditional knockout of CHARGE syndrome protein CHD7 results in stereotyped cerebellar microgyria

A. Hematoxylin and eosin staining of Ctrl (left) and CHD7 cKO (right) p56 sections of mouse cerebellum. Scale bar: 2mm
B. Zeiss Xradia Versa 520 XRM was used to perform a nano computerized tomography (nano CT) scan of Ctrl (left) and cKO (right) p56 mouse cerebella. The cerebellar vermis is highlighted blue and corresponding hemisphere regions highlighted green and yellow.
C. Graph showing number of gyri in the cerebellar vermis of the anterior basal lobe of Ctrl and cKO mice. (n=3 for each condition).

D. Bar graphs showing % change in total cerebellar (Cb) and anterior lobules (Ant. Cb) lengths upon CHD7 cKO (n = 3 for each condition). Length is shown as mean □ s.e.m for each measurement. *p<0.05, **p<0.01.

E. Nano CT scans were taken of P3, P3.5, and P4 mice cerebella. Digital 2D sections were taken through anterior basal lobe lobules. Insets show entire cerebellar section. Yellow dashed squares define region of focus.

F. Dot plot showing relative distance of fissure formation in P4 CHD7 cKO mice (n=4).

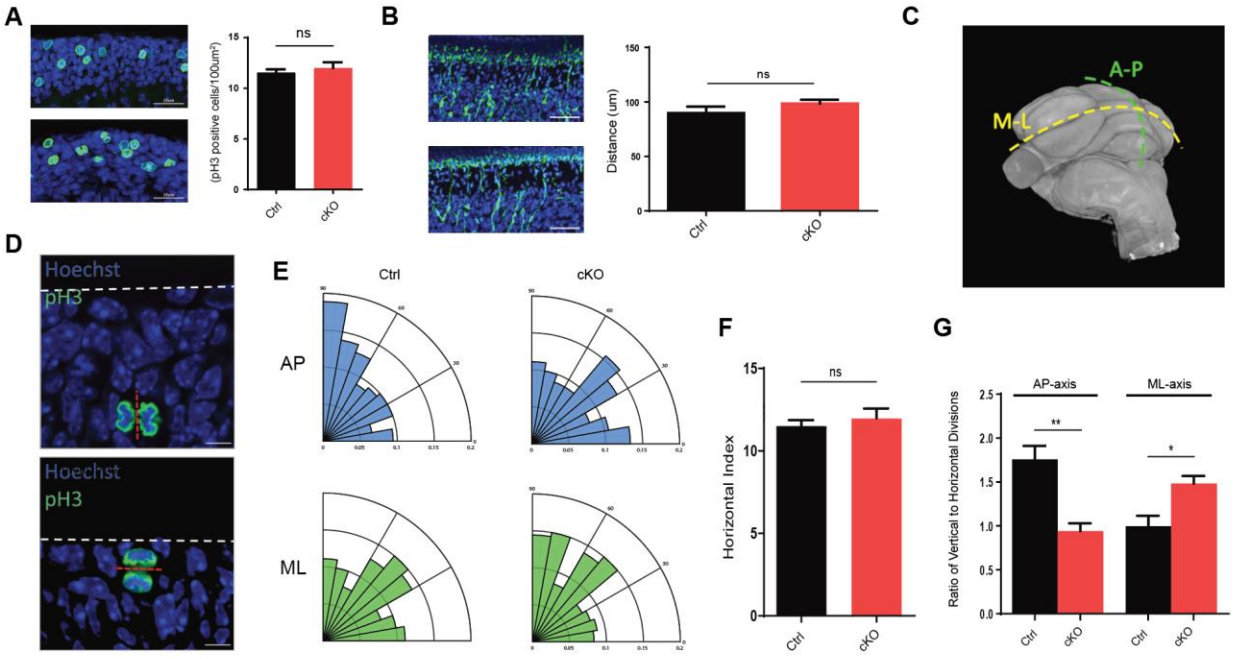

Fig. 2.2 CHD7 regulates preferred axis of granule cell precursor division from the anterior posterior to the mediolateral direction

A. Immunohistochemistry analysis of Ctrl and cKO mice with antibodies recognizing phosphorylated histone H3 (pH3), a marker of dividing cells. A representative image of the external granule layer is shown (left). Bar graphs (right) show mean pH3 positive cells per 100um2 +/- s.e.m. ns = non-significant. Paired t- test. Scale bar: 25um
B. P6 mouse pups were electroporated with the GFP expression plasmid and killed 48 hours later. Cerebella were removed, sectioned, and subjected to immunohistochemistry with antibodies recognizing GFP. Bar graphs show mean distance from EGL +/- s.e.m. ns = non-significant. Paired t- test. Scale bar: 25um
C. Image of P56 cerebellum obtained via nano CT scan (left) showing anterior-posterior axis (A-P) in green and medial-lateral axis (M-L) in yellow.
D. Immunohistochemistry analysis of axis of division of granule cell precursors, identified via pH3 staining in green. Dashed red line indicates the plane of division; dashed white

line indicates the pial surface. Example of a granule cell precursor undergoing a vertical division (top) and horizontal division (bottom) are shown.

E. Rose plot showing the distribution of axis of division angles (angle between pial surface and plane of division) for P3 Ctrl and cKO mice in A-P (top, blue) and M-L (bottom, green) axes. 180 cells were analyzed for each rose plot.

F. Bar graph showing mean number of horizontal division per 100um2 +/- s.e.m. ns = non-significant. Paired t-test.

G. Bar graph showing mean ratio of vertical to horizontal division for Ctrl and cKO mice in both A-P and M-L axes. *$p<0.05$, **$p<0.01$ Paired t-test

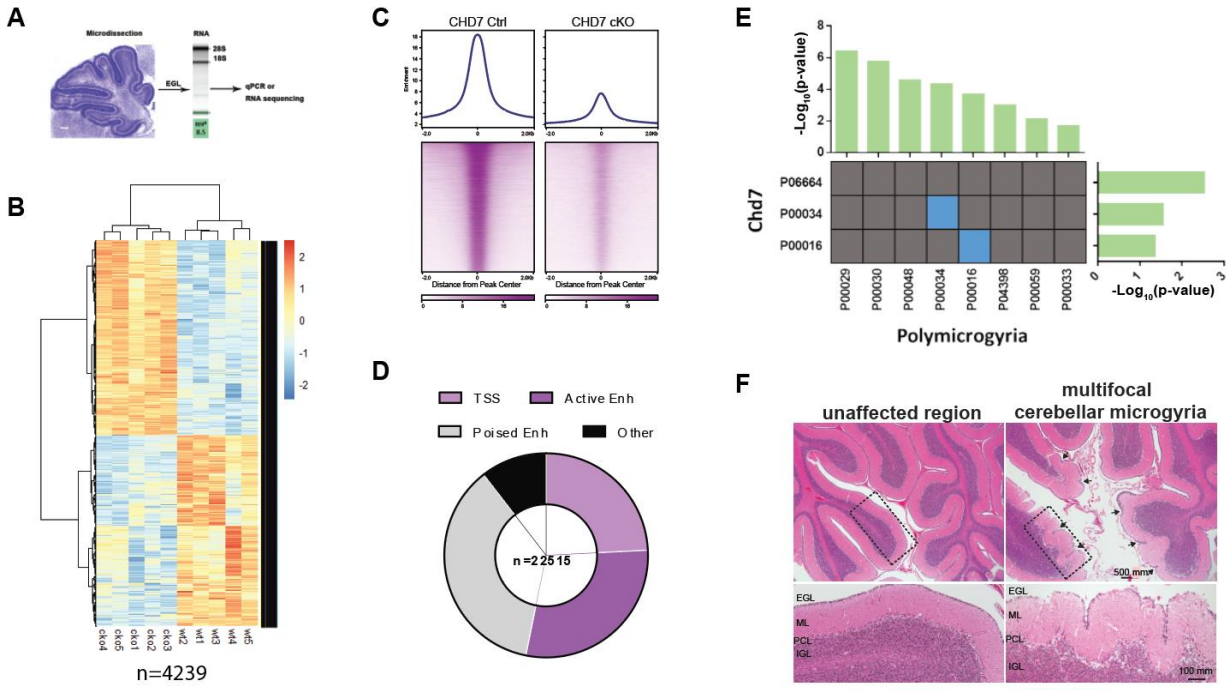

Fig. 2.3 CHD7 regulates gene pathways implicated in polymicrogyria

A. Schematic depicting laser microdissection RNA-seq of cerebellum
B. Hierarchical clustering of gene expression for Ctrl and cKO p4 mouse cerebella for genes detected as significantly dysregulated (False Discovery Rate, FDR < 0.05) in analysis of RNA-seq from Ctrl and cKO cerebella (n=5 biological replicates per genotype). Heat represents z-score of log2 cpm for a given gene.
C. Aggregate plot and heat map of ChIP-seq signal for CHD7 genomic binding sites (n=22,515) in Ctrl and cKO p4 mouse cerebella. Each CHD7 binding site is represented as a single horizontal line centered at the midpoint of each ChIP peak with flanking 2kb.
D. Pie charts displaying regulatory element distribution of CHD7 peaks. TSS, transcription start site; Enh, Enhancer.
E. Panther pathway analysis of CHD7 directly regulated genes and PMG associated genes. Significant pathways are represented as panther terms (left and bottom) while associated significance levels are shown as -log10(p-values) (right and top).

F. Hematoxylin and eosin staining of CHARGE syndrome patient cerebellum showing an unaffected region (left) and a region with multifocal cerebellar microgyria (right) with zoomed in views of insets below. Scale bar: 500mm and 100mm.

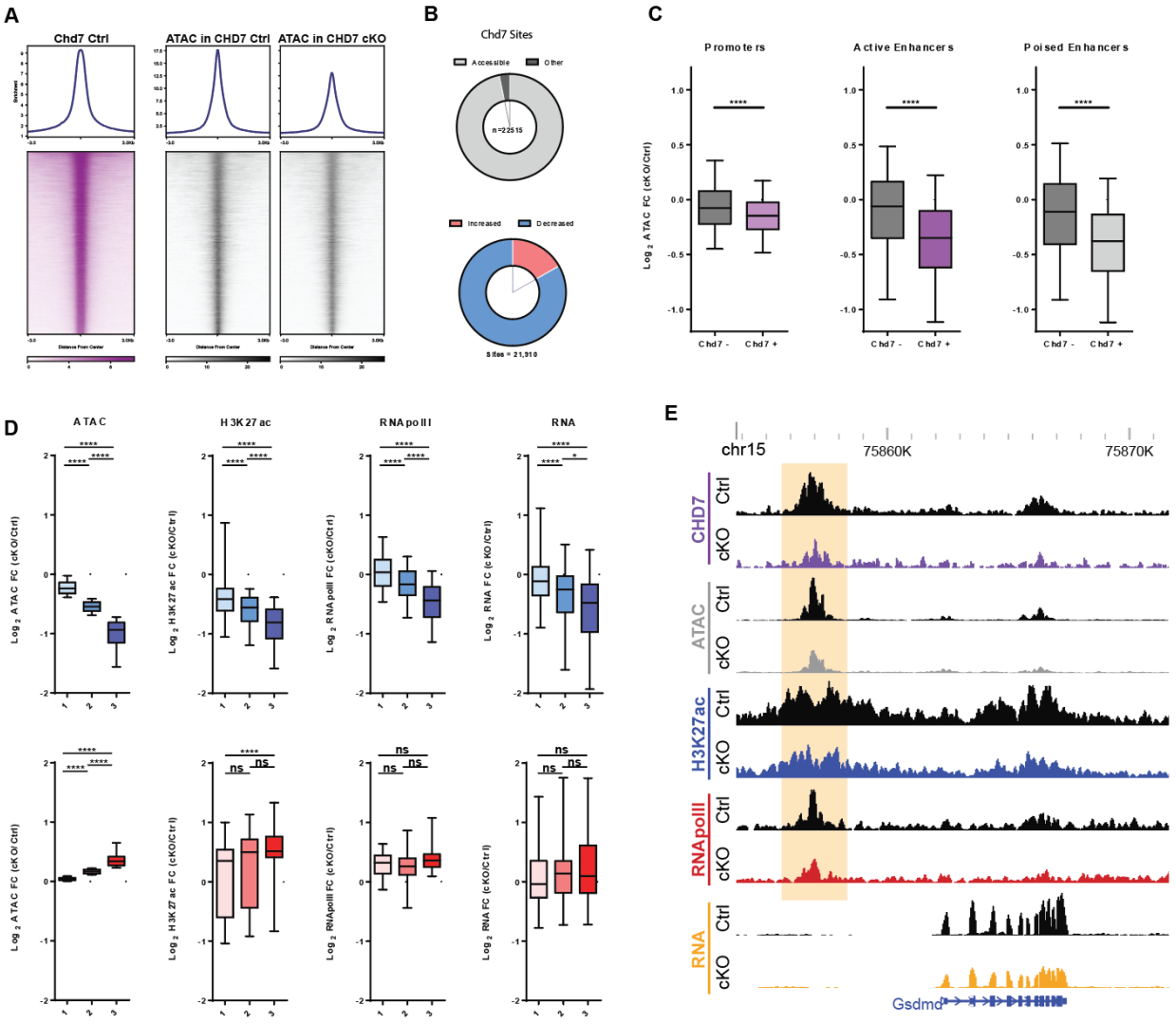

Fig. 2.4 CHD7 activates gene expression via regulation of enhancer activity

A. Aggregate plot and heatmap for ChIP-seq and ATAC-seq signal for CHD7 (n = 22,515) genomic binding sites. ChIP-seq signal for CHD7 (purple) in Ctrl and ATAC-seq signal (grey) in Ctrl and cKO from P4 mouse cerebellum centered on CHD7 binding sites.

B. Pie charts representing proportion of CHD7 sites at significantly called ATAC-seq peaks (top) and portion of CHD7 site that showed decreased or increased accessibility upon CHD7 depletion.

C. Boxplots for CHD7 non-bound and bound sites at TSS (left), active enhancers (middle) and poised enhancers (right). Box-whisker plots show median and distribution of log2-

transformed fold change of ATAC-seq signal conditional knockout mice over respective control mice. ****p < 10−4, two-sided unpaired t-test.

D. Box plots for CHD7 sites displaying significantly decreased (CHD7 activated; top, blue) and increased (CHD7 repressed; bottom, red) ATAC-seq signal upon CHD7 conditional knockout. Increased and decreased sites have been separated into three groups with low (1), medium (2) and high (3) levels of ATAC-seq signal change. Boxplots showing log2-transformed fold change of ATAC, H3K27ac, RNApolII and RNA (from left to right) for each group. ****p < 10−4, *p < 0.05, ANOVA followed by Tukey's multiple comparison test.

E. Box plots for CHD7 sites displaying significantly decreased (top, blue) and increased (bottom, red) ATAC-seq signal upon CHD7 conditional knockout. Increased and decreased sites have been separated into three groups with low (1), medium (2) and high (3) levels of ATAC-seq signal change. Boxplots showing log2-transformed fold change of ATAC, H3K27ac, RNApolII and RNA (from left to right) for each group.

F. WashU Epigenome Browser view of a CHD7 bound enhancer site (highlighted) of a direct target gene, showing CHD7, ATAC, H3K27ac, RNApolII and RNA levels in CHD7 Ctrl and cKO mice.

Chapter 3:

Chromatin accessibility and cellular state specify compensatory activity by paralogous MEF2 transcription factors

This chapter is adapted from a submitted manuscript:

Majidi SP***,** Reddy NC*, Moore MJ, Chen H, Yamada T, Andzelm MM, Cherry TJ, Hu LS, Greenberg ME, Bonni A. 2019. Chromatin accessibility and cellular state specify compensatory activity by paralogous MEF2 transcription factors. *Submitted.*

S.P.M., N.C.R., and A.B. designed the study and wrote the manuscript. S.P.M. performed all experiments. N.C.R. performed bioinformatics analyses. M.J.M. and H.C. assisted with qPCR and immunohistochemistry. T.Y. contributed to biochemical experiments. M.M.A., T.J.C., L.S.H., and M.E.G. provided mice and purified reagents.

3.1 Summary

Compensation among paralogous TFs confers genetic robustness of cellular processes. Despite the prevalence of this phenotypic phenomenon, an *in vivo* genome-scale understanding of how TFs dynamically respond within the chromatin context to paralog depletion is still lacking. We explore this question in the mammalian brain by studying the highly conserved MEF2 family of TFs in granule neurons of mouse cerebellum. We combine genetic manipulation of MEF2 family members with *in vivo* genome-wide analyses to investigate the functional consequences of compensatory activity between MEF2 family members. We uncover significant differences in functional compensation by MEF2 family members across the genome and identify genomic features that distinguish sites experiencing varying levels of compensatory activity. Furthermore, we reveal that cellular state modulates compensatory regulation of gene expression by MEF2 family members.

3.2 Introduction

The development and function of the mammalian brain requires precise control of gene expression (Cholewa-Waclaw et al., 2016, de la Torre-Ubieta and Bonni, 2011, Ziats et al., 2015). Combinatorial interactions of DNA-binding transcription factors (TFs) regulate diverse gene programs that specify neuronal sub-types, develop and refine circuits, and link sensory experience to adaptive responses of the brain (Mazzoni et al., 2013, Molyneaux et al., 2007, Kawashima et al., 2013, Pulimood et al., 2017, Sharma et al., 2019). Additionally, deregulation of TFs contributes to the pathogenesis of neurological diseases (Porter et al., 2018, Ebert and Greenberg, 2013, Li et al., 2018). Although genome-wide patterns of TF cooperation are just beginning to be revealed in the nervous system, how TF family members cooperate to orchestrate gene expression in the mammalian brain remains poorly understood.

The majority of mammalianTFs are members of multigene families that have evolved via duplication events of a single TF (Teichmann and Babu, 2004, Levine and Tjian, 2003). Members of a multigene TF family, known as paralogous TFs, typically have highly conserved DNA-binding domains. Because paralogous TFs often bind virtually identical short DNA sequences, they are thought to participate in cooperative mechanisms distinct from their non-paralogous counterparts (Weirauch et al., 2014, Wei et al., 2010, Luna-Zurita et al., 2016). However, despite the prevalence of paralogous TFs, the nature and importance of the coordinated function of paralogous TFs at a genome-wide level remains unexplored.

Importantly, paralogous TFs are thought to confer genetic robustness to cellular processes through evolutionary retention of functionally redundant activities (Macneil and Walhout, 2011). Despite the prevalence of phenotypic redundancy, the underlying molecular mechanisms by which paralogous TFs regulate this widespread phenomenon are relatively unexplored.

Individual overexpression studies of paralogous TFs in *Saccharomyces Cerevisiae* have revealed similar DNA-binding specificities to exogenous DNA sequences (Fuxman Bass et al., 2015). Recently, individual transfection of Hox proteins followed by chromatin profiling yielded insights into their binding distribution in insect cells (Porcelli et al., 2019). Although similar studies have advanced our understanding of paralogous TF binding, how endogenous TFs dynamically respond within the chromatin context to paralog depletion remains unknown and will require the integrative study of co-expressed paralogous TFs. Regional and single cell analyses of gene expression in the developing and adult brain have revealed diverse expression patterns of paralogous TFs, suggesting that they may act in concert to impart genetic robustness during brain development and function (Lyons et al., 1995, Saunders et al., 2018). However, *in vivo* mechanisms of paralogous TF interplay and their roles in neuronal gene expression and function are as of yet unknown.

The MEF2 (myocyte enhancer factor 2) proteins play fundamental roles in the development and function of the brain, and deregulation of MEF2 activity contributes to the pathogenesis of neurological diseases (Shalizi and Bonni, 2005, Yap and Greenberg, 2018, Lipton et al., 2009). However, the interdependency and functional output of paralogous MEF2 proteins on a genome-wide scale have not yet been explored. The four vertebrate MEF2 family members, MEF2A-D, share a highly conserved MADS domain that mediates DNA binding to the consensus MEF2 response element (MRE) YTAWWWWTAR (Flavell et al., 2008, Potthoff and Olson, 2007). Expression studies show different but overlapping patterns of MEF2A-D expression in the brain (Lyons et al., 1995, Potthoff and Olson, 2007), suggesting that distinct combinations of MEF2 family members coordinate gene expression (Estrella et al., 2015). MEF2 family members play key roles in neuronal survival, differentiation, and maturation (Gaudilliere

et al., 2002, Flavell et al., 2006, Yamada et al., 2013), as well as neural plasticity (Rashid et al., 2014, Chang et al., 2017, Chen et al., 2012, Pulipparacharuvil et al., 2008). Importantly, MEF2 factors are thought to confer phenotypic robustness to these neuronal processes across multiple brain regions. Despite the significant and diverse roles of MEF2 proteins in the nervous system, mechanisms of combinatorial gene regulation by these factors remain to be elucidated.

Here, we reveal an *in vivo* interdependent mechanism of gene regulation mediated by the paralogous TFs MEF2A and MEF2D in granule neurons of mouse cerebellum. Granule neuron-specific single- and double-conditional knockouts of MEF2A and MEF2D demonstrate that cerebellar-dependent motor learning is impaired following depletion of both, but not individual, paralogous TFs. Despite strong co-expression of MEF2A and MEF2D and high amino acid identity of their respective DNA-binding domains, genome wide profiling shows that MEF2D appears to be the predominant genomic regulator of gene expression in granule neurons in the mouse cerebellum. Strikingly, upon MEF2D depletion, the genomic occupancy of MEF2A robustly increases at a distinct subpopulation of formerly bound MEF2D sites, revealing differential compensation by MEF2A on a genome-wide level. Based on the presence or absence of MEF2A compensatory occupancy, we respectively define MEF2 target sites as compensatory or non-compensatory. Epigenome and transcriptome analyses reveal that sites experiencing compensatory MEF2A occupancy undergo functional compensation for genomic activation and gene expression. In contrast, a distinct population of sites without compensatory MEF2A activity undergo significant dysregulation upon loss of MEF2D. The two populations of MEF2 target sites are further stratified by relative chromatin accessibility, with compensatory MEF2A activity concentrated within more open chromatin. Cellular context also plays a key role in specifying MEF2A compensatory activity, as revealed by a dynamic switch from non-compensatory to

compensatory MEF2-dependent gene regulation in the context of motor activity. Collectively, our study defines a novel compensatory transcriptional regulatory scheme for MEF2A and MEF2D that imparts genetic robustness during mammalian brain development and function, providing to our knowledge the first *in vivo* genome-wide characterization of functional interdependency between paralogous TFs.

3.3 Results

MEF2A and MEF2D regulate cerebellar-dependent motor learning in a compensatory manner

Granule neurons of the mouse cerebellum provide a uniquely robust model to study the interplay of MEF2 family members in the mammalian brain. Whereas other neuronal subtypes express solely one MEF2 or variable levels of three or four MEF2 family members, cerebellar granule neurons strongly co-express MEF2A and MEF2D (Lyons et al., 1995). Importantly, granule neurons vastly outnumber all other cells in the cerebellum, making these neurons a suitably homogeneous cell type for *in vivo* studies of the neuronal epigenome (Yamada et al., 2014, Yang et al., 2016, Frank et al., 2015).

In granule neurons of mouse cerebellum, the temporal expression of MEF2A and MEF2D coincides with the expression of the granule neuron-enriched protein GABA(A)a6 receptor (G6R) (Lin and Bulleit, 1996). Therefore, to characterize the roles of MEF2A and MEF2D in granule neurons, we employed a G6R promoter-driven Cre transgenic line to conditionally knockout *Mef2a* (AcKO), *Mef2d* (DcKO), or both *Mef2a* and *Mef2d* (ADcKO) selectively in granule neurons (Fig. 2.1A) (Funfschilling and Reichardt, 2002, Andzelm et al., 2015, Andzelm et al., 2019). The expression of MEF2A and MEF2D proteins concurrently increased in the mouse cerebellum as granule neurons differentiate and mature (Roussel and Hatten, 2011, de la Torre-Ubieta and Bonni, 2011), reaching peak levels at postnatal day 15 (P15) and continuing into adulthood (Fig. 2.1B). MEF2A and MEF2D proteins were downregulated specifically in the internal granule layer of the cerebellar cortex during the third postnatal week in AcKO and DcKO mice, respectively (Fig. 2.1B, C). Importantly, conditional knockout of MEF2A failed to effectively alter the levels of MEF2D RNA or protein, and

conversely conditional knockout of MEF2D failed to effectively alter the levels of MEF2A RNA or protein in the cerebellum (Fig. 2.1B, D).

In immunohistochemical analyses, whereas MEF2D expression was predominantly restricted to granule neurons and Purkinje cells, MEF2A was expressed in granule neurons and other neurons of the molecular and internal granule layers (Figure 2.1C). MEF2B was undetectable, and MEF2C was expressed predominantly in Purkinje cells (Fig. 2.1C, E; (Mellen et al., 2012)). These data show that MEF2A and MEF2D are robustly expressed in granule neurons of the developing mouse cerebellum.

To determine whether MEF2A and MEF2D are required for the proper function of granule neurons, we first subjected AcKO, DcKO, and ADcKO mice to the cerebellar-dependent eyeblink conditioning learning paradigm (Fig. 2.2A) (Heiney et al., 2014, Valnegri et al., 2017). During this associative task, mice learn to blink in response to an initially neutral conditioned stimulus (blue light) after repeated pairing with an eyeblink-eliciting unconditioned stimulus (periocular air puff). As expected, the learned eyelid blink conditioned response (CR) gradually increased each session day in control littermate mice. Strikingly, the rate of CRs was significantly reduced in ADcKO mice by day three of conditioning, which persisted for the remaining session days (Fig. 2.2A). However, neither AcKO nor DcKO mice had significant learning deficits (Fig. 2.2A). In other analyses, general motor coordination assessed by the accelerating rotarod and DigiGait assays (Puram et al., 2011, Hurlock et al., 2009) was not affected upon knockout of MEF2A, MEF2D, or both proteins (Supplemental Fig. 2.2B, C). Taken together, these data reveal that MEF2A and MEF2D are required redundantly in cerebellar-dependent learning, suggesting a potential compensatory mechanism of MEF2A and MEF2D in granule neurons.

Because MEF2 family members regulate neuronal survival and synapse formation and refinement in diverse brain regions (Shalizi et al., 2006, Flavell et al., 2006, Gaudilliere et al., 2002), we next characterized the effect of combined knockout of MEF2A and MEF2D on these fundamental developmental events. The architecture of the cerebellar cortex was not altered in ADcKO mice, nor was there a detectable change in neuronal survival (Fig. 2.3A). In electron microscopy analyses, the density of granule neuron parallel fiber boutons synapses onto Purkinje neuron dendritic spines was not significantly altered in ADcKO mice (Supplemental Fig. 2.3B). Evaluation of granule neuron dendrites upon *in vivo* electroporation of granule neurons in ADcKO mice revealed no differences in dendrite length (Fig. 2.3C).

MEF2A and MEF2D exhibit complex patterns of gene regulation in the cerebellum

Because of the redundant contribution of MEF2A and MEF2D to cerebellar dependent motor learning, we reasoned that the two paralogous TFs may exert compensatory mechanisms of gene regulation. To test this possibility, we first characterized the relative effects of individual and combined conditional knockouts of MEF2A and MEF2D on gene expression in granule neurons *in vivo*. We, therefore, performed RNA-sequencing (RNA-seq) in the cerebellum from P22 mice in four biological replicates each of AcKO, DcKO, ADcKO, and respective sex-matched control littermates.

We next characterized how genetic depletion of MEF2A or MEF2D individually contributes to gene dysregulation in the combined MEF2A and MEF2D knockout. Differential mRNA expression analysis of ADcKO and control littermates led to identification of 130 “MEF2-repressed genes” that were significantly upregulated and 175 “MEF2-activated” genes that were significantly downregulated in the ADcKO mouse cerebellum. Principal component

analysis of MEF2-regulated genes showed smaller variation between control littermates for each condition, with the majority caused by differences between the three conditional knockout conditions (Fig. 2.4A). The MEF2-regulated genes were then organized into distinct clusters based on their expression in AcKO, DcKO, ADcKO, and respective control littermates by subjecting them to hierarchical clustering using the dynamic tree cut algorithm (Fig. 2.4B). This analysis yielded two major clusters each for MEF2-repressed (C1, C2) and activated genes (C3, C4), which respectively represent ~14.8, 27.9, 20.7, and 36.7% of MEF2-regulated genes. Quantitative assessment of the relative behavior of single- and double-conditional knockouts on gene expression in each cluster revealed stronger effects in DcKO and ADcKO mice relative to AcKO and control mice (Fig. 2.4B).

Two major patterns emerged upon closer examination of clusters of significantly altered genes between DcKO and ADcKO mice. First, the C1 and C3 clusters of differentially regulated genes in the mouse cerebellum displayed no significant differences between DcKO and ADcKO mice, suggesting that these groups of genes are primarily affected by depletion of MEF2D in granule neurons of the mouse cerebellum. In contrast, the C2 and C4 clusters showed significantly stronger dysregulation in ADcKO relative to DcKO mice (Fig. 2.4C, D), suggesting compensatory regulation of C2 and C4 cluster genes by MEF2A and MEF2D in granule neurons.

MEF2A displays functionally compensatory binding activity at a distinct subset of MEF2D-bound genomic sites

The gene expression patterns in single- and double-conditional knockout mice suggested shared as well as distinct roles for MEF2A and MEF2D. To better understand the underlying basis of the relationships between these two paralogous TFs, we performed ChIP-seq of MEF2A

and MEF2D in the cerebellum in control, AcKO, and DcKO mice. Among these three conditions, we identified 203 MEF2A-binding sites and 1388 MEF2D-binding sites (Fig. 2.5A). Due to the strong conservation between paralogous TFs, we validated the specificity of MEF2A and MEF2D ChIP-seq signal in the cerebellum of AcKO and DcKO mice, respectively. *De novo* motif discovery demonstrated the canonical MEF2 response element (MRE), YTAWWWTAR, as the most significantly enriched motif at >95% of peaks (Fig. 2.5B), further strengthening the conclusion that the identified MEF2A and MEF2D ChIP-seq sites represent high confidence MEF2-binding sites. Analyses of promoters and enhancers, identified based on histone modifications in ChIP-seq of the mouse cerebellum in P22 mice (Fig. 2.5A, C; (Yamada et al., 2014)), revealed that MEF2A and MEF2D bound active intergenic enhancers at a frequency higher than the normal genomic distribution. However, MEF2A proportionally bound promoters to a greater extent when compared to MEF2D (Fig. 2.5C).

Strikingly, the vast majority of MEF2A peaks exclusively appeared in DcKO mice, in which 199 sites were statistically enriched above background (Fig. 2.5A). The dynamic upregulation of MEF2A binding activity upon depletion of MEF2D was highly consistent, appearing in each of the four biological ChIP-seq replicates (Fig. 2.5A, D). In contrast, MEF2D was stably present at the majority of MEF2-bound sites in the control condition, with its occupancy mostly unaffected by conditional knockout of MEF2A. These data suggest MEF2D may play the predominant role in regulating gene expression in granule neurons.

Because MEF2A and MEF2D both bind to the canonical MRE, we next determined the extent of overlap between DcKO-induced MEF2A peaks and sites normally occupied by MEF2D. Intersectional peak analysis revealed that conditional knockout of MEF2D induced a robust increase of MEF2A mainly at sites previously bound by MEF2D (Fig. 2.6A). Specifically,

80% of MEF2A peaks that appeared in DcKO mice were occupied by MEF2D in control littermate mice. Heretofore, we refer to sites at which MEF2A increased in DcKO mice as compensatory (Fig. 2.6A), whereas the subset of MEF2D sites that did not experience MEF2A binding statistically enriched above background are termed non-compensatory (Fig. 2.6B). As an example of a compensatory MEF2 binding site, the *Inpp4b* intragenic enhancer showed binding to MEF2D in control mice, whereas MEF2A occupancy was statistically undetectable (Fig. 2.6F). However, the absence of MEF2D in DcKO mice led to significantly increased MEF2A occupancy at the *Inpp4b* intragenic enhancer. In contrast, an example of a non-compensatory binding site is a normally MEF2D-bound proximal enhancer for *Gng7*, at which no MEF2A occupancy was observed in DcKO mice (Fig. 2.6G).

The finding that MEF2A displays compensatory binding at a subset of MEF2D sites raises the question of whether the strength of MEF2D occupancy at a given site dictates the extent of MEF2A compensatory binding. We found no correlation between MEF2A and MEF2D signal intensity at compensatory sites, suggesting that the strength of MEF2D occupancy is not predictive of the degree to which MEF2A binds a given site (Fig. 2.6C).

To determine whether regulation of compensatory sites depends on MEF2A and MEF2D, we analyzed the levels of histone H3 lysine 27 acetylation (H3K27ac) at these sites upon single- or double-conditional knockout of the two TFs (Fig. 2.6D, E). As expected, because compensatory sites were predominantly bound to MEF2D in control mice, conditional knockout of MEF2A minimally affected H3K27ac levels at these sites (Fig. 2.6D). Conditional knockout of MEF2D also failed to significantly alter H3K27ac levels at these sites (Fig. 2.6D, F). By contrast, H3K27ac levels were significantly reduced at compensatory sites upon conditional knockout of both MEF2A and MEF2D (Fig. 2.6D, F), suggesting that either MEF2A or MEF2D

is sufficient for activation of these regulatory sites. Just as for compensatory sites, conditional knockout of MEF2A had minimal effects on H3K27ac levels at non-compensatory sites. In contrast, however, conditional knockout of MEF2D significantly reduced H3K27ac levels at non-compensatory sites (Fig. 2.6E, G), suggesting that MEF2D is selectively required for activation of non-compensatory sites. Taken together, our data suggest that the dynamically increased occupancy of MEF2A at compensatory sites may confer on these targets a uniquely robust ability to maintain normal activation in the presence of a single MEF2 factor.

Compensatory binding by MEF2A at a subset of MEF2-activated target genes confers genetic robustness to MEF2D depletion

To understand how MEF2A and MEF2D occupancy regulates gene expression, we first identified MEF2 target genes by performing an intersectional analysis of all MEF2 ChIP-seq and MEF2 activated/repressed genes. These analyses revealed that MEF2A and MEF2D bound in the vicinity of 49.1% of MEF2-activated genes. In contrast, only 9.2% of MEF2-repressed genes were associated with MEF2-binding sites (Fig. 2.7A). Next, we analyzed patterns of MEF2 occupancy for each of the RNA-seq clusters, C1-C4. Remarkably, the two MEF2-activated clusters, C3 and C4, exhibited distinct patterns of MEF2A and MEF2D target gene occupancy. The C3 cluster was solely enriched for MEF2D-occupied non-compensatory sites, consistent with the finding that these MEF2D-bound genes are primarily dysregulated upon depletion of MEF2D (Fig. 2.7B). In contrast, C4 was the only cluster of genes with significant enrichment of compensatory MEF2A and MEF2D occupancy (Fig. 2.7B). In other analyses, H3K27ac levels at compensatory direct target gene regulatory elements were most significantly reduced in ADcKO mice (Fig. 2.7C). At non-compensatory direct target genes, DcKO and ADcKO mice showed

similarly reduced levels of H3K27ac (Fig 2.7C), suggesting relatively stronger sensitivity to genetic perturbation of MEF2D. As an example of a compensatory MEF2 binding site, the stimulus-responsive gene *Tll1* also exhibited compensatory MEF2A occupancy at an intragenic enhancer, at which H3K27ac levels were reduced most strongly in ADcKO mice. RNA-seq coverage at *Tll1* showed substantial reduction in ADcKO mice (Fig. 2.7D). In contrast, loss of MEF2D at the intragenic enhancer of the *Blc9l* gene did not lead to compensatory MEF2A binding, which was associated with significant reduction of H3K27ac levels at this regulatory element and reduced gene expression in both DcKO and ADcKO mice (Fig. 2.7E). In summary, compensatory binding by MEF2A at a subset of MEF2-activated target genes diminishes the influence of MEF2D depletion on gene expression and associated regulatory element activation.

Chromatin accessibility and cellular state specify compensatory action of MEF2A

To investigate the basis for distinct MEF2A compensatory activities, we next compared genomic features at compensatory and non-compensatory MEF2-regulated sites. Because the MEF2 response element (MRE) directly binds both MEF2A and MEF2D, we first characterized whether MREs at compensatory versus non-compensatory sites exhibit different levels of degeneracy. These analyses revealed no significant difference in the distribution of MRE degeneracy scores between compensatory and non-compensatory sites (Fig. 2.8A), suggesting factors beyond the MRE sequence direct compensatory action of MEF2A.

In addition to binding site affinity, the chromatin environment plays a critical role in regulating permissibility of TF binding (Spitz and Furlong, 2012). To assess the relationship of chromatin accessibility and compensatory MEF2A activity, we compared DNaseI-sequencing levels between compensatory and non-compensatory sites in P22 mouse cerebellum (Yamada et

al., 2019). We found that compensatory sites displayed significantly higher chromatin accessibility than non-compensatory sites, as measured by DNaseI-sequencing read density (Fig. 2.8B). Further examination revealed that chromatin accessibility showed a graded relationship to compensatory occupancy by MEF2A. Sites of highest compensatory occupancy by MEF2A were concentrated in more accessible chromatin, whereas sites in relatively less accessible chromatin were selective for MEF2D (Fig. 2.8C, D). These data indicate that chromatin accessibility rather than MRE affinity may restrict target selection by MEF2A to a distinct subset of formerly bound MEF2D sites in conditional MEF2D knockout mice.

Because combinatorial TF occupancy serves as an energetically favorable mechanism to outcompete nucleosomes for a genomic binding site (Lambert et al., 2018; Grossman et al., 2017), we next characterized the presence of other TF binding sites that may distinguish compensatory and non-compensatory sites. Compensatory MEF2 sites in the cerebellum showed differential motif enrichment for AP-1 complex components compared to non-compensatory MEF2 sites (Fig. 2.8E, F). The AP-1 motif is the binding site for the early response proteins FOS and JUN (Eferl and Wagner, 2003, Sheng and Greenberg, 1990). Our interrogation of ChIP-seq datasets of MEF2A and MEF2C binding in cortical neurons (Telese et al., 2015) revealed that sites co-regulated by MEF2A and MEF2C were also significantly enriched for the AP-1 motif when compared to sites solely regulated by MEF2C (Fig. 2.8E, F). In accordance with higher accessibility at compensatory compared to non-compensatory sites, AP-1 is thought to increase chromatin accessibility at enhancers via recruitment of the BAF complex (Vierbuchen et al., 2017).

Neuronal stimuli significantly modify the chromatin landscape by increasing accessibility at stimulus-responsive enhancers (Su et al., 2017). Importantly, MEF2 TFs play key roles in

neuronal stimulus-dependent gene expression (Assali et al., 2019, Flavell et al., 2008, Lyons et al., 2012). Furthermore, MEF2A and MEF2D display functional redundancy for cerebellar-dependent motor learning (Fig. 2.2A), a process that likely requires stimulus-dependent gene expression to link sensory experiences to adaptive responses of the brain (Yamada et al., 2019). We asked whether neuronal state might influence the compensatory action of MEF2A (Assali et al., 2019, Malik et al., 2014, Ataman et al., 2016, Flavell et al., 2008). Analysis of MEF2A and MEF2D ChIP-seq peaks at stimulus-responsive genes revealed strongly increased MEF2A occupancy at MEF2D-bound sites upon depletion of MEF2D (Fig. 2.9A). Although expression of stimulus responsive genes is often relatively low in the mouse cerebellum, exposure of mice to forced locomotion in an accelerating rotarod paradigm triggers significant upregulation of canonical immediate early genes and other stimulus-responsive genes in the cerebellum (Fig. 2.9B; (Yang et al., 2016)). Thus, we performed the accelerating rotarod paradigm followed by qRT-PCR in ADcKO mice on several of the 113 MEF2-bound rotarod-activated genes, including the canonical immediate early genes *Fosb*, *Nr4a2*, and *Nr4a3*. The expression of MEF2-bound rotarod-activated genes was significantly reduced in the cerebellum in ADcKO mice (Fig. 2.9C), suggesting a role for MEF2 TFs in rotarod-activated gene expression.

We next employed an unbiased characterization of MEF2A and MEF2D-dependent changes in rotarod-activated gene expression by performing the rotarod paradigm followed by RNA-seq in the cerebellum of AcKO, DcKO, or ADcKO mice and their respective control littermates. Under baseline conditions, MEF2-bound rotarod-activated genes manifested similar dysregulation in both DcKO and ADcKO mice (Fig. 2.9D), suggesting that the MEF2-target genes were regulated in a non-compensatory manner. In contrast, following rotarod stimulation, MEF2-bound rotarod-activated genes were robustly dysregulated in ADcKO mice compared to

single-cKO mice (Fig. 2.9D), revealing that rotarod activity induced a switch to compensatory MEF2-dependent regulation. As expected, control rotarod-activated genes with no MEF2 binding were minimally altered in the cerebellum in AcKO, DcKO, or ADcKO mice (Fig. 2.9D). Together, these results reveal that motor activity-induced changes in neuronal state induce a dynamic switch from non-compensatory to compensatory MEF2-dependent gene regulation, demonstrating the context-dependent nature of paralogous TF interdependency.

3.4 Discussion

In this study, using the combination of genetic manipulation and genome-wide profiling, we unveil an interdependent mechanism of gene regulation mediated by the paralogous TFs MEF2A and MEF2D in granule neurons of mouse cerebellum *in vivo*. We find that MEF2D is the predominant genomic regulator of gene expression in granule neurons during brain development. Strikingly, upon depletion of MEF2D, the occupancy of MEF2A is robustly increased at a subset of sites normally bound to MEF2D, revealing differing levels of compensation by MEF2A on a genome-wide level. Based on the presence or absence of MEF2A occupancy upon MEF2D deletion, we define MEF2 target sites as compensatory or non-compensatory. Epigenome and transcriptome analyses reveal highly dissimilar responses to MEF2D depletion between compensatory and non-compensatory sites. The two populations of MEF2 target sites are further stratified by relative chromatin accessibility, with compensatory MEF2A activity concentrated within more open chromatin. In addition, motor activity induces a dynamic switch from non-compensatory to compensatory MEF2-dependent gene regulation, revealing that cellular context also plays a key role in specifying MEF2A compensatory activity. Accordingly, MEF2A and MEF2D exhibit functional redundancy for cerebellar-dependent motor learning. Collectively, our study defines a compensatory transcriptional regulatory scheme for paralogous MEF2 TFs that imparts robustness to genetic perturbation during mammalian brain development and function, providing to our knowledge the first *in vivo* genome-wide characterization of functional interdependency between TF family members.

Redundancy is an inherently dynamic process that involves substitution of one paralog upon loss of the other (Macneil and Walhout, 2011). However, prior to our study, how paralogs respond to the absence of a family member at a genome-wide level remained unknown. Our

study unveils robust compensatory binding activity of MEF2A at sites normally bound to the predominant genomic occupant, MEF2D. This finding suggests competitive binding may operate among MEF2 family members, which may be a widespread phenomenon extending to some of the >20 other TF families comprised of paralogs with highly similar DNA binding domains (Messina et al., 2004).

In view of the high amino acid identity in the DNA-binding domains of TF paralogs, what features may allow MEF2D to dominate occupancy at sites co-regulated by both MEF2D and MEF2A? Paralogs may exhibit differential DNA-binding specificities (Shen et al., 2018). Although the DNA-binding domains of MEF2A and MEF2D share >95% amino acid identity, the few non-consensus amino acids may contribute to differential binding (Potthoff and Olson, 2007). Sampling frequency and target site occupancy is also sensitive to the local concentrations of available TFs, as recently demonstrated for the cooperative TFs Sox2 and Oct4 in embryonic stem cells (Chen et al., 2014). Although MEF2 proteins are expressed at variable concentrations in neuronal cell types, these differences probably do not apply to granule neurons, which fortuitously co-express high levels of both MEF2A and MEF2D (Lyons et al., 1995). The disparity between MEF2A and MEF2D occupancies may arise from their highly divergent transactivation domains. Crystal structure of a MEF2A homodimer demonstrates that the highly divergent region beyond the DNA-binding domain may interact with the genome, possibly conferring distinct binding activities to different MEF2 family members (Wu et al., 2010). Beyond its potential interaction with DNA, the transactivation domain of each MEF2 family member may undergo unique post-translational modifications or bind distinct co-factors that stabilize binding of one paralog over the other (Shalizi et al., 2006, Shalizi and Bonni, 2005).

Importantly, true redundancy is defined as little or no change in output following perturbation of one factor because another one masks the effect (Macneil and Walhout, 2011, Conant and Wagner, 2004). Surprisingly, however, the molecular consequences of paralog occupancy have not yet been adequately explored. Integration of unbiased epigenome and transcriptome analyses in our study reveals that increased MEF2A occupancy upon loss of MEF2D is functionally compensatory. These findings provide a tangible explanation for a common observation in which TF binding sites detected by ChIP appear to be nonfunctional due to the unchanged mRNA levels of target genes following depletion of the assayed TF (Li et al., 2008, Cao et al., 2010, Andzelm et al., 2015).

Although we have discovered the compensatory genomic features of MEF2A and MEF2D, we also find a large number of non-compensatory MEF2D-bound sites. Following gene duplication, TF paralogs are thought to maintain a degree of ancestral function, while also gaining new specificities termed "neo-functionalization" (Badis et al., 2009, Macneil and Walhout, 2011). The identification of both compensatory and non-compensatory MEF2 sites supports the occurrence of these dual evolutionary processes for MEF2A and MEF2D. Global analyses of paralog evolution suggest that non-compensatory sites arising from neo-functionalization of MEF2D may have emerged via evolution of co-factor interactions. TF paralogs arising from local duplication events undergo rapid divergence of protein-protein interactions, with older paralogs acquiring relatively more protein interactions (Guan et al., 2007, Reece-Hoyes et al., 2013, Grove et al., 2009). As phylogenetic analysis indicates that MEF2D arose from an earlier local duplication event, it may have developed more co-factor interactions than MEF2A, thereby acquiring non-compensatory binding sites in granule neurons (Wu et al., 2011).

The chromatin environment plays a critical role in regulating permissibility of TF binding (Spitz and Furlong, 2012). Concentration of MEF2A compensatory activity within more open chromatin suggests that chromatin accessibility may play a key role in directing the compensatory activity of paralogous TFs. Therefore, compensatory activity by MEF2A may be influenced by competition with nucleosomes at formerly bound MEF2D sites. Neuronal activity dynamically increases accessibility at enhancers of stimulus-responsive genes (Su et al., 2017). State-dependent alterations in the chromatin environment may explain how motor activity increases MEF2A compensatory activity at formerly non-compensatory sites. Combinatorial TF occupancy serves as an energetically favorable mechanism to outcompete nucleosomes for a genomic binding site (Lambert et al., 2018; Grossman et al., 2017). We show compensatory sites are differentially enriched for AP-1 motifs. Recent evidence reveals the importance of AP-1 for increasing chromatin accessibility via recruitment of the BAF complex (Vierbuchen et al., 2017). Upon depletion of MEF2D, AP-1 may be sufficient to maintain adequate chromatin accessibility for incoming MEF2A. Collectively, these data suggest a model whereby collaborative TFs increase chromatin accessibility via recruitment of chromatin remodelers, thus allowing for compensatory regulation by multiple MEF2 family members.

Redundant mechanisms are thought to mediate robustness for genes that are essential, such as ETS family co-occupancy at housekeeping genes and HOX factors at developmental patterning genes (Macneil and Walhout, 2011, Hollenhorst et al., 2007, Slattery et al., 2011). Because stimulus-responsive genes experience compensatory redundancy by MEF2A and MEF2D, this gene program may represent a shared feature of the MEF2 family. Interestingly, stimulus responsive genes are common targets of MEF2 family members in multiple cell types including cardiac myocytes, T-cells, fibroblasts and neurons (Andzelm et al., 2015, Black and

Olson, 1998). Furthermore, as stimulus-dependent gene expression links sensory experience to adaptive responses of the brain (West and Greenberg, 2011, Alberini and Kandel, 2014, Zovkic et al., 2014), the identification of compensatory regulation of motor activity-induced gene expression may explain the redundancy of MEF2A and MEF2D in cerebellar-dependent learning.

Non-compensatory MEF2D sites may represent more specialized gene targets in granule neurons. Consistently, in photoreceptors, MEF2D is recruited away from stimulus responsive genes to retinal-specific genes via cooperativity with CRX, a photoreceptor-specific TF (Andzelm et al., 2015). Thus, it will be interesting to determine whether MEF2D plays a more specialized biological role in granule neurons.

Although we have focused on compensatory functions for MEF2A and MEF2D as well as MEF2D-predominant roles in the regulation of transcriptional activation, MEF2 proteins also play critical roles in transcriptional repression as revealed by studies of sumoylated MEF2 (Gregoire and Yang, 2005, Shalizi et al., 2006, Yamada et al., 2013, Shalizi et al., 2007). In addition, *in vivo* knockdown and structure-function studies in rat pups during the first two postnatal weeks suggest that sumoylated MEF2A drives the formation of postsynaptic dendritic claw differentiation and the maturation of presynaptic sites in the rat cerebellum (Shalizi et al., 2006, Yamada et al., 2013). The absence of major changes in transcriptomic analyses of the cerebellum in P22 AcKO mice raises the question of whether sumoylated MEF2A operates at a distinct developmental temporal window to repress transcription and trigger consequent developmental effects.

Due to the diverse states a neuron undergoes during development and plasticity, the context-dependent nature of compensation by TF family members should advance our

understanding of brain development and function. As we learn more about the interdependency of paralogous TFs, we should gain further insight into how paralogs respond to TF loss-of-function mutations in the context of disease (Ebert and Greenberg, 2013, Sudhof, 2017, Li et al., 2018). Furthermore, identifying the genomic signatures of non-compensatory sites may allow us to predict regulatory elements that might be more susceptible to gene dysregulation upon perturbation of different TF paralogs in disease states.

3.5 Conclusions

In this study, we define an *in vivo* compensatory transcriptional regulatory scheme for the paralogous TFs MEF2A and MEF2D that imparts robustness to genetic perturbation during mammalian brain development and function. Prior to our study, how paralogous TFs respond to the absence of a family member at a genome-wide level had not been explored. We present the first *in vivo* genome-wide assessment of functional interdependency between TF paralogs. Here, we discover distinct populations of MEF2 target sites that experience highly disparate levels of compensatory activity by MEF2A upon depletion of the predominant genomic regulator, MEF2D. Our analyses reveal a graded relationship between chromatin accessibility and compensatory occupancy by MEF2A. Sites of highest compensatory MEF2A occupancy are concentrated in more accessible chromatin, whereas sites selective for MEF2D are in relatively less accessible chromatin. This suggests that the chromatin accessibility landscape specifies the extent of compensation performed by paralogous TFs. Finally, we reveal a significant influence of neuronal state on compensatory activity at MEF2 target genes, thus providing a molecular basis for the functionally redundant regulation of cerebellar-dependent motor learning by MEF2 TFs. In summary, our study provides a genome-scale perspective on compensatory activity mediated by paralogous TFs, which are stratified by chromatin accessibility and dynamically altered by cellular state. We suggest that insights gained by this assessment will be relevant to some of the >20 other TF families comprised of paralogs with highly similar DNA binding domains.

3.6 Future Directions

MEF2A and MEF2D share high amino acid identity in their DNA-binding domains. Therefore it is unexpected that one factor can be the predominant genomic occupant, MEF2D in granule neurons and MEF2A in C2C12 (Estrella et al., 2015). As TF family member dominance in gene regulation is seen in different cells, it is important to understand which cellular and genetic features determine this dominance. One feature that could determine which factor is the dominant regulator of gene expression is the level of TF expression. Here we show that both MEF2A and MEF2D are highly expressed but a more quantitative assessment is needed. To best understand the importance of the level of TF expression, we would start by overexpressing both factors in varying ratios. We would then perform ChIP-seq experiments of MEF2A and MEF2D and analyze the changes in genomic occupancy of these factors.

Another feature that could determine TF family member dominance is DNA sequence. Paralogs have highly conserved DNA binding domains; however, subtly differences in sequence specificity have been shown to favor binding of one family member over another (Shen et al., 2018). However, these studies do not consider co-expression of multiple factors in the same cells. The co-expression of MEF2A and MEFD in granule neurons offers an opportunity to assess for subtle differences in DNA-binding specificity between highly related proteins. In order to pursue this question, we could use CRISPR technologies to change specific amino acids withing the MEF2A and MEF2D DNA-binding domains and assess how these changes alter the genomic occupancy of these factors.

Similarly, differences in other protein domains could also confer specificity of genomic occupancy. For example, MEF2A and MEF2D binding could be regulated through their highly divergent transactivation domains. These domains may undergo unique post-translational

modifications or bind co-factors that stabilize binding of one paralog over the other (Shalizi and Bonni, 2005). To clarify the role of the transactivation domain in genomic occupancy, we could swap the entire transactivation domain of one factor for the other and then assess genomic occupancy. Furthermore, we could identify distinct interacting co-factors of MEF2A and MEF2D by conducting comparative mass spectrometry analysis. This could be done in the presence and absence of each factor. If unique factors were found to interact with MEF2 family members, we could profile the genomic occupancy of those factors and assess the proximity of co-factor binding to MEF2 TFs binding.

Additionally, further investigating interaction between and among MEF2A and MEF2D molecules would provide a better understanding of how these factors control gene expression. A recent study showed that non-paralogous factors Nkx2.5 and Tbx5 form heterotypic interactions that mediate co-binding of these factors to their respective motifs or a composite motif at the same cis-regulatory elements (Luna-Zurita et al., 2016). However, knockout of either factor results in redistribution of the remaining partner to ectopic binding sites that also contain its consensus motif. This scenario is likely irrelevant for paralogous TFs, as they recognize the same consensus motif; however, homotypic hetero- and homo-dimerization may still provide additional specification to MEF2 TF function. Therefore, it will be interesting to study the homo- and hetero-dimerization of MEF2 paralog. This can be done initially by conducting ChIP-re-ChIP experiments to identify genomic regions that are occupied MEF2 homodimers, heterodimers or both. Additionally, mouse models with tagged MEF2A and MEF2D proteins could allow us to more accurately assess hetero and homo dimer binding by eliminating issues of antibody specificity and efficiency.

3.7 Materials and Methods

Mice

Mice were maintained in a pathogen-free environment. All procedures involving animals were performed according to protocols approved by the Animal Studies Committee of Washington University School of Medicine and in accordance with both the National Institute of Health Standings Committee on Animals as well as the National Institutes of Health guidelines. MEF2A fl/fl, MEF2D fl/fl and GABAa(6)R-Cre have been described (Andzelm et al 2019; Andzelm et al 2015; Funfschilling and Reichardt, 2002). For all experiments, control mice are sex-matched double floxed littermate mice without the G6R-Cre transgene.

Antibodies

Antibodies to Calbindin (Abcam ab1778), Mef2a (Santa Cruz sc-313x), Mef2c (Protein-Tech 18290-1-AP), 14-3-3 (Santa Cruz sc1675), Cre (Millipore 69050-3), histone H3K27ac (Abcam ab4729), cleaved caspase 3 (Cell Signaling, 9661S), GFP (Abcam ab13970) were purchased. Antibodies to Mef2a and Mef2d have been described (Flavell et al., 2008, Andzelm et al., 2015).

Immunohistochemistry

The cerebellum from mice was fixed with 4% PFA and 4% sucrose and subjected to cryo-sectioning on the Leica CM3050S Cryostat. Sections were blocked with blocking buffer (10% goat serum, 3% BSA, and 0.4% Triton X in PBS). Subsequently, sections were incubated overnight with relevant primary antibodies followed by a two-hour incubation with Alexa Fluor conjugated secondary antibodies. Confocal images were acquired with a Zeiss LSM 880 II Airyscan FAST Confocal Microscope or an Olympus FV1200 Confocal Microscope.

Delay eye-blink conditioning

Delay eye-blink conditioning assay was adapted from the procedure used by Heiney et al., 2014. Sex-matched littermate conditional MEF2A, MEF2D, MEF2A/D cKO or control mice at five to eight weeks of age were used. Surgical procedures were performed as described (Yang et al., 2016). Head plates were implanted and stabilized with screws using Metabond cement (Parkell) over the Bregma skull landmark in mice anesthetized with ketamine/xylazine (100mg/kg; 10mg/kg). After five days of post-surgical recovery, head-fixed mice underwent two consecutive days of one hour habituation sessions on a cylindrical treadmill. After training, mice underwent experimental testing in the head-fixed eyeblink conditioning apparatus. In the paradigm, mice gradually associate a conditioned stimulus (CS; blue LED) with an eye-blink-eliciting unconditioned stimulus (US, 20psi periocular air puff through a 25-gauge needle; CS-US inter-stimulus interval, 150 msec). 100 trials of CS-US pairings were performed each day over six consecutive days. The learned eyelid conditioned response was recorded using a high-speed monochrome camera (Allied Vision). Fraction of eyelid closure, ranging from 0 (fully open) to 1 (fully closed), was calculated on each frame as described previously (Heiney et al., 2014). During the inter-stimulus period, eyelid closure >0.1 was designated as a conditioned eyelid response (CR). Our measure for motor learning was the percentage of CR-positive trials on each session day (Percent CR).

DigiGait analysis

The DigiGait imaging platform (Mouse Specifics Inc, Quincy, MA, USA) was employed to assess gait dynamics in sex-matched littermate five-week-old conditional knockout and control

mice as described (Valnegri et al., 2017, Puram et al., 2011, Amende et al., 2005). During mouse ambulation on a transparent treadmill (20 cm/s), digital paw prints were captured by high-speed camera. Subsequently, gait-related variables were quantified and analyzed by software specialized for the DigiGait imaging system.

Accelerating rotarod behavior assay

The accelerating rotarod assay was performed using sex-matched littermate five-week-old MEF2A/D cKO and control mice. On the first day, mice underwent habituation on the rotarod apparatus (IITC) at a constant 5 rotations per minute (rpm) for 10 min. Following habituation, mice underwent three consecutive days of testing, with each session day consisting of 5 trials of forced ambulation at 5 to 40 rpm over a period of 3 minutes, with a 1 minute inter-trial interval (15 trials total). Latency to falling (sec) from the rod onto the platform below was recorded.

In vivo electroporation

In vivo electroporation of postnatal mouse pups was performed as described (Yamada et al., 2014, Konishi et al., 2004, Kim et al., 2009, Yang et al., 2009, Chen et al., 2019). P12-P14 littermate conditional MEF2A/D knockout and control mouse pups were injected with pCAG-GFP, and subjected to four electric pulses of 135mV with 950ms intervals. Electroporated pups were returned to moms and examined in a blinded manner by immunofluorescence confocal microscopy eight days later.

Electron microscopy

P24-P28 mice were perfusion fixed with warmed (37˚C) mammalian Ringer's solution for 2 minutes followed by a mixture of 2.5% glutaraldehyde and 2% paraformaldehyde in 0.15 M

cacodylate buffer containing 2mM $CaCl_2$, pH 7.4 for 5 minutes. Mouse brains were carefully dissected and placed into excess fixative overnight. The following day, 100 µm vibratome sections were taken of the cerebellum. Tissue slices were then stained according the methods described by Deerinck et. al 2010. In brief, coverslips were rinsed in cacodylate buffer 3 times for 10 minutes each, and subjected to a secondary fixation for one hour in 2% osmium tetroxide/1.5% potassium ferrocyanide in cacodylate buffer for one hour, rinsed in ultrapure water 3 times for 10 minutes each, and stained in an aqueous solution of 1% thiocarbohydrazide for one hour. After this, the coverslips were once again stained in aqueous 2% osmium tetroxide for one hour, rinsed in ultrapure water 3 times for 10 minutes each, and stained overnight in 1% uranyl acetate at 4˚C. The samples were then again washed in ultrapure water 3 times for 10 minutes each and *en bloc* stained for 30 minutes with 20 mM lead aspartate at 60˚C. After staining was complete, coverslips were briefly washed in ultrapure water, dehydrated in a graded acetone series (50%, 70%, 90%, 100% x2) for 10 minutes in each step, and infiltrated with microwave assistance (Pelco BioWave Pro, Redding, CA) into Durcupan resin, and flat embedded between two slides that had previously been coated with PTFE release agent (Miller-Stephenson #MS-143XD, Danbury, CT) and clamped with binder clips. Samples were cured in an oven at 60˚C for 48 hours. Post resin curing, the slides were separated and regions containing central vermal lobules of the cerebellum were cut out by saw and mounted onto blank resin stubs before 70 nm thick sections were cut and placed onto silicon wafer chips. These chips were then adhered to SEM pins with carbon adhesive tabs and large areas (~ 200 x 200 µm) were then imaged at high resolution in a FE-SEM (Zeiss Merlin, Oberkochen, Germany) using the ATLAS (Fibics, Ottowa, Canada) scan engine to tile large regions of interest. High-resolution tiles were captured at 20,480 x 20,480 pixels at 10 nm/pixel with a 8 µs dwell time and line average of 2.

The SEM was operated at 8 KeV and 900 pA using the solid-state backscatter detector. Tiles were aligned and exported using ATLAS 5.

qRT-PCR

Reverse transcription reactions were performed with Superscript III (Invitrogen) according to manufacturer's protocol. Real-time PCR reactions using iTaq Universal SYBR Green Supermix (BioRad) were performed on the LightCycler 480 II (Roche).

RNA-sequencing

For RNA-seq, total RNA was extracted from the cerebellum of sex-matched littermate mice using Trizol (ThermoFisher) according to the manufacturer's instructions. RNA was reverse-transcribed with oligo-dT priming and the cDNA was sequenced on an Illumina HiSeq 2500 (Genome Technology Access Center at Washington University). Four biological replicates were sequenced in all experiments.

Chromatin immunoprecipitation

ChIP-seq assays were performed with P22 mouse cerebella as described with modifications (Andzelm et al., 2015). For MEF2A and MEF2D ChIP-seq, prior to immunoprecipitation, the respective antibody was coupled with Dynabeads protein A (ThermoFisher). For histone H3K27ac ChIP-seq, prior to immunoprecipitation, the antibody was coupled to Dynabeads protein G (ThermoFisher). Following immunoprecipitation, MEF2 ChIP library prep and sequencing was performed at the Genome Technology Access Center at Washington University as described (Yang et al., 2016). H3K27ac ChIP libraries were prepared with Accel-NGS 2S

Plus DNA Library Kit (Swift Biosciences) and sequenced on the Illumina NextSeq 500 platform at the Center for Genomic Sciences (Washington University in St. Louis School of Medicine). Three to four biological ChIP replicates were sequenced in all experiments.

Rotarod activation paradigm

Five- to eight-week-old sex-matched littermate AcKO, DcKO, ADcKO and control mice were trained on an accelerating rotarod on the first day for 30 min (6 trials for each of the following speeds: 5-10rpm, 5-15rpm, 5-20rpm; trial duration: 90s; inter-trial interval: 10s; ramp speed: 90s). On the second day, mice were placed on the rotarod for 1 hour (36 trials of 5-20rpm; trial duration: 90s; inter-trial interval 10s; ramp speed: 90s), immediately followed by extraction of total RNA from cerebellum using Trizol (Thermo Fisher Scientific) according to the manufacturer's instructions. ~100 ng of RNA was treated with NEBNext rRNA Depletion Kit and libraries prepared with NEBNext Ultra II Directional RNA Library Prep Kit for Illumina (New England Biolabs) and sequenced on the Illumina NextSeq 500 platform at the Center for Genomic Sciences (Washington University in St. Louis School of Medicine) to obtain 75bp single-end reads. Four biological replicates were performed in all experiments.

QUANTIFICATION AND STATISTICAL ANALYSIS

Statistical Analysis

Statistical analysis for each experiment is detailed in the figure legends. For analysis of genomic distribution, the distribution of enhancers and promoters bound by MEF2A and MEF2D were compared to the genomic distribution of all enhancers and promoters. Statistical significance was

evaluated using a two-tailed Chi-squared test. Box-whisker plots display median value with whiskers representing the 5^{th} and 95^{th} percentile. Significance testing for box-whisker plots were performed using two-tailed unpaired t-test or ANOVA with Tukey multiple comparison test, when appropriate. MEF2-bound genes were defined as the single nearest gene based on distance to a MEF2 ChIP-seq peak. Significance for overlap of RNA-seq clusters with MEF2A and MEF2D peaks identified in various ChIP-seq conditions was evaluated by hypergeometric test followed by Bonferroni multiple comparison. For behavioral experiments, independent t-test and repeated measures ANOVA followed by Sidak's multiple comparison correction were used when appropriate. Threshold for calling statistical significance for all analyses mentioned above was $p < 0.05$. Statistical analyses were performed using Graphpad PRISM 6.0.

ChIP-seq alignment and peak calling

Single-end reads of 50 or 75 base pairs were obtained for all datasets. Samples were sequenced to a minimum depth of 18.5 million reads and aligned to the mm10 genome using Bowtie2 with default parameters for Galaxy platform. Reads were then filtered for a map quality score greater than 10 (mapQuality >10). Peaks were called using MACS2 on pooled data. Blacklist regions were subsequently removed prior to downstream analysis and visualization of ChIP-seq data.

Motif Analysis

MEME suite was used to perform *de novo* motif discovery for MEF2A and MEF2D peaks, with similarly sized flanking regions of MEF2A and MEF2D peaks serving as genomic background. MRE degeneracy was determined by scanning MEF2A and MEF2D peaks for a consensus MRE using FIMO software. Identification of motifs relatively enriched in compensatory sites

compared to non-compensatory sites was performed using AME software, in which compensatory sites served as the experimental dataset and non-compensatory sites as the control dataset.

RNA-seq analysis

Differential mRNA-seq analysis was performed for RNA extracted from the cerebellum of P22 AcKO, DcKO, ADcKO, and control mice. Reduction of potential line-specific differences between conditional knockout lines was performed by overlapping genes identified by two types of differential mRNA analyses, one in which conditional knockout mice were compared to respective control littermates and another in which they were compared to controls from all conditional lines.

DNaseI-seq analysis

DNaseI-seq peaks were called using MACS2 at a q-value of less than 0.01 (-q 0.01) without model building (--nomodel), an extension of 200bp (--extsize 200), and a shift of -100bp (--shift -100). DNaseI-hypersensitivity performed in two biological replicates of cerebellum harvested from p22 mouse in Yamada et al 2019 (Yamada et al., 2019).

3.8 Declarations

Ethics approval

Mice were maintained in a pathogen-free environment. All procedures involving animals were performed according to protocols approved by the Animal Studies Committee of Washington University School of Medicine and in accordance with both the National Institute of Health Standings Committee on Animals as well as the National Institutes of Health guidelines.

Availability of data and materials

The datasets generated and/or analyzed during the current study are available in the Box repository, https://wustl.box.com/s/lyzp9e7rxoz23zysw8mfhg4todm4xnm3.

Publicly available data on which conclusions of the paper rely are included below:

Telese F, Ma Q, Perez PM, Notani D et al. LRP8-Reelin-Regulated Neuronal Enhancer Signature Underlying Learning and Memory Formation. Gene Expression Omnibus (GEO). 2015. https://www.ncbi.nlm.nih.gov/geo/query/acc.cgi?acc=GSE66710

Yamada T, Yang Y, Hemberg M, Yoshida T, Cho HY, Murphy JP, Fioravante D, Regehr WG, Gygi SP, Georgopoulos K, Bonni A. Promoter decommissioning by the NuRD chromatin remodeling complex triggers synaptic connectivity in the mammalian brain. Gene Expression Omnibus (GEO). 2014. https://www.ncbi.nlm.nih.gov/geo/query/acc.cgi?acc=GSE57758

Yamada T, Yang Y, Valnegri P, Juric I, Abnousi A, Markwalter KH, Guthrie AN, Godec A, Oldenborg A, Hu M, Holy TE, Bonni A. Sensory experience remodels genome architecture in

neural circuit to drive motor learning. Gene Expression Omnibus (GEO). 2019. https://www.ncbi.nlm.nih.gov/geo/query/acc.cgi?acc=GSE127995

Acknowledgements

We thank members of the Bonni and Gabel laboratories for helpful discussions and critical reading of the manuscript, James Fitzpatrick and Matthew Joens of the Washington University Center for Cellular Imaging (WUCCI) and Krikor Dikranian for their insights in imaging analyses, and the Genome Technology Access Center (GTAC) and Center for Genomic Sciences (CGS) at Washington University in St. Louis for sequencing analyses. This work was supported by NIH grant NS041021 (A.B), the Mathers Foundations (A.B.), and NIH grant R37 NS028829 (M.E.G).

3.8 Figure

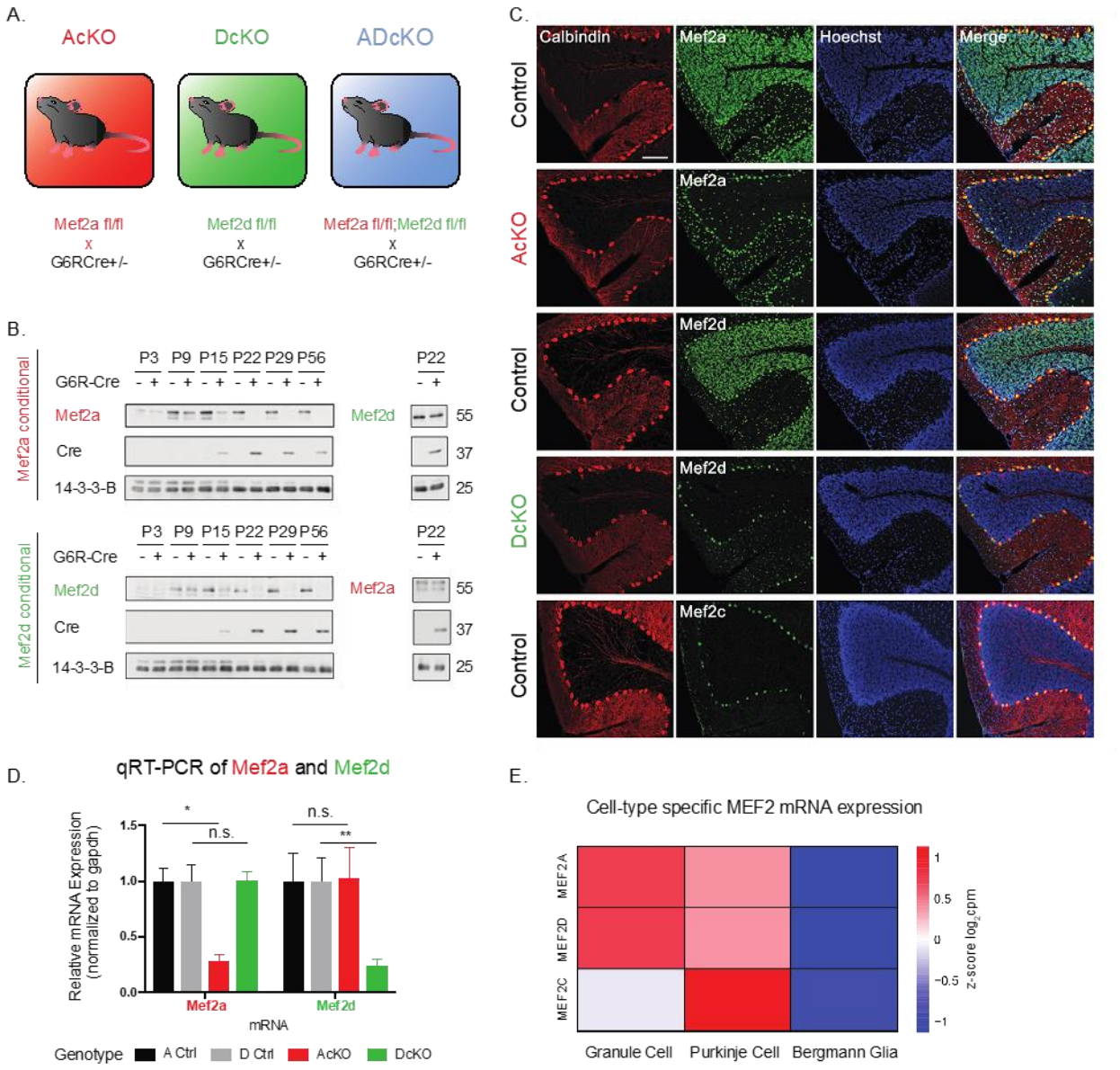

Fig. 3.1 Conditional knockout of MEF2A and/or MEF2D in cerebellar granule neurons.

A. Schematic depiction of single- and double-conditional knockouts of MEF2A and MEF2D in cerebellar granule neurons in mice. Transgenic mice expressing the recombinase Cre downstream of the granule neuron-enriched GABA(A)a6-receptor (G6R) gene promoter are crossed to mice harboring conditional alleles for *Mef2a*, *Mef2d*, or both *Mef2a* and *Mef2d* to

generate *Mef2a$^{fl/fl}$;G6RCre$^{+/-}$* (AcKO); *Mef2d$^{fl/fl}$;G6RCre$^{+/-}$* (DcKO); *Mef2a/d$^{fl/fl}$;G6RCre$^{+/-}$* (ADcKO), respectively. For all experiments, control mice are double floxed sex-matched littermates without the G6R-Cre transgene.

B. Immunoblot analysis with antibodies recognizing MEF2A, MEF2D, Cre, and 14-3-3β, the latter as loading control. Postnatal developmental expression and conditional knockout of MEF2A (top left) and MEF2D (bottom left) in lysates of the cerebellum harvested from postnatal day 3 through 56 (P3-P56) AcKO (top) and DcKO (bottom) mice, respectively. MEF2A and MEF2D proteins showed similar temporal profiles of expression in the developing and adult mouse cerebellum. Downregulation of MEF2A and MEF2D peaked by P22 in AcKO and DcKO mice, respectively. Immunoblotting analysis was also performed for MEF2D in P22 AcKO mice (top right) and MEF2A in P22 DcKO mice (bottom right). Conditional knockout of MEF2A failed to effectively alter the levels of MEF2D protein, and conversely conditional knockout of MEF2D failed to effectively alter the levels of MEF2A protein in the cerebellum.

C. Sagittal sections of P22 cerebellum from different MEF2 conditional knockout mouse lines were subjected to immunohistochemistry using antibodies recognizing Calbindin (first column), which labels Purkinje cells that outline the internal granule layer, and brain-enriched MEF2 family members (second column), as well as the DNA dye Bisbenzimide (Hoechst) (third column). Immunohistochemical analyses using the MEF2A antibody was performed on control (top row) and AcKO (second row) mouse cerebellum, the MEF2D antibody on control (third row) and DcKO (fourth row) mouse cerebellum, and the MEF2C antibody on control (fifth row) mouse cerebellum. MEF2A and MEF2D protein expression was co-localized in the internal granule layer of control cerebellum and selectively depleted in granule neurons of AcKO and DcKO mice, respectively. MEF2C expression was restricted to Purkinje cells. Scale bar: 100μm, 20X magnification.

D. qRT-PCR of Mef2a and Mef2d in AcKO, DcKO, and respective control P22 mouse cerebellum. For each mRNA species, each cKO condition is normalized to Gapdh and its respective control.

E. Analysis of cell type-specific Mef2 mRNA expression obtained from TRAP-seq (Mellen et al., 2012) on granule cells, Purkinje cells, and Bergmann glia from the cerebellar cortex. Heat represents z-score of $\log_2$ cpm.

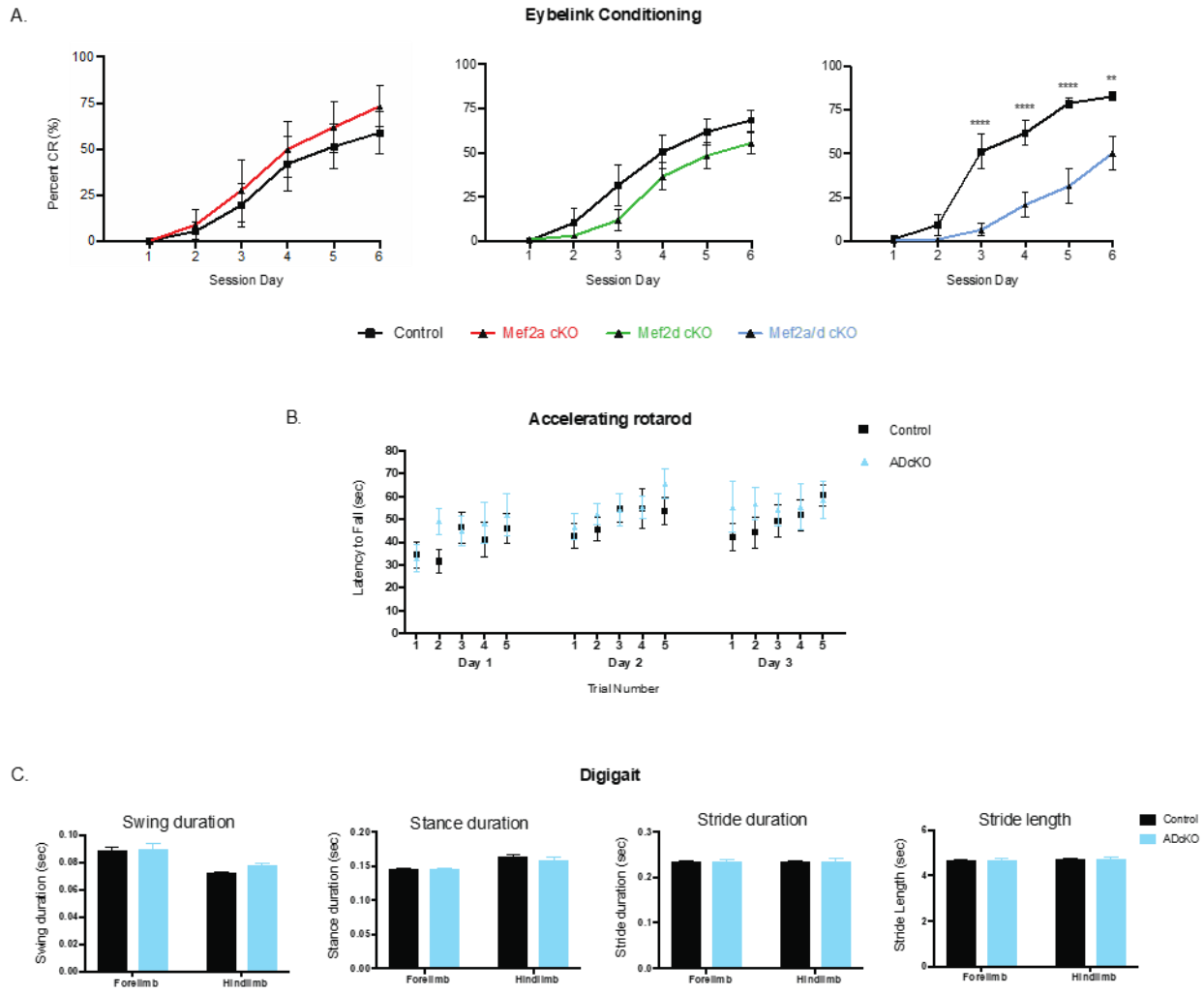

Figure 3.2 MEF2A and MEF2D regulate cerebellar-dependent motor learning in a compensatory manner, but are not required for gross motor coordination.

A. Cerebellar-dependent eyeblink conditioning learning paradigm was performed on AcKO and control (n=6 per genotype), DcKO and control (n=7 and n=8, respectively), and ADcKO and control (n=11 and n=9, respectively) mice. Percent conditioned response (CR) is shown as mean ± s.e.m. for each session day. ADcKO mice displayed impaired learning, exhibiting significantly reduced rate of CR by day three of conditioning that persisted for the remaining session days. However, neither AcKO nor DcKO mice had significant learning deficits. ****$p<10^{-4}$, **$p<10^{-2}$ repeated measures ANOVA, Sidak's multiple comparison test.

B. Accelerating rotarod of ADcKO (n= 9) and respective control (n=10) mice performed over three consecutive days for five trials each. Latency to fall in seconds was recorded.

C. Analysis of gait dynamics by Digigait Assay did not reveal deficits in sex-matched ADcKO (n=4) relative to control (n=5) littermates on stride-related variables for both the forelimbs and hindlimbs. Two-way ANOVA with Sidak's multiple comparison test.

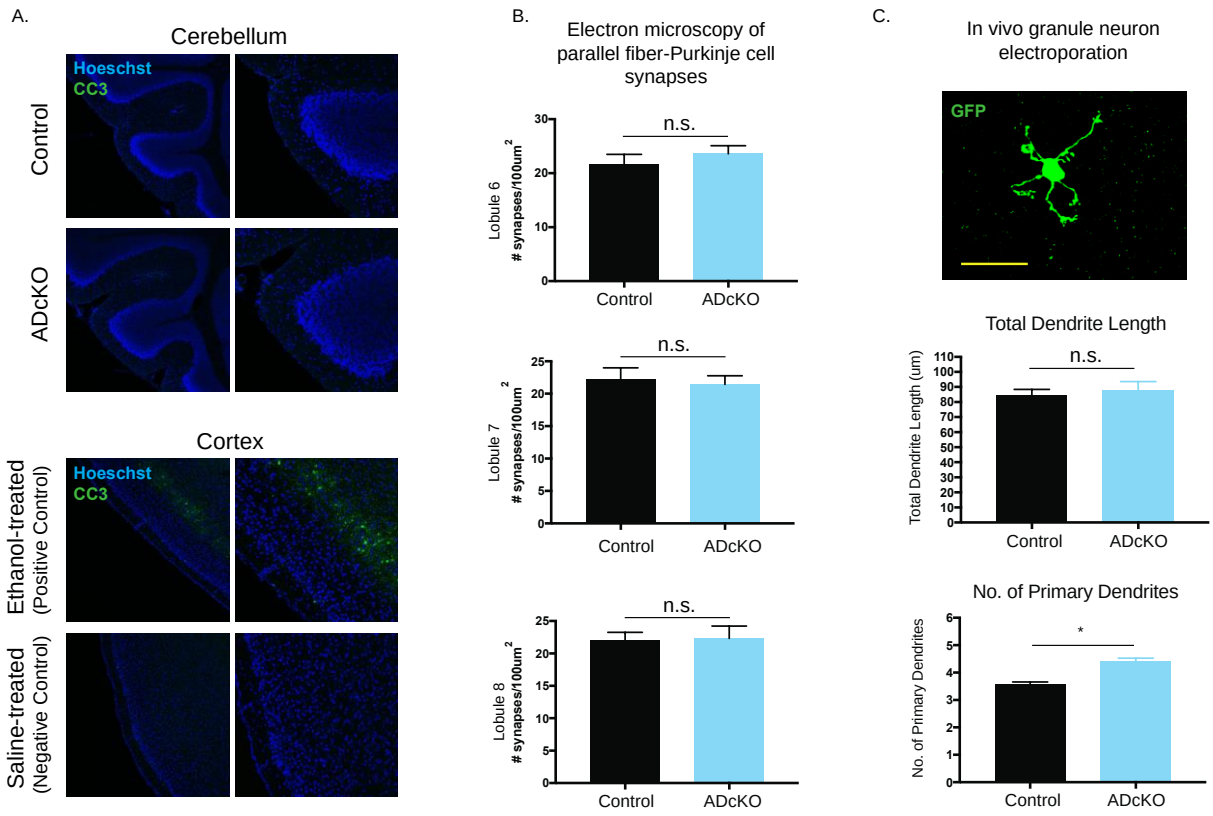

Fig. 3.3 Conditional knockout of MEF2A and MEF2D does not result in granule neuron apoptosis or deficits of pre- or post-synaptic differentiation

A. Representative images of immunohistochemistical analyses performed with antibodies for cleaved caspase 3 (CC3) and the DNA dye Bisbenzimide (Hoechst) in the cerebellar cortex from control and ADcKO sex-matched littermates. Because few cerebellar cells are normally CC3-positive, for positive control we induced apoptosis in the mouse frontal cortex using two consecutive subcutaneous injections, two hours apart, of 20% ethanol 2.5g/kg into P7 mice and saline as negative control. Magnification 10X (left) and 20X (right).

B. Electron Microscopy analysis of synapses between cerebellar granule neuron parallel fibers with Purkinje cell dendritic spines in the cerebellar cortex of ADcKO (n=5 mice) and control (n=6 mice) sex-matched littermates.

C. *In vivo* electroporation of GFP expression plasmid into the cerebellar cortex of ADcKO (n=4) and control (5) sex-matched littermate mice labels developing granule neurons. Eight

days post-electroporation, immunohistochemical analyses were performed using a GFP antibody (top). Number (No.) of primary dendrites (middle) and dendrite length (bottom) analyzed in GFP-positive granule neurons. * $p<10^{-1}$, Mann Whitney test. n.s., not significant.

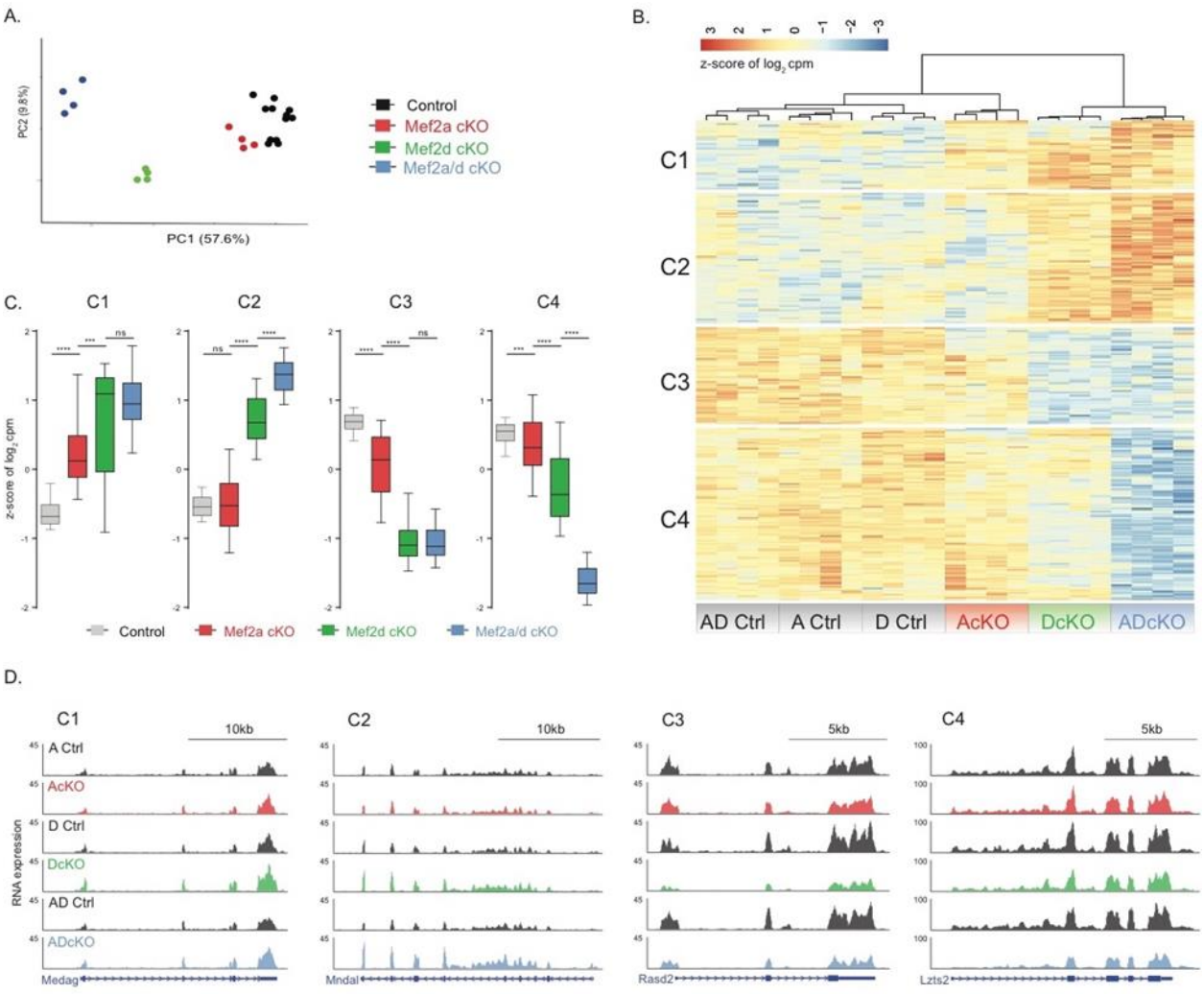

Fig. 3.4 MEF2A and MEF2D exhibit complex patterns of gene regulation in cerebellum.

A. Principal component (PC) analysis of RNA-seq samples, including four replicates each of AcKO (red), DcKO (green), ADcKO (blue), and respective sex-match littermate control mice (black).

B. Hierarchical clustering of gene expression of AcKO, DcKO, ADcKO, and respective control (Ctrl) P22 mouse cerebellum for genes detected as significantly dysregulated (false discovery rate, FDR < 0.05) in analysis of RNA-seq from Ctrl and ADcKO cerebellum (n=4 biological replicates per genotype). Four clusters are indicated on the left side of the heat map. Heat represents z-score of $\log_2$ cpm for a given gene.

C. Box-whisker plots representing median and distribution of the z-score of $\log_2$ cpm for control, AcKO, DcKO, and ADcKO mice show distinct trends in gene expression for each of the four clusters (C1-C4) of genes identified in Figure 2.4B, providing quantitative assessment of the relative effects of single- and double-conditional knockouts on gene expression for each cluster. C1 and C2 represent MEF2-repressed genes, while C3 and C4 represent MEF2-activated genes. One major trend, represented by C1 and C3, showed no significant difference in gene expression between DcKO and ADcKO mice. In contrast, C2 and C4 followed a different trend, in which gene expression in ADcKO mice was more significantly altered compared to DcKO mice. Horizontal line inside box represents the median. Whiskers represent the 5^{th} and 95^{th} percentile; ****$p<10^{-4}$, ***$p<10^{-3}$, one-way ANOVA, Tukey's multiple comparison test; n.s., not significant.

D. WashU Epigenome browser view of RNA-seq coverage from AcKO, DcKO, ADcKO, and respective control (Ctrl) mice, illustrating changes in gene expression for each of the four clusters (C1-C4).

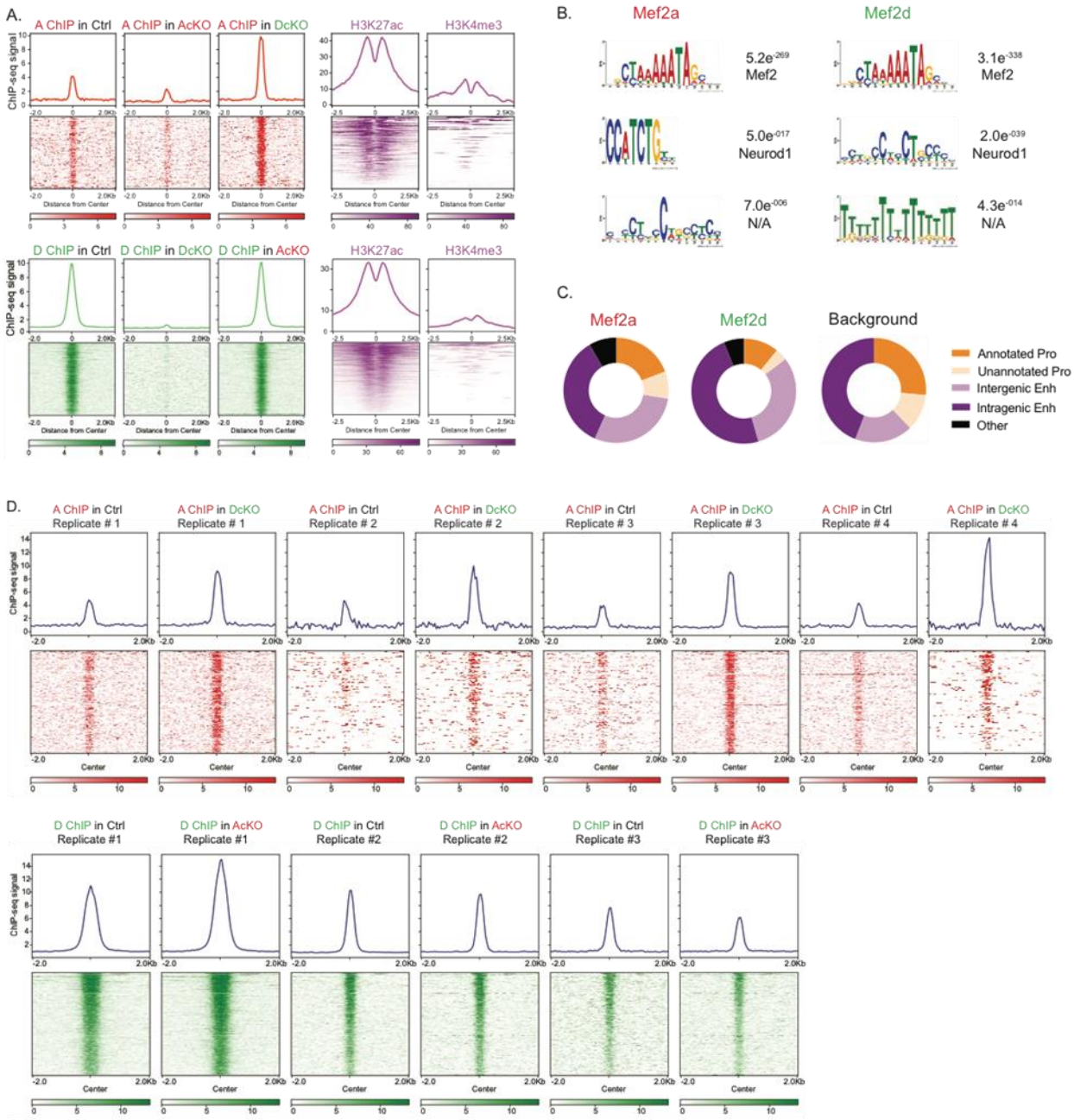

Fig. 3.5 Genomic distribution and enriched motifs of MEF2A and MEF2D-bound sites.

A. Aggregate plot and heat map of ChIP-seq signal for MEF2A (red, n=203) and MEF2D (green, n = 1388) genomic binding sites in Ctrl, AcKO, and DcKO P22 mouse cerebellum. Each MEF2 binding site is represented as a single horizontal line centered at the midpoint of each ChIP peak with flanking 2kb. ChIP-seq signal for H3K27ac and H3K4me3 (purple)

from P22 mouse cerebellum centered on each MEF2 genomic binding site with flanking 2.5 kb. ChIP-seq antibody specificity was validated by performing MEF2A and MEF2D ChIP-seq in AcKO and DcKO mice, respectively. Upon depletion of MEF2D in DcKO mice, MEF2A showed a striking increase in genomic occupancy. In contrast, MEF2D occupancy appeared relatively unchanged in AcKO mice.

B. Significantly enriched *de novo* binding motifs at MEF2A and MEF2D peaks. To the right of each position weighted matrix is the E-value followed by the most significant match to a TF motif in a database (see Methods). Canonical MEF2 response element (MRE), YTAWWWTAR, was the most significantly enriched motif at >95% of peaks.

C. Pie charts displaying regulatory element distribution of peak regions for MEF2A (left) and MEF2D (middle) as well as genomic background (right). Pro = promoter; Enh = enhancer. MEF2A and MEF2D both bind active intergenic enhancers at a frequency higher than the normal genomic distribution.

D. Aggregate plot and heatmap of ChIP-seq signal for four pairs of biological replicates for MEF2A in control (Ctrl) and DcKO (red, top) and three biological replicates of MEF2D in control (Ctrl) and AcKO (green, bottom) P22 mouse cerebellum.

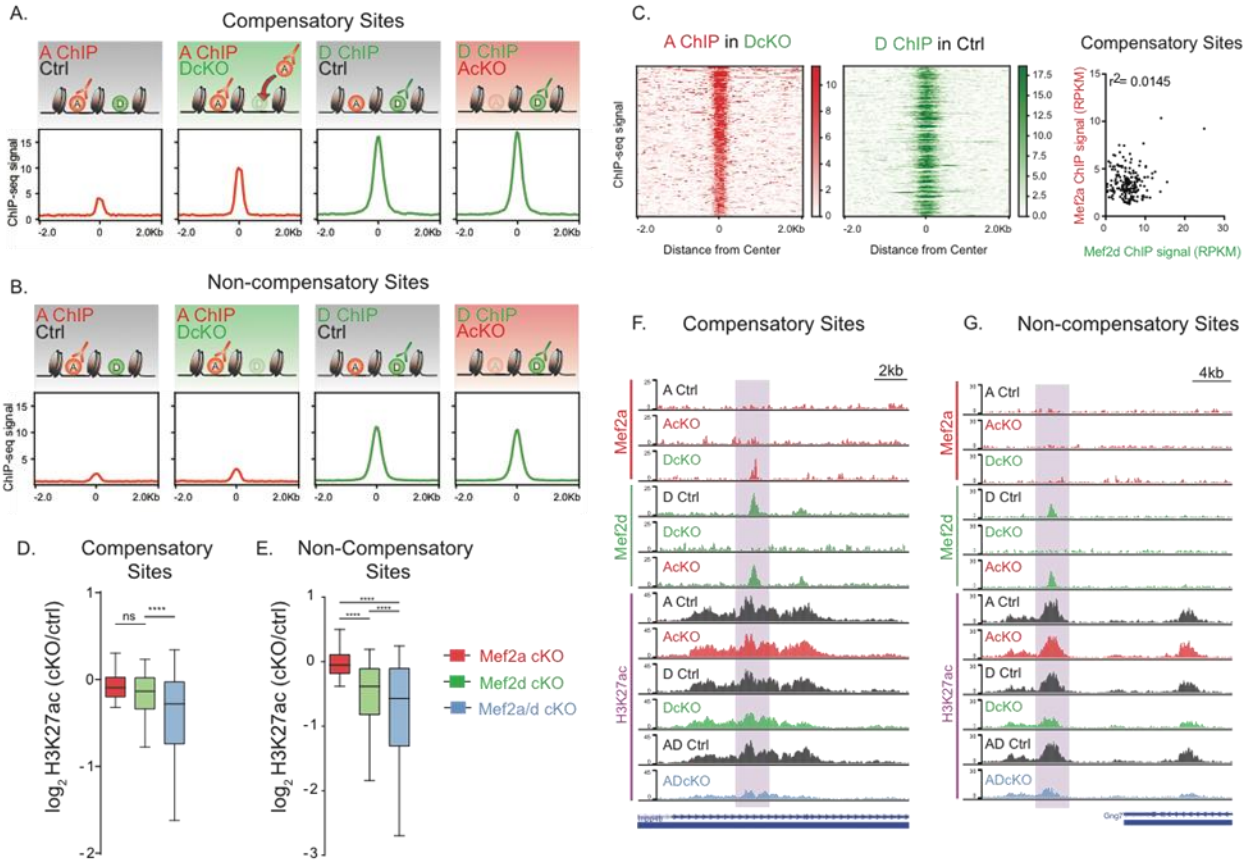

Fig. 3.6 MEF2A displays functionally compensatory binding at a distinct subset of MEF2D-bound genomic sites.

A. Conditional knockout of MEF2D robustly increased MEF2A mainly at a subset of sites previously bound by MEF2D. MEF2D sites experiencing increased MEF2A occupancy in DcKO mouse cerebellum are termed “compensatory.” Aggregate plots are shown for MEF2A and MEF2D ChIP-seq performed in different control (Ctrl) or cKO mice. A schematic depicts outcome based on the ChIP-seq peak signal detected in each condition.

B. “Non-compensatory” sites, defined as control MEF2D sites without increased MEF2A binding in DcKO mouse cerebellum, are shown. Aggregate plots are shown for MEF2A and MEF2D ChIP-seq performed in different control (Ctrl) or cKO mice. A schematic depicts outcome based on the ChIP-seq peak signal detected in each condition.

C. Heat map of ChIP-seq signal for MEF2A (left) and MEF2D (right) at compensatory sites. Sites are the same in both heat maps and sorted in descending order based on MEF2A ChIP-seq signal. Scatterplot of MEF2A and MEF2D ChIP-seq signal (RPKM) at compensatory sites. Coefficient of determination using Pearson correlation. Within compensatory sites, there is no correlation between MEF2A and MEF2D signal intensity.

D. For compensatory genomic-binding sites, box-whisker plots show median and distribution for $\log_2$ transformed fold-change of H3K27ac in AcKO, DcKO, and ADcKO over respective control mice. H3K27ac levels were significantly reduced at compensatory sites in ADcKO mice, whereas they were not altered significantly in AcKO or DcKO mice. Horizontal line inside box represents the median. Whiskers represent the 5^{th} and 95^{th} percentile; **** $p<10^{-4}$, ANOVA followed by Tukey's multiple comparison test. n.s., not significant.

E. For non-compensatory genomic-binding sites: box-whisker plots of $\log_2$ transformed fold-change of H3K27ac in AcKO, DcKO, and ADcKO over respective controls. Horizontal line inside box represents the median. Whiskers represent the 5^{th} and 95^{th} percentile; **** $p<10^{-4}$, ANOVA followed by Tukey's multiple comparison test.

F. WashU Epigenome Browser view of a compensatory site (highlighted), showing MEF2A, MEF2D, and H3K27ac ChIP-seq coverage from AcKO, DcKO, ADcKO and respective control (Ctrl) mice, illustrates that ADcKO has the strongest effects on H3K27ac at genomic site experiencing compensatory MEF2A occupancy in DcKO.

G. Same format as Figure 2.6F for non-compensatory sites, illustrating that DcKO and ADcKO have similar effects on H3K27ac at genomic sites *without* compensatory occupancy by MEF2A in DcKO, in contrast to example in Figure 3I.

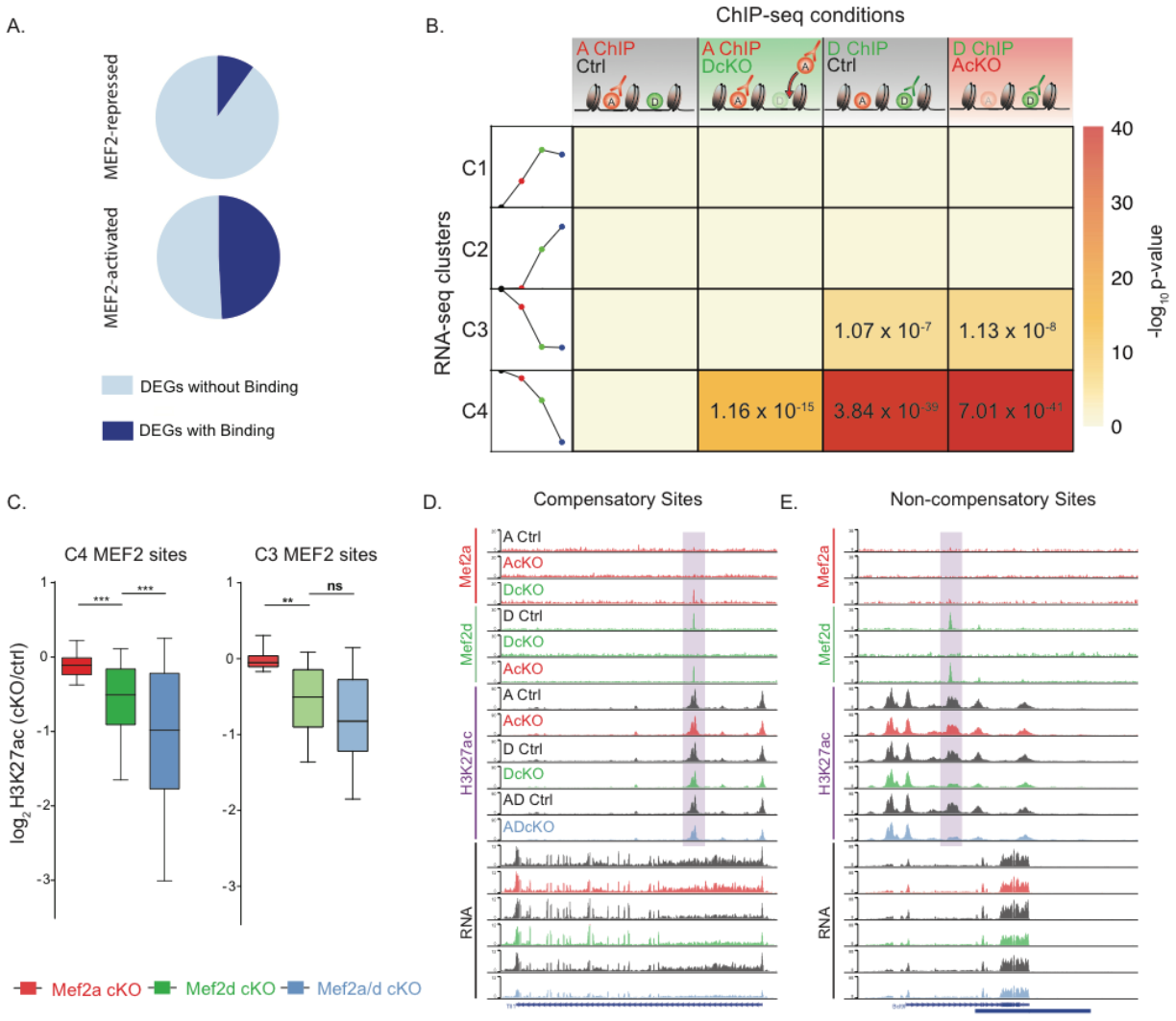

Fig. 3.7 Compensatory binding by MEF2A at a subset of MEF2-activated target genes confers genetic robustness to MEF2D depletion

A. Pie chart representing proportion of MEF2-repressed (top) and MEF2-activated (bottom) genes associated with MEF2A and/or MEF2D genomic binding sites.

B. Table represents significance of overlap of RNA-seq clusters with MEF2A and MEF2D peaks identified in various ChIP-seq conditions. Columns from left to right: MEF2A ChIP in control mice; MEF2A ChIP in DcKO mice (compensatory sites); MEF2D ChIP in control mice; MEF2D ChIP in AcKO mice. Rows from top to bottom represent RNA-seq Clusters 1, 2, 3, and 4 (C1, C2, C3, C4), as depicted by a schematic of the trends in gene expression

(schematization of Fig. 2.4C): control (Black circle), AcKO (Red circle), DcKO (Green circle) and AD cKO (Blue circle) mice. Heat represents $-\log_{10}$ p-value significance of overlap determined by hypergeometric test, with significant values displayed.

C. For compensatory direct target genes (defined as genes from compensatory C4 Cluster associated with MEF2-bound sites): Box-whisker plots show median and distribution of $\log_2$ transformed fold-change of H3K27ac in different conditional knockout mice over respective control mice. Horizontal line inside box represents the median. Whiskers represent the 5^{th} and 95^{th} percentile; ***$p<10^{-3}$, ANOVA followed by Tukey's multiple comparison test. For non-compensatory direct target MEF2-activated genes (defined as genes from non-compensatory C3 Cluster associated with MEF2-bound sites): Box-whisker plots of $\log_2$ transformed fold-change of H3K27ac in different cKO conditions over respective controls. Horizontal line inside box represents the median. Whiskers represent the 5^{th} and 95^{th} percentile; **$p<10^{-2}$, ANOVA followed by Tukey's multiple comparison test. n.s. not significant.

D. WashU Epigenome Browser view of an intragenic enhancer site (highlighted) of a compensatory direct target gene, showing MEF2A, MEF2D, and H3K27ac ChIP-seq and RNA-seq coverage from AcKO, DcKO, ADcKO and respective control (Ctrl) mice. ADcKO has the strongest effects on H3K27ac and RNA levels at this gene.

E. Same format as Figure 2.7D for intragenic enhancer site (highlighted) at non-compensatory direct target gene, illustrating that DcKO and ADcKO have similar effects on H3K27ac and RNA levels at genes *without* compensatory occupancy by MEF2A in DcKO, in contrast to example in Figure 2.7D.

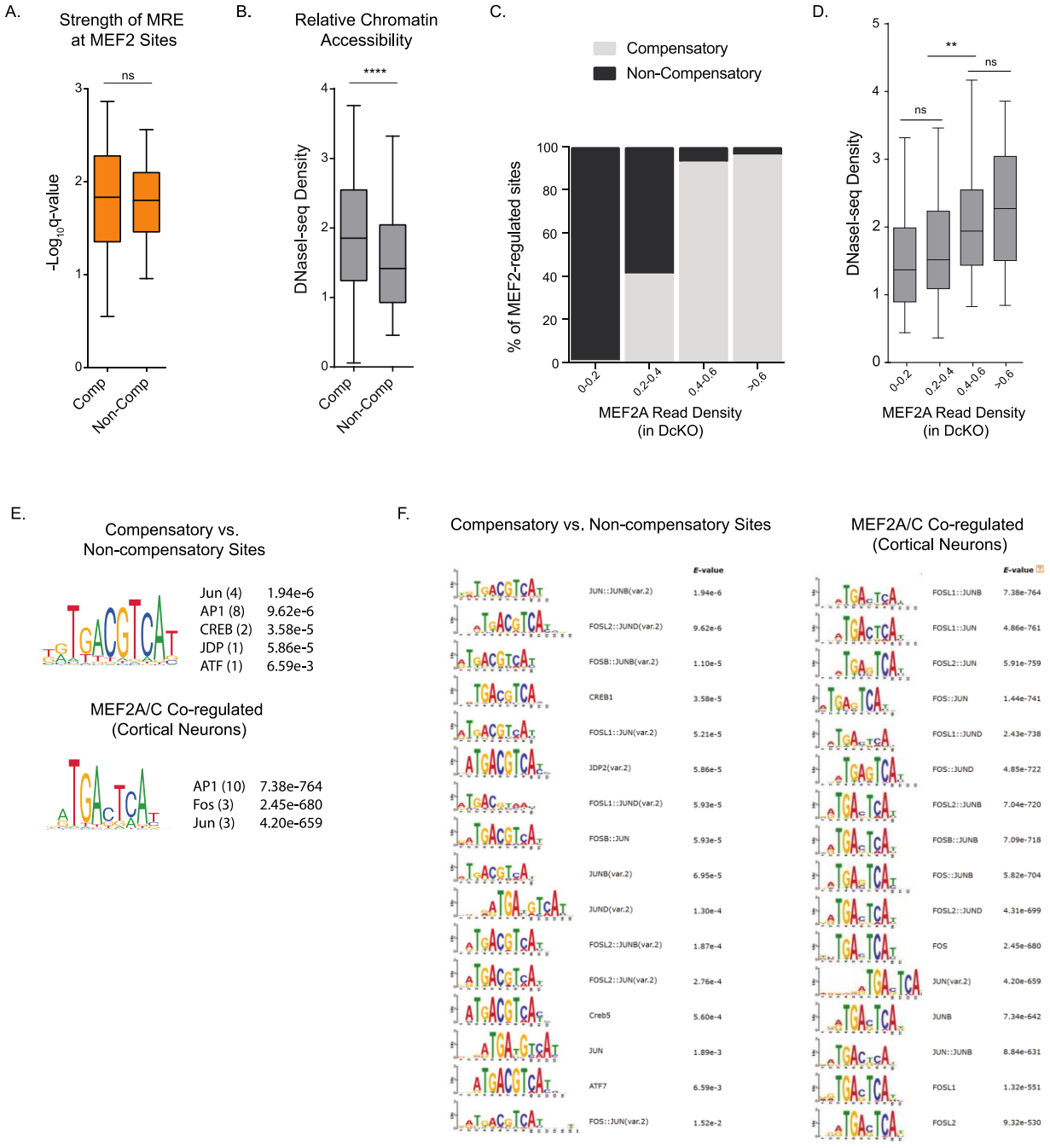

Fig. 3.8 Relative chromatin accessibility, rather than binding site affinity, distinguish compensatory and non-compensatory MEF2-regulated sites

A. Box-whisker plots show no significant difference between compensatory and non-compensatory sites in MRE degeneracy scores relative to a consensus MRE. Horizontal line

inside box represents the median. Whiskers represent the 5^{th} and 95^{th} percentile. n.s., not significant (see Methods for details).

B. Box-whisker plots show significant difference in chromatin accessibility between compensatory and non-compensatory MEF2-bound sites, as measured by DNaseI-sequencing at MEF2 peak regions. Horizontal line inside box represents the median. Whiskers represent the 5^{th} and 95^{th} percentile. Two-sided unpaired t-test, **** $p<10^{-4}$.

C. Plots represent bins of MEF2 sites sorted by increasing MEF2A peak read density in DcKO mice. Relative distribution of compensatory (light gray) and non-compensatory (black) MEF2 sites are shown as percentage (%) of regions comprising each bin. Bins of higher MEF2A density in DcKO mice are comprised primarily of compensatory sites.

D. Box-whisker plots of DNaseI-sequencing read density for bins of increasing MEF2A density in DcKO mice (classified in Figure 2.8C). Chromatin accessibility increases with higher levels of compensatory MEF2A read density. ANOVA followed by Tukey's multiple comparison test. ** $p<10^{-2}$, n.s., not significant.

E. (Top) Relative motif enrichment for compensatory sites relative to non-compensatory sites primarily identifies binding sites for multiple components of the TF AP-1, which alongside the composite motif, are individually listed as predicted binding factor, followed in parentheses by number of significant motif occurrences and the top q-value representing significance of relative enrichment. (Bottom) Cortical neuron MEF2A and MEF2C genomic-binding (Telese et al., 2015) analyzed with similar strategy. Relative motif enrichment for MEF2A genomic binding sites, some of which co-bound by MEF2C, compared to MEF2C-only sites was performed and also yielded motifs for AP-1 components (see Methods for details).

F. All significant motifs identified by AME analysis for compensatory sites relative to non-compensatory sites shown as position weight matrix (left). Same number of top significant motifs shown for MEF2A and MEF2C co-regulated sites (right) (Telese et al., 2015).

Following position weight matrix is the predicted binding factor(s), followed by q-value representing significance of relative enrichment (see Methods for details). The vast majority of identified motifs for both analyses are AP-1 components.

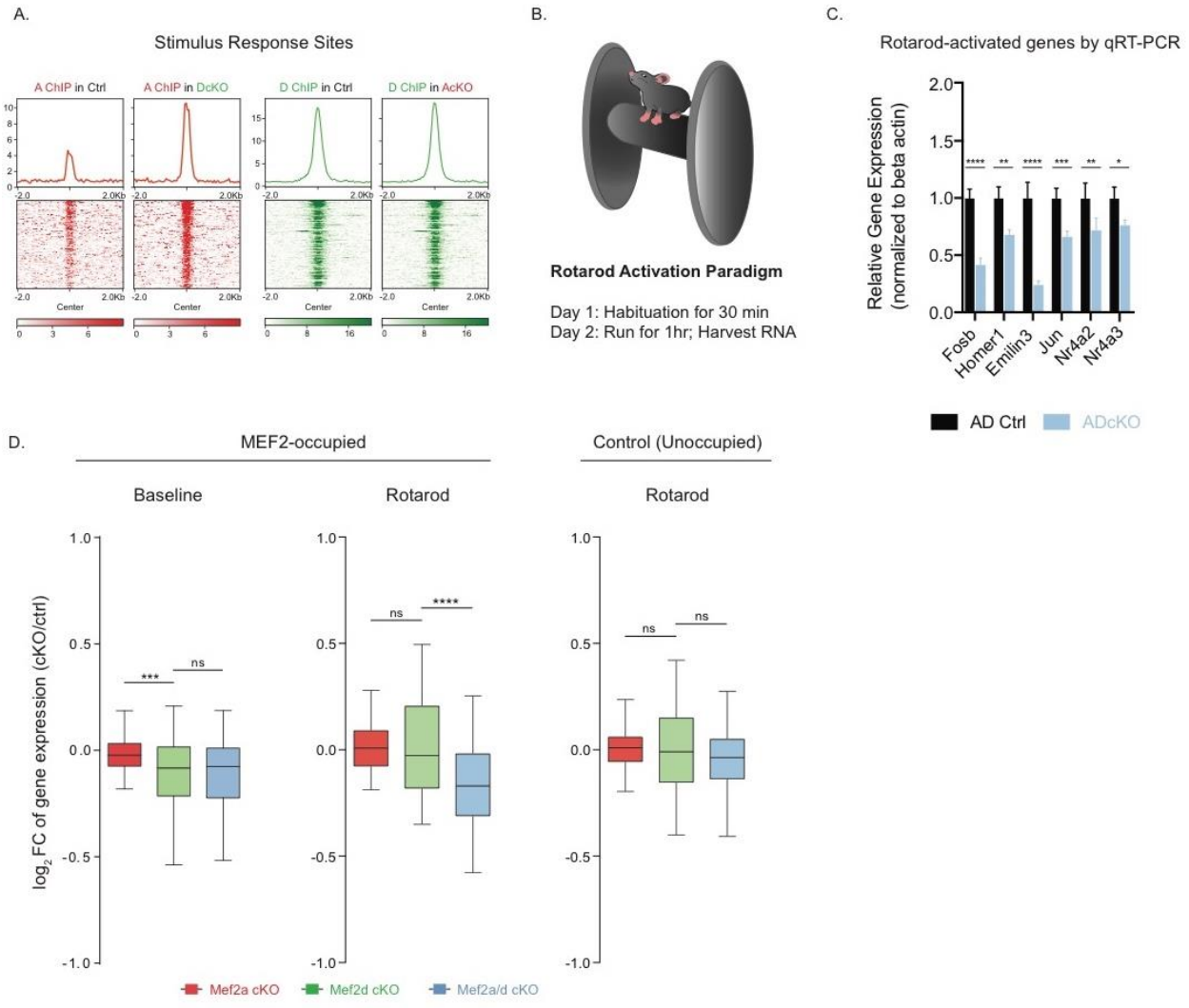

Fig. 3.9 Motor-activity induced changes in neuronal state result in a dynamic switch to compensatory regulation by MEF2A

A. ChIP-seq signal of MEF2A (red, left) and MEF2D (green, right) at stimulus responsive genes listed in the "Response to Stimulus" Gene Ontology term (GO 0050896), shows an increase in MEF2A occupancy at MEF2D-bound sites upon depletion of MEF2D.

B. Schematic depicting accelerating rotarod paradigm, in which mice undergo forced locomotion on a rotating cylinder to significantly induce expression of stimulus-responsive genes (Yang et al., 2016, Yamada et al., 2019), here termed "rotarod-activated" genes.

C. Rotarod paradigm performed for control and ADcKO mice followed by quantitative reverse transcription PCR (qRT-PCR) on cerebellar RNA for select rotarod-activated genes experiencing compensatory MEF2A binding. ****$p<10^{-4}$, ***$p<10^{-3}$, **$p<10^{-2}$, *$p<10^{-4}$, Two-way repeated measures ANOVA, Sidak's multiple comparison test.

D. Total RNA-seq analysis of rotarod-activated gene expression in the cerebellum of AcKO, DcKO, ADcKO, and respective control mice subjected to the rotarod paradigm. Box-whisker plots of log_2-transformed fold-change (FC) of gene expression in AcKO, DcKO, and ADcKO over respective control mice for MEF2-occupied rotarod activated genes at baseline (left) and after rotarod stimulation (middle), as well as unoccupied rotarod-activated genes after rotarod stimulation (right). Under baseline conditions, rotarod-activated MEF2-bound genes appeared to be regulated in a non-compensatory manner; however, after rotarod stimulation, they switched to being regulated in a compensatory manner. As expected, conditional knockout of MEF2A, MEF2D, or both TFs failed to alter expression of rotarod-activated genes that were not direct targets of MEF2. Horizontal line inside box represents the median. Whiskers represent the 5^{th} and 95^{th} percentile; **** $p<10^{-4}$, ANOVA followed by Tukey's multiple comparison test. n.s., not significant.

References

AKHTAR, M. W., KIM, M. S., ADACHI, M., MORRIS, M. J., QI, X., RICHARDSON, J. A., BASSEL-DUBY, R., OLSON, E. N., KAVALALI, E. T. & MONTEGGIA, L. M. 2012. In vivo analysis of MEF2 transcription factors in synapse regulation and neuronal survival. *PLoS One,* 7**,** e34863.

ALBERINI, C. M. & KANDEL, E. R. 2014. The regulation of transcription in memory consolidation. *Cold Spring Harb Perspect Biol,* 7**,** a021741.

ALCHINI, R., SATO, H., MATSUMOTO, N., SHIMOGORI, T., SUGO, N. & YAMAMOTO, N. 2017. Nucleocytoplasmic Shuttling of Histone Deacetylase 9 Controls Activity-Dependent Thalamocortical Axon Branching. *Sci Rep,* 7**,** 6024.

ALVAREZ-SAAVEDRA, M., DE REPENTIGNY, Y., LAGALI, P. S., RAGHU RAM, E. V., YAN, K., HASHEM, E., IVANOCHKO, D., HUH, M. S., YANG, D., MEARS, A. J., TODD, M. A., CORCORAN, C. P., BASSETT, E. A., TOKAREW, N. J., KOKAVEC, J., MAJUMDER, R., IOSHIKHES, I., WALLACE, V. A., KOTHARY, R., MESHORER, E., STOPKA, T., SKOULTCHI, A. I. & PICKETTS, D. J. 2014. Snf2h-mediated chromatin organization and histone H1 dynamics govern cerebellar morphogenesis and neural maturation. *Nat Commun,* 5**,** 4181.

AMENDE, I., KALE, A., MCCUE, S., GLAZIER, S., MORGAN, J. P. & HAMPTON, T. G. 2005. Gait dynamics in mouse models of Parkinson's disease and Huntington's disease. *J Neuroeng Rehabil,* 2**,** 20.

ANDZELM, M. M., CHERRY, T. J., HARMIN, D. A., BOEKE, A. C., LEE, C., HEMBERG, M., PAWLYK, B., MALIK, A. N., FLAVELL, S. W., SANDBERG, M. A., RAVIOLA, E. & GREENBERG, M. E. 2015. MEF2D drives photoreceptor development through a genome-wide competition for tissue-specific enhancers. *Neuron,* 86**,** 247-63.

ANDZELM, M. M., VANNESS, D., GREENBERG, M. E. & LINDEN, D. J. 2019. A Late Phase of Long-Term Synaptic Depression in Cerebellar Purkinje Cells Requires Activation of MEF2. *Cell Rep,* 26**,** 1089-1097.e3.

ARNOSTI, D. N. & KULKARNI, M. M. 2005. Transcriptional enhancers: Intelligent enhanceosomes or flexible billboards? *J Cell Biochem,* 94**,** 890-8.

ASSALI, A., HARRINGTON, A. J. & COWAN, C. W. 2019. Emerging roles for MEF2 in brain development and mental disorders. *Curr Opin Neurobiol,* 59**,** 49-58.

ATAMAN, B., BOULTING, G. L., HARMIN, D. A., YANG, M. G., BAKER-SALISBURY, M., YAP, E. L., MALIK, A. N., MEI, K., RUBIN, A. A., SPIEGEL, I., DURRESI, E., SHARMA, N., HU, L. S., PLETIKOS, M., GRIFFITH, E. C., PARTLOW, J. N., STEVENS, C. R., ADLI, M., CHAHROUR, M., SESTAN, N., WALSH, C. A., BEREZOVSKII, V. K., LIVINGSTONE, M. S. & GREENBERG, M. E. 2016. Evolution of Osteocrin as an activity-regulated factor in the primate brain. *Nature,* 539**,** 242-247.

BADIS, G., BERGER, M. F., PHILIPPAKIS, A. A., TALUKDER, S., GEHRKE, A. R., JAEGER, S. A., CHAN, E. T., METZLER, G., VEDENKO, A., CHEN, X., KUZNETSOV, H., WANG, C. F., COBURN, D., NEWBURGER, D. E., MORRIS, Q., HUGHES, T. R. & BULYK, M. L. 2009. Diversity and complexity in DNA recognition by transcription factors. *Science,* 324**,** 1720-3.

BAJPAI, R., CHEN, D. A., RADA-IGLESIAS, A., ZHANG, J., XIONG, Y., HELMS, J., CHANG, C. P., ZHAO, Y., SWIGUT, T. & WYSOCKA, J. 2010. CHD7 cooperates with PBAF to control multipotent neural crest formation. *Nature,* 463**,** 958-62.

BAYLY, P. V., OKAMOTO, R. J., XU, G., SHI, Y. & TABER, L. A. 2013. A cortical folding model incorporating stress-dependent growth explains gyral wavelengths and stress patterns in the developing brain. *Phys Biol,* 10**,** 016005.

BETIZEAU, M., CORTAY, V., PATTI, D., PFISTER, S., GAUTIER, E., BELLEMIN-MENARD, A., AFANASSIEFF, M., HUISSOUD, C., DOUGLAS, R. J., KENNEDY, H. & DEHAY, C. 2013. Precursor diversity and complexity of lineage relationships in the outer subventricular zone of the primate. *Neuron,* 80**,** 442-57.

BLACK, B. L. & OLSON, E. N. 1998. Transcriptional control of muscle development by myocyte enhancer factor-2 (MEF2) proteins. *Annu Rev Cell Dev Biol,* 14**,** 167-96.

BORRELL, V. 2018. How Cells Fold the Cerebral Cortex. *J Neurosci,* 38**,** 776-783.

BOSMAN, E. A., PENN, A. C., AMBROSE, J. C., KETTLEBOROUGH, R., STEMPLE, D. L. & STEEL, K. P. 2005. Multiple mutations in mouse CHD7 provide models for CHARGE syndrome. *Hum Mol Genet,* 14**,** 3463-76.

BOUAZOUNE, K. & KINGSTON, R. E. 2012. Chromatin remodeling by the CHD7 protein is impaired by mutations that cause human developmental disorders. *Proc Natl Acad Sci U S A,* 109**,** 19238-43.

BREKER, M., GYMREK, M. & SCHULDINER, M. 2013. A novel single-cell screening platform reveals proteome plasticity during yeast stress responses. *J Cell Biol,* 200**,** 839-50.

BUDDAY, S., STEINMANN, P. & KUHL, E. 2014. The role of mechanics during brain development. *J Mech Phys Solids,* 72**,** 75-92.

CAO, Y., YAO, Z., SARKAR, D., LAWRENCE, M., SANCHEZ, G. J., PARKER, M. H., MACQUARRIE, K. L., DAVISON, J., MORGAN, M. T., RUZZO, W. L., GENTLEMAN, R. C. & TAPSCOTT, S. J. 2010. Genome-wide MyoD binding in skeletal muscle cells: a potential for broad cellular reprogramming. *Dev Cell,* 18**,** 662-74.

CHAI, M., SANOSAKA, T., OKUNO, H., ZHOU, Z., KOYA, I., BANNO, S., ANDOH-NODA, T., TABATA, Y., SHIMAMURA, R., HAYASHI, T., EBISAWA, M., SASAGAWA, Y., NIKAIDO, I., OKANO, H. & KOHYAMA, J. 2018. Chromatin remodeler CHD7 regulates the stem cell identity of human neural progenitors. *Genes Dev,* 32**,** 165-180.

CHANG, C. H., ZANINI, M., SHIRVANI, H., CHENG, J. S., YU, H., FENG, C. H., MERCIER, A. L., HUNG, S. Y., FORGET, A., WANG, C. H., CIGNA, S. M., LU, I. L., CHEN, W. Y., LEBOUCHER, S., WANG, W. J., RUAT, M., SPASSKY, N., TSAI, J. W. & AYRAULT, O. 2019. Atoh1 Controls Primary Cilia Formation to Allow for SHH-Triggered Granule Neuron Progenitor Proliferation. *Dev Cell,* 48**,** 184-199 e5.

CHANG, C. W., WILKERSON, J. R., HALE, C. F., GIBSON, J. R. & HUBER, K. M. 2017. Distinct stages of synapse elimination are induced by burst firing of CA1 neurons and differentially require MEF2A/D. *Elife,* 6.

CHEN, J., ZHANG, Z., LI, L., CHEN, B. C., REVYAKIN, A., HAJJ, B., LEGANT, W., DAHAN, M., LIONNET, T., BETZIG, E., TJIAN, R. & LIU, Z. 2014. Single-molecule dynamics of enhanceosome assembly in embryonic stem cells. *Cell,* 156**,** 1274-1285.

CHEN, S. X., CHERRY, A., TARI, P. K., PODGORSKI, K., KWONG, Y. K. & HAAS, K. 2012. The transcription factor MEF2 directs developmental visually driven functional and structural metaplasticity. *Cell,* 151**,** 41-55.

CHEN, X., CHANDA, A., IKEUCHI, Y., ZHANG, X., GOODMAN, J. V., REDDY, N. C., MAJIDI, S. P., WU, D. Y., SMITH, S. E., GODEC, A., OLDENBORG, A., GABEL, H. W., ZHAO, G., BONNI, S. & BONNI, A. 2019. The Transcriptional Regulator SnoN Promotes the Proliferation of Cerebellar Granule Neuron Precursors in the Postnatal Mouse Brain. *J Neurosci,* 39**,** 44-62.

CHENG, Y., SUDAROV, A., SZULC, K. U., SGAIER, S. K., STEPHEN, D., TURNBULL, D. H. & JOYNER, A. L. 2010. The Engrailed homeobox genes determine the different foliation patterns in the vermis and hemispheres of the mammalian cerebellum. *Development,* 137**,** 519-29.

CHOLEWA-WACLAW, J., BIRD, A., VON SCHIMMELMANN, M., SCHAEFER, A., YU, H., SONG, H., MADABHUSHI, R. & TSAI, L. H. 2016. The Role of Epigenetic Mechanisms in the Regulation of Gene Expression in the Nervous System. *J Neurosci,* 36**,** 11427-11434.

CLAPIER, C. R., IWASA, J., CAIRNS, B. R. & PETERSON, C. L. 2017. Mechanisms of action and regulation of ATP-dependent chromatin-remodelling complexes. *Nat Rev Mol Cell Biol,* 18**,** 407-422.

COHEN, R., YOKOI, T., HOLLAND, J. P., PEPPER, A. E. & HOLLAND, M. J. 1987. Transcription of the constitutively expressed yeast enolase gene ENO1 is mediated by positive and negative cis-acting regulatory sequences. *Mol Cell Biol,* 7**,** 2753-61.

CONANT, G. C. & WAGNER, A. 2004. Duplicate genes and robustness to transient gene knock-downs in Caenorhabditis elegans. *Proc Biol Sci,* 271**,** 89-96.

COTNEY, J., MUHLE, R. A., SANDERS, S. J., LIU, L., WILLSEY, A. J., NIU, W., LIU, W., KLEI, L., LEI, J., YIN, J., REILLY, S. K., TEBBENKAMP, A. T., BICHSEL, C., PLETIKOS, M., SESTAN, N., ROEDER, K., STATE, M. W., DEVLIN, B. & NOONAN, J. P. 2015. The autism-associated chromatin modifier CHD8 regulates other autism risk genes during human neurodevelopment. *Nat Commun,* 6**,** 6404.

DE DIEULEVEULT, M., YEN, K., HMITOU, I., DEPAUX, A., BOUSSOUAR, F., BOU DARGHAM, D., JOUNIER, S., HUMBERTCLAUDE, H., RIBIERRE, F., BAULARD, C., FARRELL, N. P., PARK, B., KEIME, C., CARRIERE, L., BERLIVET, S., GUT, M., GUT, I., WERNER, M., DELEUZE, J. F., OLASO, R., AUDE, J. C., CHANTALAT, S., PUGH, B. F. & GERARD, M. 2016. Genome-wide nucleosome specificity and function of chromatin remodellers in ES cells. *Nature,* 530**,** 113-6.

DE JUAN ROMERO, C. & BORRELL, V. 2017. Genetic maps and patterns of cerebral cortex folding. *Curr Opin Cell Biol,* 49**,** 31-37.

DE JUAN ROMERO, C., BRUDER, C., TOMASELLO, U., SANZ-ANQUELA, J. M. & BORRELL, V. 2015. Discrete domains of gene expression in germinal layers distinguish the development of gyrencephaly. *EMBO J,* 34**,** 1859-74.

DE LA TORRE-UBIETA, L. & BONNI, A. 2011. Transcriptional regulation of neuronal polarity and morphogenesis in the mammalian brain. *Neuron,* 72**,** 22-40.

DEAN, E. J., DAVIS, J. C., DAVIS, R. W. & PETROV, D. A. 2008. Pervasive and persistent redundancy among duplicated genes in yeast. *PLoS Genet,* 4**,** e1000113.

DEL TORO, D., RUFF, T., CEDERFJALL, E., VILLALBA, A., SEYIT-BREMER, G., BORRELL, V. & KLEIN, R. 2017. Regulation of Cerebral Cortex Folding by Controlling Neuronal Migration via FLRT Adhesion Molecules. *Cell,* 169**,** 621-635 e16.

DELUNA, A., SPRINGER, M., KIRSCHNER, M. W. & KISHONY, R. 2010. Need-based up-regulation of protein levels in response to deletion of their duplicate genes. *PLoS Biol,* 8**,** e1000347.

DELUNA, A., VETSIGIAN, K., SHORESH, N., HEGRENESS, M., COLON-GONZALEZ, M., CHAO, S. & KISHONY, R. 2008. Exposing the fitness contribution of duplicated genes. *Nat Genet,* 40**,** 676-81.

DISS, G., ASCENCIO, D., DELUNA, A. & LANDRY, C. R. 2014. Molecular mechanisms of paralogous compensation and the robustness of cellular networks. *J Exp Zool B Mol Dev Evol,* 322**,** 488-99.

DOI, T., OGATA, T., YAMAUCHI, J., SAWADA, Y., TANAKA, S. & NAGAO, M. 2017. CHD7 Collaborates with Sox2 to Regulate Activation of Oligodendrocyte Precursor Cells after Spinal Cord Injury. *J Neurosci,* 37**,** 10290-10309.

EBERT, D. H. & GREENBERG, M. E. 2013. Activity-dependent neuronal signalling and autism spectrum disorder. *Nature,* 493**,** 327-37.

EFERL, R. & WAGNER, E. F. 2003. AP-1: a double-edged sword in tumorigenesis. *Nat Rev Cancer,* 3**,** 859-68.

EGAN, C. M., NYMAN, U., SKOTTE, J., STREUBEL, G., TURNER, S., O'CONNELL, D. J., RRAKLLI, V., DOLAN, M. J., CHADDERTON, N., HANSEN, K., FARRAR, G. J., HELIN, K., HOLMBERG, J. & BRACKEN, A. P. 2013. CHD5 is required for neurogenesis and has a dual role in facilitating gene expression and polycomb gene repression. *Dev Cell,* 26**,** 223-36.

EL-BROLOSY, M. A., KONTARAKIS, Z., ROSSI, A., KUENNE, C., GUNTHER, S., FUKUDA, N., KIKHI, K., BOEZIO, G. L. M., TAKACS, C. M., LAI, S. L., FUKUDA, R., GERRI, C., GIRALDEZ, A. J. & STAINIER, D. Y. R. 2019. Genetic compensation triggered by mutant mRNA degradation. *Nature,* 568**,** 193-197.

ENGELEN, E., AKINCI, U., BRYNE, J. C., HOU, J., GONTAN, C., MOEN, M., SZUMSKA, D., KOCKX, C., VAN IJCKEN, W., DEKKERS, D. H., DEMMERS, J., RIJKERS, E. J., BHATTACHARYA, S., PHILIPSEN, S., PEVNY, L. H., GROSVELD, F. G., ROTTIER, R. J., LENHARD, B. & POOT, R. A. 2011. Sox2 cooperates with CHD7 to regulate genes that are mutated in human syndromes. *Nat Genet,* 43**,** 607-11.

ERCEG, J., SAUNDERS, T. E., GIRARDOT, C., DEVOS, D. P., HUFNAGEL, L. & FURLONG, E. E. 2014. Subtle changes in motif positioning cause tissue-specific effects on robustness of an enhancer's activity. *PLoS Genet,* 10**,** e1004060.

ESTRELLA, N. L., DESJARDINS, C. A., NOCCO, S. E., CLARK, A. L., MAKSIMENKO, Y. & NAYA, F. J. 2015. MEF2 transcription factors regulate distinct gene programs in mammalian skeletal muscle differentiation. *J Biol Chem,* 290**,** 1256-68.

FARLEY, E. K., OLSON, K. M., ZHANG, W., BRANDT, A. J., ROKHSAR, D. S. & LEVINE, M. S. 2015. Suboptimization of developmental enhancers. *Science,* 350**,** 325-8.

FENG, W., KAWAUCHI, D., KORKEL-QU, H., DENG, H., SERGER, E., SIEBER, L., LIEBERMAN, J. A., JIMENO-GONZALEZ, S., LAMBO, S., HANNA, B. S., HARIM, Y., JANSEN, M., NEUERBURG, A., FRIESEN, O., ZUCKERMANN, M., RAJENDRAN, V., GRONYCH, J., AYRAULT, O., KORSHUNOV, A., JONES, D. T., KOOL, M., NORTHCOTT, P. A., LICHTER, P., CORTES-

LEDESMA, F., PFISTER, S. M. & LIU, H. K. 2017a. CHD7 is indispensable for mammalian brain development through activation of a neuronal differentiation programme. *Nat Commun,* 8**,** 14758.

FENG, W., SHAO, C. & LIU, H. K. 2017b. Versatile Roles of the Chromatin Remodeler CHD7 during Brain Development and Disease. *Front Mol Neurosci,* 10**,** 309.

FLAVELL, S. W., COWAN, C. W., KIM, T. K., GREER, P. L., LIN, Y., PARADIS, S., GRIFFITH, E. C., HU, L. S., CHEN, C. & GREENBERG, M. E. 2006. Activity-dependent regulation of MEF2 transcription factors suppresses excitatory synapse number. *Science,* 311**,** 1008-12.

FLAVELL, S. W., KIM, T. K., GRAY, J. M., HARMIN, D. A., HEMBERG, M., HONG, E. J., MARKENSCOFF-PAPADIMITRIOU, E., BEAR, D. M. & GREENBERG, M. E. 2008. Genome-wide analysis of MEF2 transcriptional program reveals synaptic target genes and neuronal activity-dependent polyadenylation site selection. *Neuron,* 60**,** 1022-38.

FLORIO, M., ALBERT, M., TAVERNA, E., NAMBA, T., BRANDL, H., LEWITUS, E., HAFFNER, C., SYKES, A., WONG, F. K., PETERS, J., GUHR, E., KLEMROTH, S., PRUFER, K., KELSO, J., NAUMANN, R., NUSSLEIN, I., DAHL, A., LACHMANN, R., PAABO, S. & HUTTNER, W. B. 2015. Human-specific gene ARHGAP11B promotes basal progenitor amplification and neocortex expansion. *Science,* 347**,** 1465-70.

FRANK, C. L., LIU, F., WIJAYATUNGE, R., SONG, L., BIEGLER, M. T., YANG, M. G., VOCKLEY, C. M., SAFI, A., GERSBACH, C. A., CRAWFORD, G. E. & WEST, A. E. 2015. Regulation of chromatin accessibility and Zic binding at enhancers in the developing cerebellum. *Nat Neurosci,* 18**,** 647-56.

FRANKEL, N., DAVIS, G. K., VARGAS, D., WANG, S., PAYRE, F. & STERN, D. L. 2010. Phenotypic robustness conferred by apparently redundant transcriptional enhancers. *Nature,* 466**,** 490-3.

FUNFSCHILLING, U. & REICHARDT, L. F. 2002. Cre-mediated recombination in rhombic lip derivatives. *Genesis,* 33**,** 160-9.

FUXMAN BASS, J. I., SAHNI, N., SHRESTHA, S., GARCIA-GONZALEZ, A., MORI, A., BHAT, N., YI, S., HILL, D. E., VIDAL, M. & WALHOUT, A. J. M. 2015. Human gene-centered transcription factor networks for enhancers and disease variants. *Cell,* 161**,** 661-673.

GALLEGOS, D. A., CHAN, U., CHEN, L. F. & WEST, A. E. 2018. Chromatin Regulation of Neuronal Maturation and Plasticity. *Trends Neurosci,* 41**,** 311-324.

GAUDILLIERE, B., SHI, Y. & BONNI, A. 2002. RNA interference reveals a requirement for myocyte enhancer factor 2A in activity-dependent neuronal survival. *J Biol Chem,* 277**,** 46442-6.

GOODMAN, J. V. & BONNI, A. 2019. Regulation of neuronal connectivity in the mammalian brain by chromatin remodeling. *Curr Opin Neurobiol,* 59**,** 59-68.

GREGOIRE, S. & YANG, X. J. 2005. Association with class IIa histone deacetylases upregulates the sumoylation of MEF2 transcription factors. *Mol Cell Biol,* 25**,** 2273-87.

GROSSMAN, S. R., ENGREITZ, J., RAY, J. P., NGUYEN, T. H., HACOHEN, N. & LANDER, E. S. 2018. Positional specificity of different transcription factor classes within enhancers. *Proc Natl Acad Sci U S A,* 115**,** E7222-E7230.

GROVE, C. A., DE MASI, F., BARRASA, M. I., NEWBURGER, D. E., ALKEMA, M. J., BULYK, M. L. & WALHOUT, A. J. 2009. A multiparameter network reveals extensive divergence between C. elegans bHLH transcription factors. *Cell,* 138**,** 314-27.

GU, Z., STEINMETZ, L. M., GU, X., SCHARFE, C., DAVIS, R. W. & LI, W. H. 2003. Role of duplicate genes in genetic robustness against null mutations. *Nature,* 421**,** 63-6.

GUAN, Y., DUNHAM, M. J. & TROYANSKAYA, O. G. 2007. Functional analysis of gene duplications in Saccharomyces cerevisiae. *Genetics,* 175**,** 933-43.

GURDON, J. B., LASKEY R. A., REEVES O. R. 1975. The developmental capacity of nuclei transplanted from keratinized skin cells of adult frogs. *Journal of Embryology and Experimental Morphology* 34, 93–112

HANADA, K., KUROMORI, T., MYOUGA, F., TOYODA, T., LI, W. H. & SHINOZAKI, K. 2009. Evolutionary persistence of functional compensation by duplicate genes in Arabidopsis. *Genome Biol Evol,* 1**,** 409-14.

HARTMAN, J. L. T., GARVIK, B. & HARTWELL, L. 2001. Principles for the buffering of genetic variation. *Science,* 291**,** 1001-4.

HE, D., MARIE, C., ZHAO, C., KIM, B., WANG, J., DENG, Y., CLAVAIROLY, A., FRAH, M., WANG, H., HE, X., HMIDAN, H., JONES, B. V., WITTE, D., ZALC, B., ZHOU, X., CHOO, D. I., MARTIN, D. M., PARRAS, C. & LU, Q. R. 2016. CHD7 cooperates with Sox10 and regulates the onset of CNS myelination and remyelination. *Nat Neurosci,* 19**,** 678-689.

HEINEY, S. A., WOHL, M. P., CHETTIH, S. N., RUFFOLO, L. I. & MEDINA, J. F. 2014. Cerebellar-dependent expression of motor learning during eyeblink conditioning in head-fixed mice. *J Neurosci,* 34**,** 14845-53.

HOFFMANN, A., LEUNG, T. H. & BALTIMORE, D. 2003. Genetic analysis of NF-kappaB/Rel transcription factors defines functional specificities. *EMBO J,* 22**,** 5530-9.

HOLLENHORST, P. C., SHAH, A. A., HOPKINS, C. & GRAVES, B. J. 2007. Genome-wide analyses reveal properties of redundant and specific promoter occupancy within the ETS gene family. *Genes Dev,* 21**,** 1882-94.

HONG, J. W., HENDRIX, D. A. & LEVINE, M. S. 2008. Shadow enhancers as a source of evolutionary novelty. *Science,* 321**,** 1314.

HOTA, S. K. & BRUNEAU, B. G. 2016. ATP-dependent chromatin remodeling during mammalian development. *Development,* 143**,** 2882-97.

HSIAO, T. L. & VITKUP, D. 2008. Role of duplicate genes in robustness against deleterious human mutations. *PLoS Genet,* 4**,** e1000014.

HURLOCK, E. C., BOSE, M., PIERCE, G. & JOHO, R. H. 2009. Rescue of motor coordination by Purkinje cell-targeted restoration of Kv3.3 channels in Kcnc3-null mice requires Kcnc1. *J Neurosci,* 29**,** 15735-44.

JANSSEN, N., BERGMAN, J. E., SWERTZ, M. A., TRANEBJAERG, L., LODAHL, M., SCHOOTS, J., HOFSTRA, R. M., VAN RAVENSWAAIJ-ARTS, C. M. & HOEFSLOOT, L. H. 2012. Mutation update on the CHD7 gene involved in CHARGE syndrome. *Hum Mutat,* 33**,** 1149-60.

JIANG, X., ZHOU, Y., XIAN, L., CHEN, W., WU, H. & GAO, X. 2012. The mutation in CHD7 causes misexpression of Bmp4 and developmental defects in telencephalic midline. *Am J Pathol,* 181**,** 626-41.

JOLMA, A., YAN, J., WHITINGTON, T., TOIVONEN, J., NITTA, K. R., RASTAS, P., MORGUNOVA, E., ENGE, M., TAIPALE, M., WEI, G., PALIN, K., VAQUERIZAS, J. M., VINCENTELLI, R., LUSCOMBE, N. M., HUGHES, T. R., LEMAIRE, P., UKKONEN, E., KIVIOJA, T. & TAIPALE, J. 2013. DNA-binding specificities of human transcription factors. *Cell,* 152**,** 327-39.

JOLMA, A., YIN, Y., NITTA, K. R., DAVE, K., POPOV, A., TAIPALE, M., ENGE, M., KIVIOJA, T., MORGUNOVA, E. & TAIPALE, J. 2015. DNA-dependent formation of transcription factor pairs alters their binding specificity. *Nature,* 527**,** 384-8.

JONGMANS, M. C., ADMIRAAL, R. J., VAN DER DONK, K. P., VISSERS, L. E., BAAS, A. F., KAPUSTA, L., VAN HAGEN, J. M., DONNAI, D., DE RAVEL, T. J., VELTMAN, J. A., GEURTS VAN KESSEL, A., DE VRIES, B. B., BRUNNER, H. G., HOEFSLOOT, L. H. & VAN RAVENSWAAIJ, C. M. 2006. CHARGE syndrome: the phenotypic spectrum of mutations in the CHD7 gene. *J Med Genet,* 43**,** 306-14.

JUNION, G., SPIVAKOV, M., GIRARDOT, C., BRAUN, M., GUSTAFSON, E. H., BIRNEY, E. & FURLONG, E. E. 2012. A transcription factor collective defines cardiac cell fate and reflects lineage history. *Cell,* 148**,** 473-86.

KASAH, S., ODDY, C. & BASSON, M. A. 2018. Autism-linked CHD gene expression patterns during development predict multi-organ disease phenotypes. *J Anat,* 233**,** 755-769.

KAWASHIMA, T., KITAMURA, K., SUZUKI, K., NONAKA, M., KAMIJO, S., TAKEMOTO-KIMURA, S., KANO, M., OKUNO, H., OHKI, K. & BITO, H. 2013. Functional labeling of neurons and their projections using the synthetic activity-dependent promoter E-SARE. *Nat Methods,* 10**,** 889-95.

KIM, A. H., PURAM, S. V., BILIMORIA, P. M., IKEUCHI, Y., KEOUGH, S., WONG, M., ROWITCH, D. & BONNI, A. 2009. A centrosomal Cdc20-APC pathway controls dendrite morphogenesis in postmitotic neurons. *Cell,* 136**,** 322-36.

KIM, T. K., HEMBERG, M., GRAY, J. M., COSTA, A. M., BEAR, D. M., WU, J., HARMIN, D. A., LAPTEWICZ, M., BARBARA-HALEY, K., KUERSTEN, S., MARKENSCOFF-PAPADIMITRIOU, E., KUHL, D., BITO, H., WORLEY, P. F., KREIMAN, G. & GREENBERG, M. E. 2010. Widespread transcription at neuronal activity-regulated enhancers. *Nature,* 465**,** 182-7.

KITANO, H. 2004. Biological robustness. *Nat Rev Genet,* 5**,** 826-37.

KONISHI, Y., STEGMULLER, J., MATSUDA, T., BONNI, S. & BONNI, A. 2004. Cdh1-APC controls axonal growth and patterning in the mammalian brain. *Science,* 303**,** 1026-30.

KROENKE, C. D. & BAYLY, P. V. 2018. How Forces Fold the Cerebral Cortex. *J Neurosci,* 38**,** 767-775.

LAI, W. K. M. & PUGH, B. F. 2017. Understanding nucleosome dynamics and their links to gene expression and DNA replication. *Nat Rev Mol Cell Biol,* 18**,** 548-562.

LAMBERT, S. A., JOLMA, A., CAMPITELLI, L. F., DAS, P. K., YIN, Y., ALBU, M., CHEN, X., TAIPALE, J., HUGHES, T. R. & WEIRAUCH, M. T. 2018. The Human Transcription Factors. *Cell,* 175**,** 598-599.

LAWTON, A. K., ENGSTROM, T., ROHRBACH, D., OMURA, M., TURNBULL, D. H., MAMOU, J., ZHANG, T., SCHWARZ, J. M. & JOYNER, A. L. 2019. Cerebellar folding is initiated by mechanical constraints on a fluid-like layer without a cellular pre-pattern. *Elife,* 8.

LAZZARO, M. A. & PICKETTS, D. J. 2001. Cloning and characterization of the murine Imitation Switch (ISWI) genes: differential expression patterns suggest distinct developmental roles for Snf2h and Snf2l. *J Neurochem,* 77**,** 1145-56.

LEGENDRE, M., ABADIE, V., ATTIE-BITACH, T., PHILIP, N., BUSA, T., BONNEAU, D., COLIN, E., DOLLFUS, H., LACOMBE, D., TOUTAIN, A., BLESSON, S., JULIA, S., MARTIN-COIGNARD, D., GENEVIEVE, D., LEHEUP, B., ODENT, S., JOUK, P. S., MERCIER, S., FAIVRE, L., VINCENT-

DELORME, C., FRANCANNET, C., NAUDION, S., MATHIEU-DRAMARD, M., DELRUE, M. A., GOLDENBERG, A., HERON, D., PARENT, P., TOURAINE, R., LAYET, V., SANLAVILLE, D., QUELIN, C., MOUTTON, S., FRADIN, M., JACQUETTE, A., SIGAUDY, S., PINSON, L., SARDA, P., GUERROT, A. M., ROSSI, M., MASUREL-PAULET, A., EL CHEHADEH, S., PIGUEL, X., RODRIGUEZ-BALLESTEROS, M., RAGOT, S., LYONNET, S., BILAN, F. & GILBERT-DUSSARDIER, B. 2017. Phenotype and genotype analysis of a French cohort of 119 patients with CHARGE syndrome. *Am J Med Genet C Semin Med Genet,* 175**,** 417-430.

LEGENDRE, M., GONZALES, M., GOUDEFROYE, G., BILAN, F., PARISOT, P., PEREZ, M. J., BONNIERE, M., BESSIERES, B., MARTINOVIC, J., DELEZOIDE, A. L., JOSSIC, F., FALLET-BIANCO, C., BUCOURT, M., TANTAU, J., LOGET, P., LOEUILLET, L., LAURENT, N., LEROY, B., SALHI, H., BIGI, N., ROULEAU, C., GUIMIOT, F., QUELIN, C., BAZIN, A., ALBY, C., ICHKOU, A., GESNY, R., KITZIS, A., VILLE, Y., LYONNET, S., RAZAVI, F., GILBERT-DUSSARDIER, B., VEKEMANS, M. & ATTIE-BITACH, T. 2012. Antenatal spectrum of CHARGE syndrome in 40 fetuses with CHD7 mutations. *J Med Genet,* 49**,** 698-707.

LEGUE, E., GOTTSHALL, J. L., JAUMOUILLE, E., ROSELLO-DIEZ, A., SHI, W., BARRAZA, L. H., WASHINGTON, S., GRANT, R. L. & JOYNER, A. L. 2016. Differential timing of granule cell production during cerebellum development underlies generation of the foliation pattern. *Neural Dev,* 11**,** 17.

LEGUE, E., RIEDEL, E. & JOYNER, A. L. 2015. Clonal analysis reveals granule cell behaviors and compartmentalization that determine the folded morphology of the cerebellum. *Development,* 142**,** 1661-71.

LEJEUNE, E., DORTDIVANLIOGLU, B., KUHL, E. & LINDER, C. 2019. Understanding the mechanical link between oriented cell division and cerebellar morphogenesis. *Soft Matter,* 15**,** 2204-2215.

LESSARD, J., WU, J. I., RANISH, J. A., WAN, M., WINSLOW, M. M., STAAHL, B. T., WU, H., AEBERSOLD, R., GRAEF, I. A. & CRABTREE, G. R. 2007. An essential switch in subunit composition of a chromatin remodeling complex during neural development. *Neuron,* 55**,** 201-15.

LEVINE, M. & TJIAN, R. 2003. Transcription regulation and animal diversity. *Nature,* 424**,** 147-51.

LI, M., SANTPERE, G., IMAMURA KAWASAWA, Y., EVGRAFOV, O. V., GULDEN, F. O., POCHAREDDY, S., SUNKIN, S. M., LI, Z., SHIN, Y., ZHU, Y., SOUSA, A. M. M., WERLING, D. M., KITCHEN, R. R., KANG, H. J., PLETIKOS, M., CHOI, J., MUCHNIK, S., XU, X., WANG, D., LORENTE-GALDOS, B., LIU, S., GIUSTI-RODRIGUEZ, P., WON, H., DE LEEUW, C. A., PARDINAS, A. F., HU, M., JIN, F., LI, Y., OWEN, M. J., O'DONOVAN, M. C., WALTERS, J. T. R., POSTHUMA, D., REIMERS, M. A., LEVITT, P., WEINBERGER, D. R., HYDE, T. M., KLEINMAN, J. E., GESCHWIND, D. H., HAWRYLYCZ, M. J., STATE, M. W., SANDERS, S. J., SULLIVAN, P. F., GERSTEIN, M. B., LEIN, E. S., KNOWLES, J. A. & SESTAN, N. 2018. Integrative functional genomic analysis of human brain development and neuropsychiatric risks. *Science,* 362.

LI, X. Y., MACARTHUR, S., BOURGON, R., NIX, D., POLLARD, D. A., IYER, V. N., HECHMER, A., SIMIRENKO, L., STAPLETON, M., LUENGO HENDRIKS, C. L., CHU, H. C., OGAWA, N., INWOOD, W., SEMENTCHENKO, V., BEATON, A., WEISZMANN, R., CELNIKER, S. E., KNOWLES, D. W., GINGERAS, T., SPEED, T. P., EISEN, M. B. & BIGGIN, M. D. 2008.

Transcription factors bind thousands of active and inactive regions in the Drosophila blastoderm. *PLoS Biol,* 6**,** e27.

LIN, X. & BULLEIT, R. F. 1996. Cell intrinsic mechanisms regulate mouse cerebellar granule neuron differentiation. *Neurosci Lett,* 220**,** 81-4.

LIPTON, S. A., LI, H., ZAREMBA, J. D., MCKERCHER, S. R., CUI, J., KANG, Y. J., NIE, Z., SOUSSOU, W., TALANTOVA, M., OKAMOTO, S. & NAKANISHI, N. 2009. Autistic phenotype from MEF2C knockout cells. *Science,* 323**,** 208.

LLINARES-BENADERO, C. & BORRELL, V. 2019. Deconstructing cortical folding: genetic, cellular and mechanical determinants. *Nat Rev Neurosci,* 20**,** 161-176.

LOHMANN, G., VON CRAMON, D. Y. & COLCHESTER, A. C. 2008. Deep sulcal landmarks provide an organizing framework for human cortical folding. *Cereb Cortex,* 18**,** 1415-20.

LONG, H. K., PRESCOTT, S. L. & WYSOCKA, J. 2016. Ever-Changing Landscapes: Transcriptional Enhancers in Development and Evolution. *Cell,* 167**,** 1170-1187.

LUNA-ZURITA, L., STIRNIMANN, C. U., GLATT, S., KAYNAK, B. L., THOMAS, S., BAUDIN, F., SAMEE, M. A., HE, D., SMALL, E. M., MILEIKOVSKY, M., NAGY, A., HOLLOWAY, A. K., POLLARD, K. S., MULLER, C. W. & BRUNEAU, B. G. 2016. Complex Interdependence Regulates Heterotypic Transcription Factor Distribution and Coordinates Cardiogenesis. *Cell,* 164**,** 999-1014.

LYONS, G. E., MICALES, B. K., SCHWARZ, J., MARTIN, J. F. & OLSON, E. N. 1995. Expression of mef2 genes in the mouse central nervous system suggests a role in neuronal maturation. *J Neurosci,* 15**,** 5727-38.

LYONS, M. R., SCHWARZ, C. M. & WEST, A. E. 2012. Members of the myocyte enhancer factor 2 transcription factor family differentially regulate Bdnf transcription in response to neuronal depolarization. *J Neurosci,* 32**,** 12780-5.

MA, K., CHAN, J. K., ZHU, G. & WU, Z. 2005. Myocyte enhancer factor 2 acetylation by p300 enhances its DNA binding activity, transcriptional activity, and myogenic differentiation. *Mol Cell Biol,* 25**,** 3575-82.

MA, Q. & TELESE, F. 2015. Genome-wide epigenetic analysis of MEF2A and MEF2C transcription factors in mouse cortical neurons. *Commun Integr Biol,* 8**,** e1087624.

MACNEIL, L. T. & WALHOUT, A. J. 2011. Gene regulatory networks and the role of robustness and stochasticity in the control of gene expression. *Genome Res,* 21**,** 645-57.

MALIK, A. N., VIERBUCHEN, T., HEMBERG, M., RUBIN, A. A., LING, E., COUCH, C. H., STROUD, H., SPIEGEL, I., FARH, K. K., HARMIN, D. A. & GREENBERG, M. E. 2014. Genome-wide identification and characterization of functional neuronal activity-dependent enhancers. *Nat Neurosci,* 17**,** 1330-9.

MANNING, B. J. & YUSUFZAI, T. 2017. The ATP-dependent chromatin remodeling enzymes CHD6, CHD7, and CHD8 exhibit distinct nucleosome binding and remodeling activities. *J Biol Chem,* 292**,** 11927-11936.

MARTIN, D. M. 2010. Chromatin remodeling in development and disease: focus on CHD7. *PLoS Genet,* 6**,** e1001010.

MARTINEZ, S., ANDREU, A., MECKLENBURG, N. & ECHEVARRIA, D. 2013. Cellular and molecular basis of cerebellar development. *Front Neuroanat,* 7**,** 18.

MAZZONI, E. O., MAHONY, S., CLOSSER, M., MORRISON, C. A., NEDELEC, S., WILLIAMS, D. J., AN, D., GIFFORD, D. K. & WICHTERLE, H. 2013. Synergistic binding of transcription factors to cell-specific enhancers programs motor neuron identity. *Nat Neurosci,* 16**,** 1219-27.

MELLEN, M., AYATA, P., DEWELL, S., KRIAUCIONIS, S. & HEINTZ, N. 2012. MeCP2 binds to 5hmC enriched within active genes and accessible chromatin in the nervous system. *Cell,* 151**,** 1417-30.

MESSINA, D. N., GLASSCOCK, J., GISH, W. & LOVETT, M. 2004. An ORFeome-based analysis of human transcription factor genes and the construction of a microarray to interrogate their expression. *Genome Res,* 14**,** 2041-7.

MILLER, J. A. & WIDOM, J. 2003. Collaborative competition mechanism for gene activation in vivo. *Mol Cell Biol,* 23**,** 1623-32.

MITERKO, L. N., LACKEY, E. P., HECK, D. H. & SILLITOE, R. V. 2018. Shaping Diversity Into the Brain's Form and Function. *Front Neural Circuits,* 12**,** 83.

MOLYNEAUX, B. J., ARLOTTA, P., MENEZES, J. R. & MACKLIS, J. D. 2007. Neuronal subtype specification in the cerebral cortex. *Nat Rev Neurosci,* 8**,** 427-37.

NARAYANAN, R., PIROUZ, M., KERIMOGLU, C., PHAM, L., WAGENER, R. J., KISZKA, K. A., ROSENBUSCH, J., SEONG, R. H., KESSEL, M., FISCHER, A., STOYKOVA, A., STAIGER, J. F. & TUOC, T. 2015. Loss of BAF (mSWI/SNF) Complexes Causes Global Transcriptional and Chromatin State Changes in Forebrain Development. *Cell Rep,* 13**,** 1842-54.

NITARSKA, J., SMITH, J. G., SHERLOCK, W. T., HILLEGE, M. M., NOTT, A., BARSHOP, W. D., VASHISHT, A. A., WOHLSCHLEGEL, J. A., MITTER, R. & RICCIO, A. 2016. A Functional Switch of NuRD Chromatin Remodeling Complex Subunits Regulates Mouse Cortical Development. *Cell Rep,* 17**,** 1683-1698.

NONAKA-KINOSHITA, M., REILLO, I., ARTEGIANI, B., MARTINEZ-MARTINEZ, M. A., NELSON, M., BORRELL, V. & CALEGARI, F. 2013. Regulation of cerebral cortex size and folding by expansion of basal progenitors. *EMBO J,* 32**,** 1817-28.

O'ROAK, B. J., STESSMAN, H. A., BOYLE, E. A., WITHERSPOON, K. T., MARTIN, B., LEE, C., VIVES, L., BAKER, C., HIATT, J. B., NICKERSON, D. A., BERNIER, R., SHENDURE, J. & EICHLER, E. E. 2014. Recurrent de novo mutations implicate novel genes underlying simplex autism risk. *Nat Commun,* 5**,** 5595.

O'ROAK, B. J., VIVES, L., GIRIRAJAN, S., KARAKOC, E., KRUMM, N., COE, B. P., LEVY, R., KO, A., LEE, C., SMITH, J. D., TURNER, E. H., STANAWAY, I. B., VERNOT, B., MALIG, M., BAKER, C., REILLY, B., AKEY, J. M., BORENSTEIN, E., RIEDER, M. J., NICKERSON, D. A., BERNIER, R., SHENDURE, J. & EICHLER, E. E. 2012. Sporadic autism exomes reveal a highly interconnected protein network of de novo mutations. *Nature,* 485**,** 246-50.

PACIORKOWSKI, A. R., TRAYLOR, R. N., ROSENFELD, J. A., HOOVER, J. M., HARRIS, C. J., WINTER, S., LACASSIE, Y., BIALER, M., LAMB, A. N., SCHULTZ, R. A., BERRY-KRAVIS, E., PORTER, B. E., FALK, M., VENKAT, A., VANZO, R. J., COHEN, J. S., FATEMI, A., DOBYNS, W. B., SHAFFER, L. G., BALLIF, B. C. & MARSH, E. D. 2013. MEF2C Haploinsufficiency features consistent hyperkinesis, variable epilepsy, and has a role in dorsal and ventral neuronal developmental pathways. *Neurogenetics,* 14**,** 99-111.

PERRY, M. W., BOETTIGER, A. N., BOTHMA, J. P. & LEVINE, M. 2010. Shadow enhancers foster robustness of Drosophila gastrulation. *Curr Biol,* 20**,** 1562-7.

PFEIFFER, B. E., ZANG, T., WILKERSON, J. R., TANIGUCHI, M., MAKSIMOVA, M. A., SMITH, L. N., COWAN, C. W. & HUBER, K. M. 2010. Fragile X mental retardation protein is required for synapse elimination by the activity-dependent transcription factor MEF2. *Neuron,* 66**,** 191-7.

PIAO, X., CHANG, B. S., BODELL, A., WOODS, K., BENZEEV, B., TOPCU, M., GUERRINI, R., GOLDBERG-STERN, H., SZTRIHA, L., DOBYNS, W. B., BARKOVICH, A. J. & WALSH, C. A. 2005. Genotype-phenotype analysis of human frontoparietal polymicrogyria syndromes. *Ann Neurol,* 58**,** 680-7.

PORCELLI, D., FISCHER, B., RUSSELL, S. & WHITE, R. 2019. Chromatin accessibility plays a key role in selective targeting of Hox proteins. *Genome Biol,* 20**,** 115.

PORTER, R. S., JAAMOUR, F. & IWASE, S. 2018. Neuron-specific alternative splicing of transcriptional machineries: Implications for neurodevelopmental disorders. *Mol Cell Neurosci,* 87**,** 35-45.

POTTHOFF, M. J. & OLSON, E. N. 2007. MEF2: a central regulator of diverse developmental programs. *Development,* 134**,** 4131-40.

PUC, J. & ROSENFELD, M. G. 2011. SOX2 and CHD7 cooperatively regulate human disease genes. *Nat Genet,* 43**,** 505-6.

PULIMOOD, N. S., RODRIGUES, W. D. S. J., ATKINSON, D. A., MOONEY, S. M. & MEDINA, A. E. 2017. The Role of CREB, SRF, and MEF2 in Activity-Dependent Neuronal Plasticity in the Visual Cortex. *J Neurosci,* 37**,** 6628-6637.

PULIPPARACHARUVIL, S., RENTHAL, W., HALE, C. F., TANIGUCHI, M., XIAO, G., KUMAR, A., RUSSO, S. J., SIKDER, D., DEWEY, C. M., DAVIS, M. M., GREENGARD, P., NAIRN, A. C., NESTLER, E. J. & COWAN, C. W. 2008. Cocaine regulates MEF2 to control synaptic and behavioral plasticity. *Neuron,* 59**,** 621-33.

PURAM, S. V., RICCIO, A., KOIRALA, S., IKEUCHI, Y., KIM, A. H., CORFAS, G. & BONNI, A. 2011. A TRPC5-regulated calcium signaling pathway controls dendrite patterning in the mammalian brain. *Genes Dev,* 25**,** 2659-73.

RAJKOVICH, K. E., LOERWALD, K. W., HALE, C. F., HESS, C. T., GIBSON, J. R. & HUBER, K. M. 2017. Experience-Dependent and Differential Regulation of Local and Long-Range Excitatory Neocortical Circuits by Postsynaptic Mef2c. *Neuron,* 93**,** 48-56.

RASHID, A. J., COLE, C. J. & JOSSELYN, S. A. 2014. Emerging roles for MEF2 transcription factors in memory. *Genes Brain Behav,* 13**,** 118-25.

REECE-HOYES, J. S., PONS, C., DIALLO, A., MORI, A., SHRESTHA, S., KADREPPA, S., NELSON, J., DIPRIMA, S., DRICOT, A., LAJOIE, B. R., RIBEIRO, P. S., WEIRAUCH, M. T., HILL, D. E., HUGHES, T. R., MYERS, C. L. & WALHOUT, A. J. 2013. Extensive rewiring and complex evolutionary dynamics in a C. elegans multiparameter transcription factor network. *Mol Cell,* 51**,** 116-27.

REILLO, I., DE JUAN ROMERO, C., GARCIA-CABEZAS, M. A. & BORRELL, V. 2011. A role for intermediate radial glia in the tangential expansion of the mammalian cerebral cortex. *Cereb Cortex,* 21**,** 1674-94.

REIK, W. 2007. Stability and flexibility of epigenetic gene regulation in mammalian development. *Nature*, 447(7143):425-32.

REITER, F., WIENERROITHER, S. & STARK, A. 2017. Combinatorial function of transcription factors and cofactors. *Curr Opin Genet Dev,* 43**,** 73-81.

RICHMAN, D. P., STEWART, R. M., HUTCHINSON, J. W. & CAVINESS, V. S., JR. 1975. Mechanical model of brain convolutional development. *Science,* 189**,** 18-21.

RONAN, J. L., WU, W. & CRABTREE, G. R. 2013. From neural development to cognition: unexpected roles for chromatin. *Nat Rev Genet,* 14**,** 347-59.

ROUSSEL, M. F. & HATTEN, M. E. 2011. Cerebellum development and medulloblastoma. *Curr Top Dev Biol,* 94**,** 235-82.

SAUNDERS, A., MACOSKO, E. Z., WYSOKER, A., GOLDMAN, M., KRIENEN, F. M., DE RIVERA, H., BIEN, E., BAUM, M., BORTOLIN, L., WANG, S., GOEVA, A., NEMESH, J., KAMITAKI, N., BRUMBAUGH, S., KULP, D. & MCCARROLL, S. A. 2018. Molecular Diversity and Specializations among the Cells of the Adult Mouse Brain. *Cell,* 174**,** 1015-1030.e16.

SHALIZI, A., BILIMORIA, P. M., STEGMULLER, J., GAUDILLIERE, B., YANG, Y., SHUAI, K. & BONNI, A. 2007. PIASx is a MEF2 SUMO E3 ligase that promotes postsynaptic dendritic morphogenesis. *J Neurosci,* 27**,** 10037-46.

SHALIZI, A., GAUDILLIERE, B., YUAN, Z., STEGMULLER, J., SHIROGANE, T., GE, Q., TAN, Y., SCHULMAN, B., HARPER, J. W. & BONNI, A. 2006. A calcium-regulated MEF2 sumoylation switch controls postsynaptic differentiation. *Science,* 311**,** 1012-7.

SHALIZI, A., LEHTINEN, M., GAUDILLIERE, B., DONOVAN, N., HAN, J., KONISHI, Y. & BONNI, A. 2003. Characterization of a neurotrophin signaling mechanism that mediates neuron survival in a temporally specific pattern. *J Neurosci,* 23**,** 7326-36.

SHALIZI, A. K. & BONNI, A. 2005. brawn for brains: the role of MEF2 proteins in the developing nervous system. *Curr Top Dev Biol,* 69**,** 239-66.

SHARMA, N., POLLINA, E. A., NAGY, M. A., YAP, E. L., DIBIASE, F. A., HRVATIN, S., HU, L., LIN, C. & GREENBERG, M. E. 2019. ARNT2 Tunes Activity-Dependent Gene Expression through NCoR2-Mediated Repression and NPAS4-Mediated Activation. *Neuron*.

SHEN, N., ZHAO, J., SCHIPPER, J. L., ZHANG, Y., BEPLER, T., LEEHR, D., BRADLEY, J., HORTON, J., LAPP, H. & GORDAN, R. 2018. Divergence in DNA Specificity among Paralogous Transcription Factors Contributes to Their Differential In Vivo Binding. *Cell Syst,* 6**,** 470-483.e8.

SHENG, M. & GREENBERG, M. E. 1990. The regulation and function of c-fos and other immediate early genes in the nervous system. *Neuron,* 4**,** 477-85.

SIERSBAEK, R., RABIEE, A., NIELSEN, R., SIDOLI, S., TRAYNOR, S., LOFT, A., POULSEN, L. C., ROGOWSKA-WRZESINSKA, A., JENSEN, O. N. & MANDRUP, S. 2014. Transcription factor cooperativity in early adipogenic hotspots and super-enhancers. *Cell Rep,* 7**,** 1443-1455.

SILLITOE, R. V., STEPHEN, D., LAO, Z. & JOYNER, A. L. 2008. Engrailed homeobox genes determine the organization of Purkinje cell sagittal stripe gene expression in the adult cerebellum. *J Neurosci,* 28**,** 12150-62.

SLATTERY, M., RILEY, T., LIU, P., ABE, N., GOMEZ-ALCALA, P., DROR, I., ZHOU, T., ROHS, R., HONIG, B., BUSSEMAKER, H. J. & MANN, R. S. 2011. Cofactor binding evokes latent differences in DNA binding specificity between Hox proteins. *Cell,* 147**,** 1270-82.

SMITH, R. P., TAHER, L., PATWARDHAN, R. P., KIM, M. J., INOUE, F., SHENDURE, J., OVCHARENKO, I. & AHITUV, N. 2013. Massively parallel decoding of mammalian

regulatory sequences supports a flexible organizational model. *Nat Genet,* 45**,** 1021-1028.
SOKPOR, G., XIE, Y., ROSENBUSCH, J. & TUOC, T. 2017. Chromatin Remodeling BAF (SWI/SNF) Complexes in Neural Development and Disorders. *Front Mol Neurosci,* 10**,** 243.
SON, E. Y. & CRABTREE, G. R. 2014. The role of BAF (mSWI/SNF) complexes in mammalian neural development. *Am J Med Genet C Semin Med Genet,* 166C**,** 333-49.
SPITZ, F. & FURLONG, E. E. 2012. Transcription factors: from enhancer binding to developmental control. *Nat Rev Genet,* 13**,** 613-26.
SRINIVASAN, S., DORIGHI, K. M. & TAMKUN, J. W. 2008. Drosophila Kismet regulates histone H3 lysine 27 methylation and early elongation by RNA polymerase II. *PLoS Genet,* 4**,** e1000217.
STAHL, R., WALCHER, T., DE JUAN ROMERO, C., PILZ, G. A., CAPPELLO, S., IRMLER, M., SANZ-AQUELA, J. M., BECKERS, J., BLUM, R., BORRELL, V. & GOTZ, M. 2013. Trnp1 regulates expansion and folding of the mammalian cerebral cortex by control of radial glial fate. *Cell,* 153**,** 535-49.
STOPKA, T. & SKOULTCHI, A. I. 2003. The ISWI ATPase Snf2h is required for early mouse development. *Proc Natl Acad Sci U S A,* 100**,** 14097-102.
SU, Y., SHIN, J., ZHONG, C., WANG, S., ROYCHOWDHURY, P., LIM, J., KIM, D., MING, G. L. & SONG, H. 2017. Neuronal activity modifies the chromatin accessibility landscape in the adult brain. *Nat Neurosci,* 20**,** 476-483.
SUDAROV, A. & JOYNER, A. L. 2007. Cerebellum morphogenesis: the foliation pattern is orchestrated by multi-cellular anchoring centers. *Neural Dev,* 2**,** 26.
SUDHOF, T. C. 2017. Molecular Neuroscience in the 21(st) Century: A Personal Perspective. *Neuron,* 96**,** 536-541.
TAKAHASHI, K. & YAMANAKA, S. 2006. Induction of pluripotent stem cells from mouse embryonic and adult fibroblast cultures by defined factors. *Cell,* 126**,** 663-76.
TEICHMANN, S. A. & BABU, M. M. 2004. Gene regulatory network growth by duplication. *Nat Genet,* 36**,** 492-6.
TELESE, F., MA, Q., PEREZ, P. M., NOTANI, D., OH, S., LI, W., COMOLETTI, D., OHGI, K. A., TAYLOR, H. & ROSENFELD, M. G. 2015. LRP8-Reelin-Regulated Neuronal Enhancer Signature Underlying Learning and Memory Formation. *Neuron,* 86**,** 696-710.
THANOS, D. & MANIATIS, T. 1995. Virus induction of human IFN beta gene expression requires the assembly of an enhanceosome. *Cell,* 83**,** 1091-100.
TSAI, N. P., WILKERSON, J. R., GUO, W., MAKSIMOVA, M. A., DEMARTINO, G. N., COWAN, C. W. & HUBER, K. M. 2012. Multiple autism-linked genes mediate synapse elimination via proteasomal degradation of a synaptic scaffold PSD-95. *Cell,* 151**,** 1581-94.
TU, S., AKHTAR, M. W., ESCORIHUELA, R. M., AMADOR-ARJONA, A., SWARUP, V., PARKER, J., ZAREMBA, J. D., HOLLAND, T., BANSAL, N., HOLOHAN, D. R., LOPEZ, K., RYAN, S. D., CHAN, S. F., YAN, L., ZHANG, X., HUANG, X., SULTAN, A., MCKERCHER, S. R., AMBASUDHAN, R., XU, H., WANG, Y., GESCHWIND, D. H., ROBERTS, A. J., TERSKIKH, A. V., RISSMAN, R. A., MASLIAH, E., LIPTON, S. A. & NAKANISHI, N. 2017. NitroSynapsin therapy for a mouse MEF2C haploinsufficiency model of human autism. *Nat Commun,* 8**,** 1488.

VALNEGRI, P., HUANG, J., YAMADA, T., YANG, Y., MEJIA, L. A., CHO, H. Y., OLDENBORG, A. & BONNI, A. 2017. RNF8/UBC13 ubiquitin signaling suppresses synapse formation in the mammalian brain. *Nat Commun,* 8**,** 1271.

VAN ESSEN, D. C. 1997. A tension-based theory of morphogenesis and compact wiring in the central nervous system. *Nature,* 385**,** 313-8.

VAN RAVENSWAAIJ-ARTS, C. & MARTIN, D. M. 2017. New insights and advances in CHARGE syndrome: Diagnosis, etiologies, treatments, and research discoveries. *Am J Med Genet C Semin Med Genet,* 175**,** 397-406.

VETERE, G., RESTIVO, L., COLE, C. J., ROSS, P. J., AMMASSARI-TEULE, M., JOSSELYN, S. A. & FRANKLAND, P. W. 2011. Spine growth in the anterior cingulate cortex is necessary for the consolidation of contextual fear memory. *Proc Natl Acad Sci U S A,* 108**,** 8456-60.

VIERBUCHEN, T., LING, E., COWLEY, C. J., COUCH, C. H., WANG, X., HARMIN, D. A., ROBERTS, C. W. M. & GREENBERG, M. E. 2017. AP-1 Transcription Factors and the BAF Complex Mediate Signal-Dependent Enhancer Selection. *Mol Cell,* 68**,** 1067-1082.e12.

VOSS, T. C. & HAGER, G. L. 2014. Dynamic regulation of transcriptional states by chromatin and transcription factors. *Nat Rev Genet,* 15**,** 69-81.

WANG, L., HOU, S. & HAN, Y. G. 2016. Hedgehog signaling promotes basal progenitor expansion and the growth and folding of the neocortex. *Nat Neurosci,* 19**,** 888-96.

WEI, G. H., BADIS, G., BERGER, M. F., KIVIOJA, T., PALIN, K., ENGE, M., BONKE, M., JOLMA, A., VARJOSALO, M., GEHRKE, A. R., YAN, J., TALUKDER, S., TURUNEN, M., TAIPALE, M., STUNNENBERG, H. G., UKKONEN, E., HUGHES, T. R., BULYK, M. L. & TAIPALE, J. 2010. Genome-wide analysis of ETS-family DNA-binding in vitro and in vivo. *Embo j,* 29**,** 2147-60.

WEIRAUCH, M. T., YANG, A., ALBU, M., COTE, A. G., MONTENEGRO-MONTERO, A., DREWE, P., NAJAFABADI, H. S., LAMBERT, S. A., MANN, I., COOK, K., ZHENG, H., GOITY, A., VAN BAKEL, H., LOZANO, J. C., GALLI, M., LEWSEY, M. G., HUANG, E., MUKHERJEE, T., CHEN, X., REECE-HOYES, J. S., GOVINDARAJAN, S., SHAULSKY, G., WALHOUT, A. J. M., BOUGET, F. Y., RATSCH, G., LARRONDO, L. F., ECKER, J. R. & HUGHES, T. R. 2014. Determination and inference of eukaryotic transcription factor sequence specificity. *Cell,* 158**,** 1431-1443.

WERNER, T., HAMMER, A., WAHLBUHL, M., BOSL, M. R. & WEGNER, M. 2007. Multiple conserved regulatory elements with overlapping functions determine Sox10 expression in mouse embryogenesis. *Nucleic Acids Res,* 35**,** 6526-38.

WEST, A. E. & GREENBERG, M. E. 2011. Neuronal activity-regulated gene transcription in synapse development and cognitive function. *Cold Spring Harb Perspect Biol,* 3.

WHITE, J. J., ARANCILLO, M., STAY, T. L., GEORGE-JONES, N. A., LEVY, S. L., HECK, D. H. & SILLITOE, R. V. 2014. Cerebellar zonal patterning relies on Purkinje cell neurotransmission. *J Neurosci,* 34**,** 8231-45.

WHITE, J. K., GERDIN, A. K., KARP, N. A., RYDER, E., BULJAN, M., BUSSELL, J. N., SALISBURY, J., CLARE, S., INGHAM, N. J., PODRINI, C., HOUGHTON, R., ESTABEL, J., BOTTOMLEY, J. R., MELVIN, D. G., SUNTER, D., ADAMS, N. C., SANGER INSTITUTE MOUSE GENETICS, P., TANNAHILL, D., LOGAN, D. W., MACARTHUR, D. G., FLINT, J., MAHAJAN, V. B., TSANG, S. H., SMYTH, I., WATT, F. M., SKARNES, W. C., DOUGAN, G., ADAMS, D. J., RAMIREZ-SOLIS,

R., BRADLEY, A. & STEEL, K. P. 2013. Genome-wide generation and systematic phenotyping of knockout mice reveals new roles for many genes. *Cell,* 154**,** 452-64.
WHITE, M. A., KWASNIESKI, J. C., MYERS, C. A., SHEN, S. Q., CORBO, J. C. & COHEN, B. A. 2016. A Simple Grammar Defines Activating and Repressing cis-Regulatory Elements in Photoreceptors. *Cell Rep,* 17**,** 1247-1254.
WHITTAKER, D. E., KASAH, S., DONOVAN, A. P. A., ELLEGOOD, J., RIEGMAN, K. L. H., VOLK, H. A., MCGONNELL, I., LERCH, J. P. & BASSON, M. A. 2017. Distinct cerebellar foliation anomalies in a CHD7 haploinsufficient mouse model of CHARGE syndrome. *Am J Med Genet C Semin Med Genet,* 175.
WILMUT, I., SCHNIEKE, A. E., MCWHIR, J., KIND, A.J., CAMPBELL, K. H. S. 2007. Viable offspring derived from fetal and adult mammalian cells. *Nature* 385, 810–813
WU, J. I., LESSARD, J., OLAVE, I. A., QIU, Z., GHOSH, A., GRAEF, I. A. & CRABTREE, G. R. 2007. Regulation of dendritic development by neuron-specific chromatin remodeling complexes. *Neuron,* 56**,** 94-108.
WU, W., DE FOLTER, S., SHEN, X., ZHANG, W. & TAO, S. 2011. Vertebrate paralogous MEF2 genes: origin, conservation, and evolution. *PLoS One,* 6**,** e17334.
WU, Y., DEY, R., HAN, A., JAYATHILAKA, N., PHILIPS, M., YE, J. & CHEN, L. 2010. Structure of the MADS-box/MEF2 domain of MEF2A bound to DNA and its implication for myocardin recruitment. *J Mol Biol,* 397**,** 520-33.
XU, G., KNUTSEN, A. K., DIKRANIAN, K., KROENKE, C. D., BAYLY, P. V. & TABER, L. A. 2010. Axons pull on the brain, but tension does not drive cortical folding. *J Biomech Eng,* 132**,** 071013.
YAMADA, T., YANG, Y., HEMBERG, M., YOSHIDA, T., CHO, H. Y., MURPHY, J. P., FIORAVANTE, D., REGEHR, W. G., GYGI, S. P., GEORGOPOULOS, K. & BONNI, A. 2014. Promoter decommissioning by the NuRD chromatin remodeling complex triggers synaptic connectivity in the mammalian brain. *Neuron,* 83**,** 122-34.
YAMADA, T., YANG, Y., HUANG, J., COPPOLA, G., GESCHWIND, D. H. & BONNI, A. 2013. Sumoylated MEF2A coordinately eliminates orphan presynaptic sites and promotes maturation of presynaptic boutons. *J Neurosci,* 33**,** 4726-40.
YAMADA, T., YANG, Y., VALNEGRI, P., JURIC, I., ABNOUSI, A., MARKWALTER, K. H., GUTHRIE, A. N., GODEC, A., OLDENBORG, A., HU, M., HOLY, T. E. & BONNI, A. 2019. Sensory experience remodels genome architecture in neural circuit to drive motor learning. *Nature*.
YANG, Y., KIM, A. H., YAMADA, T., WU, B., BILIMORIA, P. M., IKEUCHI, Y., DE LA IGLESIA, N., SHEN, J. & BONNI, A. 2009. A Cdc20-APC ubiquitin signaling pathway regulates presynaptic differentiation. *Science,* 326**,** 575-8.
YANG, Y., YAMADA, T., HILL, K. K., HEMBERG, M., REDDY, N. C., CHO, H. Y., GUTHRIE, A. N., OLDENBORG, A., HEINEY, S. A., OHMAE, S., MEDINA, J. F., HOLY, T. E. & BONNI, A. 2016. Chromatin remodeling inactivates activity genes and regulates neural coding. *Science,* 353**,** 300-305.
YAP, E. L. & GREENBERG, M. E. 2018. Activity-Regulated Transcription: Bridging the Gap between Neural Activity and Behavior. *Neuron,* 100**,** 330-348.

YIP, D. J., CORCORAN, C. P., ALVAREZ-SAAVEDRA, M., DEMARIA, A., RENNICK, S., MEARS, A. J., RUDNICKI, M. A., MESSIER, C. & PICKETTS, D. J. 2012. Snf2l regulates Foxg1-dependent progenitor cell expansion in the developing brain. *Dev Cell,* 22**,** 871-8.

YU, T., MEINERS, L. C., DANIELSEN, K., WONG, M. T., BOWLER, T., REINBERG, D., SCAMBLER, P. J., VAN RAVENSWAAIJ-ARTS, C. M. & BASSON, M. A. 2013. Deregulated FGF and homeotic gene expression underlies cerebellar vermis hypoplasia in CHARGE syndrome. *Elife,* 2**,** e01305.

ZARET, K. S. & CARROLL, J. S. 2011. Pioneer transcription factors: establishing competence for gene expression. *Genes Dev,* 25**,** 2227-41.

ZENTNER, G. E., LAYMAN, W. S., MARTIN, D. M. & SCACHERI, P. C. 2010. Molecular and phenotypic aspects of CHD7 mutation in CHARGE syndrome. *Am J Med Genet A,* 152a**,** 674-86.

ZHOU, K., GAULLIER, G. & LUGER, K. 2019. Nucleosome structure and dynamics are coming of age. *Nat Struct Mol Biol,* 26**,** 3-13.

ZIATS, M. N., GROSVENOR, L. P. & RENNERT, O. M. 2015. Functional genomics of human brain development and implications for autism spectrum disorders. *Transl Psychiatry,* 5**,** e665.

ZOVKIC, I. B., PAULUKAITIS, B. S., DAY, J. J., ETIKALA, D. M. & SWEATT, J. D. 2014. Histone H2A.Z subunit exchange controls consolidation of recent and remote memory. *Nature,* 515**,** 582-6.

PUBLICATIONS

*__Reddy NC__, *Majidi SP**,** Ferguson CJ, Moore MJ, Liu HK, Bonni A. Conditional knockout of CHD7 leads to cerebellar polymicrogyria. *In preparation.*

***__Majidi SP, *Reddy NC__, Moore MJ, Chen H, Yamada T, Andzelm MM, Cherry TJ, Hu LS, Greenberg ME, Bonni A. (2019) Chromatin Environment and Cellular Context Specify Compensatory Activity of Paralogous MEF2 Transcription Factors. *Cell Reports*. 9:2001-2015.e5

Chen X, Chanda A, Ikeuchi Y, Zhang X, Goodman JV, **Reddy NC,** Majidi SP**,** Wu DY, Smith SE, Godec A, Oldenborg A, Gabel HW, Zhao G, Bonni S, Bonni A. 2018. The transcriptional regulator SnoN promotes the proliferation of granule neuron precursors in the brain in a temporally specific manner. *Journal of Neuroscience*. 39 (1): 44-62.

Yang Y, Yamada T, Hill KK, Hemberg M, **Reddy NC**, Cho HY, Guthrie AN, Oldenborg A, Heiney SA, Ohmae S, Medina JF, Holy TE, Bonni A. 2016. Chromatin remodeling inactivates activity genes and regulates neural coding. *Science*. 353:300-305.

Crisp MJ, Mawuenyega KG, Patterson BW, **Reddy NC**, Chott R, Self WK, Weihl CC, Jockel-Balsarotti J, Varadhachary AS, Bucelli RC, Yarasheski KE, Bateman RJ, Miller TM. 2015. In vivo kinetic approach reveals slow SOD1 turnover in the CNS. *Journal of Clinical Investigations*. 125:2772-80.

TEACHING/MENTORSHIP EXPERIENCE

2017-2019: Undergraduate student
2018: PhD rotating student
2016-2017: PhD rotating student
2014-2015: Teaching Assistant for Principles of the Nervous System